

# **STUDIES ON ATMOSPHERIC ELECTRIC PARAMETERS**

Thesis submitted to the  
**COCHIN UNIVERSITY OF SCIENCE AND TECHNOLOGY**  
for the degree of  
**DOCTOR OF PHILOSOPHY**  
under the  
**FACULTY OF SCIENCE**

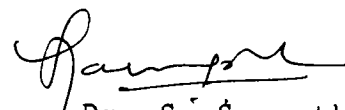
**S. MURALI DAS**

**ATMOSPHERIC SCIENCES DIVISION  
CENTRE FOR EARTH SCIENCE STUDIES  
THIRUVANANTHAPURAM-695 031**

**March 1993**

**CERTIFICATE**

This is to certify that this Thesis is an authentic record of research work carried out by Mr. S. Murali Das under my supervision and guidance in the Centre for Earth Science Studies for Ph.D. Degree of the Cochin University of Science and Technology and no part of it has previously formed the basis for the award of any other degree in any University.



Dr. S. Sampath  
(Research Guide)  
Head

Atmospheric Science Division  
Centre for Earth Science Studies  
Thiruvananthapuram -695031

Thiruvananthapuram  
March 19, 1993.

# C O N T E N T S

|   | Page No    |
|---|------------|
| <b>Chapter 1. INTRODUCTION</b>                                  | <b>1</b>   |
| 1.1. The atmosphere   | 1          |
| 1.2. Ionisation, ionising radiation and the ionosphere          | 4          |
| 1.3. Atmospheric electric field and the electrosphere           | 12         |
| 1.4. The atmospheric electric circuit                           | 15         |
| 1.5. The relevance of atmospheric electric parameters           | 20         |
| 1.6. Conductivity   | 22         |
| 1.7. Measurement of conductivity - Techniques and previous work | 24         |
| 1.8. Present work   | 29         |
| <br>  |            |
| <b>Chapter 2. TECHNIQUE OF MEASUREMENT</b>                      | <b>42</b>  |
| 2.1. Principle  | 42         |
| 2.2. Theory of operation  | 46         |
| 2.3. Sources of error   | 55         |
| 2.4. Operation  | 69         |
| 2.5. The sensor - Practical considerations                      | 72         |
| 2.6. Summary  | 77         |
| <br>  |            |
| <b>Chapter 3. UPPER ATMOSPHERIC MEASUREMENTS</b>                | <b>78</b>  |
| 3.1. Payload  | 78         |
| 3.2. Discussion   | 101        |
| 3.3. Errors in measurement                                      | 119        |
| <br>  |            |
| <b>Chapter 4. LOWER ATMOSPHERIC MEASUREMENTS</b>                | <b>121</b> |
| 4.1. Experimental details                                       | 121        |
| 4.2. Results and discussion                                     | 151        |
| 4.3. Errors in measurement                                      | 167        |

|  |            |
|--|------------|
| <b>Chapter 5. SUMMARY AND CONCLUSION</b> | <b>168</b> |
| 5.1. Summary                             | 168        |
| 5.2. Achievements of the work            | 169        |
| 5.3. An overview of the results          | 171        |
| 5.4. Future perspectives                 | 175        |

REFERENCES

PUBLICATIONS IN JOURNALS / PRESENTED IN SYMPOSIA

=====

## CHAPTER - 1

### INTRODUCTION

#### 1.1. THE ATMOSPHERE:

The atmosphere is a gaseous envelope surrounding the earth, held by gravity, having its maximum density just above the solid surface and becoming gradually thinner with distance from the ground until it finally becomes indistinguishable from inter planetary gas. Therefore there is no well defined upper limit or top of the atmosphere. It is classified into different layers based on its characteristics. The classification is not unique and differs with the type of characteristic on which the classification is based.

Based on its composition the atmosphere is classified broadly into two layers, namely the *homosphere* and the *heterosphere*. The layer of atmosphere below about 100 km altitude is of constant chemical composition (except for water vapour and certain trace gases) and is therefore called the homosphere. In the homosphere the mean free path is so short that the time required for vertical separation of the heavier and lighter constituents by molecular diffusion is many orders of magnitude longer than the time required for turbulent fluid motions to homogenise them. The layer of atmosphere above 100

km is of varying composition and for that reason is called the heterosphere. In this region vertical mixing of atmospheric constituents is essentially controlled by molecular diffusion. The level of transition, at 100 km, from the region of turbulent mixing to molecular diffusion is called the *turbopause*.

Again, the atmosphere is classified into thinner layers, based on the temperature profile and the associated characteristics. In the lowest layer, starting from the surface and extending up to about 7 to 17 km, the temperature usually decreases with altitude at a rate of about 5 to 7 degrees  $\text{km}^{-1}$ . The rate of decrease of temperature (lapse rate) is highly variable from place to place; but it never exceeds 10 degree  $\text{km}^{-1}$  except near ground. This lowest layer of atmosphere is the *troposphere* and is characterized by strong vertical mixing. This is the seat of all weather phenomena that affect us at ground and contains about 80% of the total air mass. The upper limit of troposphere is defined by a sudden change in temperature trend. The temperature stops decreasing more or less suddenly and remains constant or starts increasing slightly. This is the *tropopause* and its altitude varies with latitude from 17 km to 7 km (being higher at the equator). The tropopause temperature near the equator is about  $-80^{\circ}\text{C}$  and that in the middle latitude is about  $-55^{\circ}\text{C}$ .

The next region of atmosphere shows a gradual increase of temperature reaching a maximum of about  $0^{\circ}\text{C}$  at

about 50 km. This region is characterized by very small vertical mixing and is known as the *stratosphere* (the layered or stratified sphere). Its upper limit, at the temperature maximum, is the *stratopause*. Then the temperature drops again through the region called *mesosphere* to a minimum of the order of  $-100^{\circ}\text{C}$  defining the *mesopause*, at about 85 km. In this region vertical air motions are not strongly inhibited. During summer there is enough lifting to produce thin cloud layers (*noctilucent clouds* - nucleated over meteoric dust) in the upper mesosphere over parts of the polar regions.

From thereon the temperature increases steadily and the region beyond 85 km, from the temperature point of view, is called the *thermosphere*. It extends upward to an altitude of several hundred kilometers where the temperature range from  $500^{\circ}\text{K}$  to as much as  $2000^{\circ}\text{K}$  depending on the amount of solar activity. Above 500 km the molecular collisions are so infrequent that temperature as such is difficult to define. At these levels neutral particles and charged particles move more or less independently and thus there is no reason why their temperatures should be the same.

It may be mentioned here that the pressure at stratopause is about 1 mb. Thus the troposphere and stratosphere together account for about 99.9% of the atmospheric mass. Of the remaining mass, 99% is contained in the mesosphere and the rest 1% in the thermosphere.

## 1.2. IONISATION, IONISING RADIATION AND THE IONOSPHERE:

Ionisation means removing an electron from the outer shell of a gas molecule or atom. The ionisation energy is supplied either by a colliding particle of sufficient kinetic energy or by the energy quantum  $h\nu$  ( $\nu$  is the frequency and  $h$  is the Planck's constant) of incident electromagnetic radiation.

Four types of ionising agencies produce ionisation in the atmosphere. They are

1. Solar radiation
2. Galactic cosmic rays
3. Radiations of radioactive origin, consisting of
  - a.  $\alpha$  radiation
  - b.  $\beta$  radiation and
  - c.  $\gamma$  radiation.
4. Ions or electrons which have reached the threshold energy for impact ionisation in high electric fields.

Above about 60 km solar radiation is the dominant source of ionisation and the contribution by other sources of ionisation is relatively insignificant. Similarly ionisation by galactic cosmic rays dominate below 60 km altitude. Near the surface over land, ionisation caused by radioactive substances and radioactive gases dominate.

Because of the rapid increase in mean free path of molecules with altitude and the transition to more stable



species of ions at higher levels, the free electrons produced by sun's ionising radiation in the upper atmosphere have much longer life times than those resulting from various sources at lower levels. Hence, most of the atmospheres' free electrons are located at levels above 60 km where they exist in sufficient number to affect radio propagation. This region of the atmosphere is called the *ionosphere* (or some times the *Heaviside layer*). The concentration of free electrons increases monotonically with height from very small values below 60 km to a maximum value near 300 km.

The ionosphere is classified into four regions namely D, E, F<sub>1</sub>, and F<sub>2</sub> layers. Table 1.1 gives their height ranges and typical order of electron concentration.

Table 1.1.

Ionospheric layers; their height ranges and typical order of electron concentration.

| Region                               | Height<br>(km) | Electron concentration (m <sup>-3</sup> )<br>Typical order of magnitude |
|--------------------------------------|----------------|---|
| D                                    | 60 - 90        | 10 <sup>9</sup> - 10 <sup>10</sup>                                      |
| E                                    | 90 - 140       | 10 <sup>11</sup>  |
| F <sub>1</sub> }<br>F <sub>2</sub> } | > 140          | Minimum of 10 <sup>12</sup> in the region<br>of 250 to 500 km.          |

The D region is observed during day time only and the regions  $F_1$  and  $F_2$  become a single region ( or  $F_1$  disappears) during night. Above 500 km the collision between individual particles are so infrequent that there is relatively little interaction between charged particles and the neutral constituents of the atmosphere. At these levels motions of charged particles are strongly contained by the presence of earth's magnetic field lines and so this region is named *magnetosphere*. The earth's magnetosphere acts as an obstacle to the solar wind, with the *magnetopause* separating solar wind particles which flow around the magnetosphere, from charged particles trapped within the magnetosphere.

In the succeeding sections characteristics of different types of ionising agencies are discussed. The discussion pertains to the region of atmosphere below about 90km.

#### 1.2.1. CHARACTERISTICS OF SOLAR RADIATION:

The discussion of the characteristics of solar radiation is limited to the region of atmosphere below 90 km only, which is of interest here.

Normally the effect of solar ionising radiation is seen only down to 60 km. The layer of atmosphere between 60 and 90 km, namely the D-region, is effectively shielded by the upper layers from most of the solar short wave radiation which is capable of ionising air molecules. In the wavelength

region from 102 to 122 nm there are certain windows in which no absorption occurs above the D-region. In particular the Hydrogen line, Lyman  $\alpha$  of wave length 121.6 nm reaches these levels through one of the windows and is able to ionise NO and is thus largely responsible for the existence of the D-region. More details regarding this are given in chapter - 3.

Among the ionospheric layers, formation of negative ion is a characteristic of the D-region. They are produced by electron attachment and such a reaction requires a third body (neutral molecule or atom) to carry away excess energy. Because of the requirement of a molecule or atom for attachment and of a third body, the concentration of negative ions is expected to decrease rapidly with increase in altitude, like the pressure.

#### 1.2.1.1. Solar activity indices and periodic variations:

Generally two types of indices are used to quantify the level of solar activity. One is the sunspot number  $\mathcal{R}$  which represents in a complex way, the number and area of sun spots. Sun spots are patches of comparative darkness frequently visible on the sun. The sun spot number provides an approximate measure of the strength of the XUV radiation. The magnitude of  $\mathcal{R}$  varies between 0 and 200 with a quasi period of 11 years throughout the solar cycle. The energy flux in the ultra violet part of the spectrum is approximately proportional to  $(1+0.01\mathcal{R})$ .

The flux of decimetric radio waves of 10.7 cm wave length, emitted from the sun has been found to be a better measure of XUV strength. This flux, denoted by  $S$  or  $F_{10.7}$ , is measured in units of  $10^{-22} \text{W m}^{-2} \text{Hz}^{-1}$ .

The strength of XUV often varies rapidly within hours or days (Ratcliffe, 1972). There is a tendency for this variation to show a periodicity of about 27 days, the period of solar rotation, as though the radiation were emitted in comparatively narrow beams.

#### 1.2.1.2. Particle radiation - the solar wind:

The solar coronal plasma is accelerated outward to form the solar wind. This consists of a stream of protons and electrons. There are strong magnetic fields on the sun and as the solar wind moves through them currents are induced and the original field is distorted. If the conditions are suitable the distorted field appears to be carried with the wind as though it were frozen into the moving plasma. Because of the 27 day rotation of the sun the particles emitted in succession are later distributed along a spiral; they carry the magnetic field with them to give it the same spiral shape. Near the earth the radial velocity of the wind combined with the circumferential velocity of the sun corresponding to the 27 day rotation causes the field lines to make an angle of about  $45^\circ$  with the radial direction. The spiral magnetic field is often divided into four or six sectors of roughly equal size,

such that in the neighbouring ones the field is in opposite directions. The sectors rotate with the sun so that at the earth there are four or six reversals of the field during each solar rotation. The sectors are formed gradually and often persist for many solar rotations.

#### 1.2.1.3. Solar disturbances:

Sometimes, disturbances occur on the sun, accompanied by the emission of one or more of the following radiation, each of which can produce its own type of disturbance in the ionosphere.

1. *Solar flare* - Intense bursts of high energy particles emanating from the sun's outer atmosphere with an increase in the intensity of the visible H- $\alpha$  line. A typical flare lasts of the order of an hour.

2. *X-ray flare* - A sudden increase in the strength of X radiation.

3. *Solar plasma event* - The emission of a group of protons and electrons so dense that interaction between the particles gives it the characteristics of a plasma cloud. It forms an enhancement of the solar wind. It reaches the earth after about 36 hours.

4. *Solar proton event* - The emission of energetic particles and electrons with such small concentration that they travel like independent charged particles. They reach the earth in a few hours.

X-ray flares, plasma events, and proton events often accompany solar flares. The frequencies of all types of disturbance follow the 11 year solar cycle.

#### 1.2.2.CHARACTERISTICS OF GALACTIC COSMIC RAYS:

Galactic cosmic radiation is the dominant source of ionisation below about 60 km. Because the collision cross section of these energetic particles is small the ion production rate above 30 km is directly proportional to the atmospheric particle number density. Between about 30 and 15 km increasing number of secondary cosmic ray particles cause a rapid increase in the ionisation rate. The secondary cosmic ray particles associated with primary cosmic rays penetrate to the ground level before reaching the end of their path.

Cosmic ray ionisation is a function of several variables of which two are important, namely the period of sunspot cycle and the earth's geomagnetic latitude.

Galactic cosmic radiation is somewhat deviated away from the sun's neighbourhood by solar magnetic field. Since the strength of this field increases with sun spot number (solar activity) the intensity of cosmic radiation reaching the earth is weakest at sun spot maximum and strongest at sun spot minimum.

Earth's magnetic field regulates the flux of cosmic rays into the atmosphere. Only the more energetic particles have sufficiently large radii of curvature to reach the

surface near the equator before being deflected by the earth's magnetic field. At higher latitudes ionisation rate is higher as large number of ever lower energy particles have access through the magnetic field. Near the geomagnetic poles the field lines are essentially open allowing very low energy particles. Because of the latitude effect plus solar modulation of cosmic rays, a knee is found in the latitude profile of cosmic ray ionisation, i.e. a latitude above which the ionisation at any fixed altitude no longer increases with increasing latitude. During sun spot cycle minima when the solar reduction of the galactic cosmic ray flux is small the knee moves to higher latitudes and occasionally may not be present at all.

### 1.2.3. CHARACTERISTICS OF SURFACE RADIOACTIVITY:

A few meters above ground, ionisation by radiation from radioactive material at the surface and radioactive gases dominate over that by cosmic rays. Of the total number of ion pairs produced, the contribution by cosmic rays is only 20%. Of the rest 80%, radiation from the soil contributes to 35% and the remaining 45% is contributed by radioactivity of air (Bricard, 1965).  $\beta$  and  $\gamma$  radiation of air contributes to only about 1% of the the ionisation and the rest 44% is due to  $\alpha$  radiation. Similarly of the 35% ion pair production by radiation from soil, the contribution by  $\beta$  radiation is only 3% . The strength of soil radiation decreases with altitude

in such a way that by about 1 km the strength reduces to 0.1% of the surface value. The main source of  $\alpha$  radiation in the air is Radon which is exhaled into the atmosphere from the soil. It is transported to upper layers by diffusion and turbulent transport. Therefore variation of ionisation by natural radioactive sources is dependent on the concentration of Rn in the air. The rate of exhalation and the vertical transport of Rn depends on meteorological factors like pressure, temperature, frost, precipitation etc. (Junge, 1963). The mean concentration of Rn of the atmosphere near ground above continents is about 100 times that above oceans (Israel, 1971).

### 1.3. ATMOSPHERIC ELECTRIC FIELD AND THE ELECTROSPHERE:

It is well known that an electric field exists between the earth and a highly conducting layer of atmosphere (the atmospheric electric equalisation layer, also known as the *electrosphere*) above about 60 km. According to the widely accepted hypothesis, postulated by C.T.R. Wilson (1920), the earth and the electrosphere together form a spherical capacitor with the electrosphere being continuously charged by thunderstorms to about 250 kV relative to the earth. It discharges through fair weather parts of earth with a current density (current per unit area) of a few picoamperes per square meter.

Here, from the atmospheric electricity point of view



it becomes necessary to define the altitude at which the global electric equalisation takes place (The discussion below follows Israel, 1971). For this, we first determine the time taken for a charge  $Q$  that is carried to a point  $P$  at a height  $h$  in the atmosphere at time  $t=0$ , to be distributed uniformly over the spherical shell. Israel and Kasemir carried out a rough calculation assuming that conduction takes place only in a layer  $\Delta h$  km thick, which surrounds the earth concentrically at this height, and that the remaining atmosphere is non conductive (Israel, 1971). They arrived at the approximate solution

$$\frac{U_P}{U_\infty} = 6 e^{-\left(\frac{2t}{T}\right)} \quad (1)$$

This equation indicates how a potential difference  $U_P$  between  $P$  and its antipodal point approaches the final value  $U_\infty$  upon bringing a charge  $Q$  to point  $P$ .  $U_\infty$  is the potential assumed by the entire layer after the charge has spread out. The time constant  $T$  is given by

$$T = \frac{\epsilon_0 R (R+h)}{\Delta h \sigma h} \quad (2)$$

where,  $R$  is the radius of earth

$h$  is the height above earth's surface

$\sigma$  is the conductivity

$\Delta h$  is the layer thickness and

$\epsilon_0$  is the dielectric constant of air.

The time constants for various altitudes can be obtained by substituting the value of  $\sigma$  and calculating for a given thickness, say  $\Delta h = 1$  km. This means that in a non-conducting atmosphere, if a spherical conducting layer exists, a charge supplied to this layer will spread uniformly over the entire layer in the given time. If this layer of thickness  $\Delta h$  were assumed to be the counter plate of the atmospheric capacitor, this time would signify the phase delay at the antipodal point.

Observations have shown that electrical disturbances in the atmosphere are transmitted around the globe without any significant delay. For instance the thunderstorm activity are reflected in the vertical electric field measured over regions where local effects are negligible, without any phase delay. After a change in atmospheric electric conditions the time required for reestablishment of steady state is known to be approximately 10 to 15 min. This time may be taken as the 'equalisation period'.

Thus a layer of the type described above, the time constant of which is less than 10 to 15 min., would be sufficient to permit a global correlation between the potential gradient and thunderstorm activity. For generalisation, the layer thickness can be changed and corresponding values for other thicknesses can be calculated. Using the conductivity profile of the atmosphere the actual height at which the global atmospheric equalisation takes

place with the participation of all layers can be calculated. Such a computation shows (Israel, 1871) that equalisation takes place at a height of about 60 km. This layer is defined as the *Electrosphere*.

Thus the establishment of a global atmospheric balance does not fully involve the ionosphere but it takes place in a layer at a height of about 60 km. This also shows that solar or ionospheric effects need not always influence the atmospheric electricity. In the atmospheric electric sense, it may be expected that the solar effects will only be felt when they penetrate deep into the atmosphere.

#### 1.4. THE ATMOSPHERIC ELECTRIC CIRCUIT:

Figure 1.1. illustrates the general atmospheric electrical process as per the widely accepted hypothesis of C.T.R. Wilson. The equivalent circuit diagram of the same is shown in Figure 1.2. According to the hypothesis world wide thunderstorm, which in effect is a D.C generator (vertical dipole), causes a current to flow through the circuit and maintains the earth's electric field. If thunderstorms were to stop, the electrification of the earth would decay with a time constant of about 15 min. (Israel, 1971); it persists because thunderstorms occur somewhere at all times.

As mentioned earlier, atmospheric conductivity below the electrosphere is maintained by galactic cosmic radiation and so conduction currents can flow in the atmosphere.

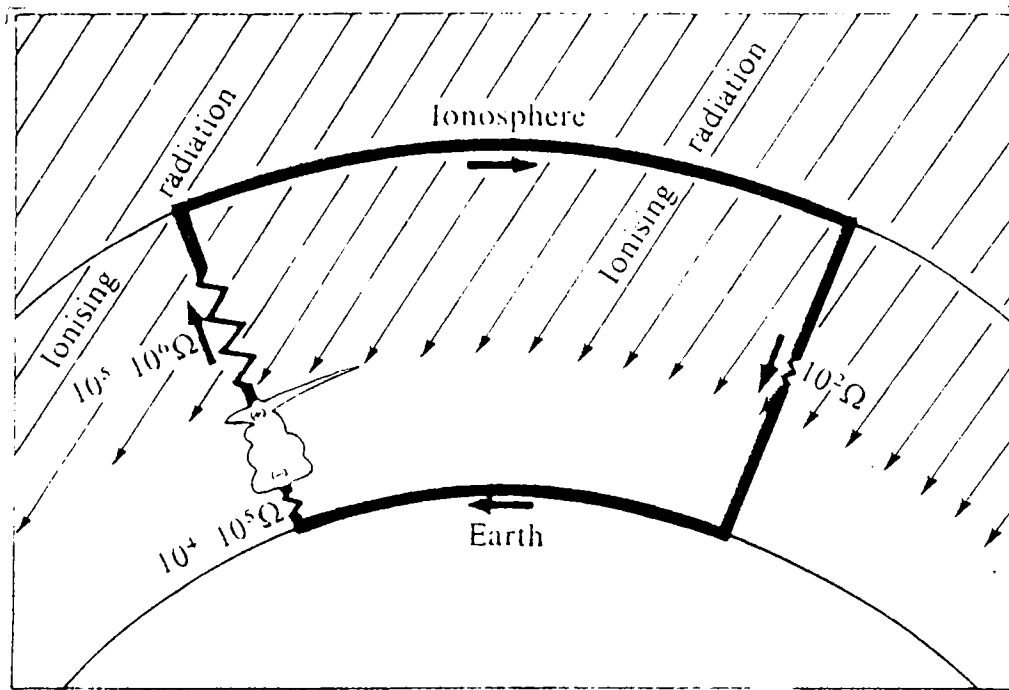


FIGURE 1.1. The atmospheric electrical global circuit. Large arrows indicate flow of positive charge. Estimated resistances of circuit elements are given (after Markson, 1978). The resistance shown on the fair weather part represents the total resistance.

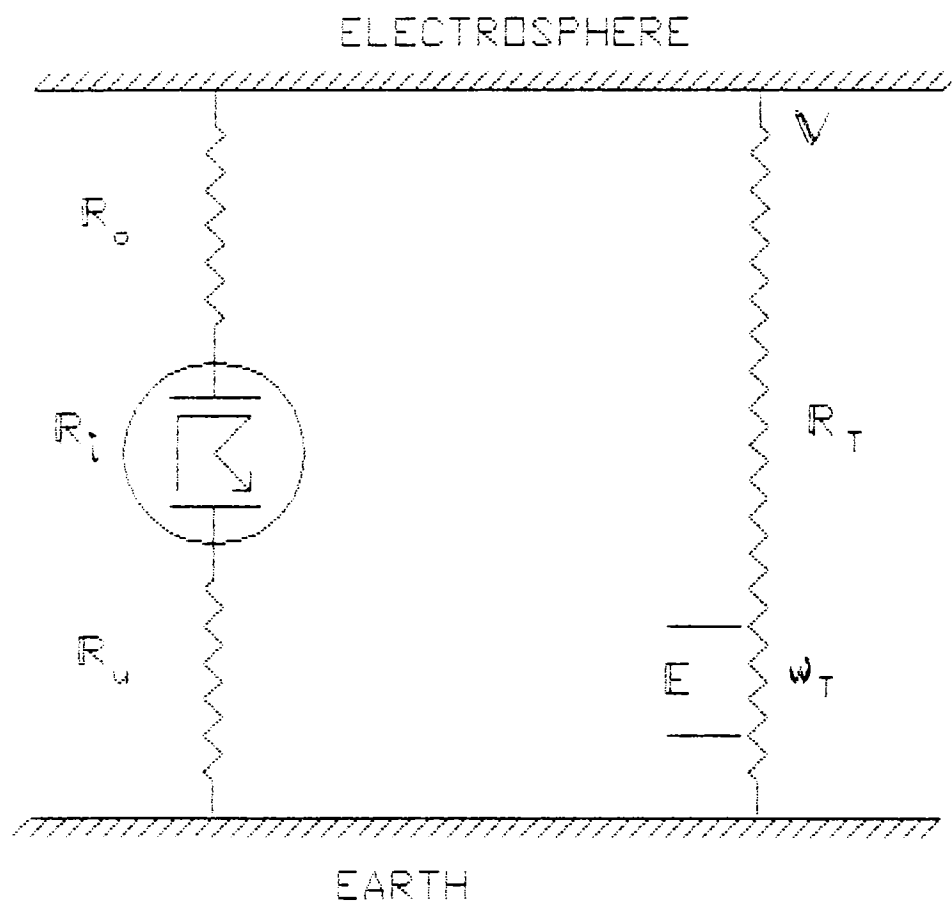


FIGURE 1.2. The atmospheric electrical global circuit - the equivalent circuit diagram.

Therefore air behaves as a leaky dielectric between the two electrodes of the spherical capacitor. A conduction current flows between the electrodes in the fair weather regions of the globe. Above the thunderstorm generator, through the charging resistor a conduction current flows between thundercloud tops and the electrosphere. This charging current maintains the electrosphere potential at about 250 kV relative to earth. This potential can be considered as an expression of the overall intensity of global atmospheric electrification. Over the fair weather parts of the globe, in the return portion of the circuit a conduction current flows through the load resistor part; positive ions drift downwards and negative ions upwards. The circuit is completed between the earth and the thunder cloud base through combined hydrometeor precipitation, conduction (including corona), convection and lightning currents.

In the equivalent circuit diagram the atmosphere in the fair weather parts is represented by  $R_T$ , which is the total resistance from the surface to the electrosphere. The thunderstorm symbol represents the D.C generator. It represents the thunderstorm activity over the entire earth in parallel per unit time and has an internal resistance  $R_i$ .  $R_o$  and  $R_u$  represent the resistances of the atmosphere above and below the thunderstorms. These two resistances connect the generator to the surface of earth and the electrosphere.  $V$  represents the potential of the electrosphere. The parameter

$E$  is the atmospheric potential gradient across a section  $\omega_T$  (representing unit thickness of the atmosphere) of the resistance, as shown in the diagram. Then

$$E = \frac{\omega_T}{R_T} V \quad (3)$$

The air-earth current  $I_T$ , which is the current flowing from the electrosphere to earth, must be independent of the height under steady state conditions and can be expressed as

$$I_T = \frac{V}{R_T} \quad (4)$$

also, 
$$I_T = \frac{E}{\omega_T} \quad (5)$$

If the values of  $R_T$  and  $\omega_T$  are replaced by columnar resistance  $R$ , which is the resistance of a column of the atmosphere of unit area of cross section, and  $\omega$  the resistivity respectively, then the air earth current density  $I$  is given by

$$I = \frac{V}{R} \quad (6)$$

and, 
$$I = \frac{E}{\omega} \quad (7)$$

Similarly eqn.(3) becomes

$$E = \frac{\omega}{R} V \quad (8)$$

In these equations the resistivity, or its reciprocal conductivity, of air is an independent variable and the potential gradient and air earth current are derived quantities which depend on the value of conductivity.

### 1.5. THE RELEVANCE OF ATMOSPHERIC ELECTRIC PARAMETERS:

It is seen from the above discussion that the electric field, which is dependent on the value of  $V$ , decreases with height because it is inversely proportional to conductivity. The field is modified by periodic and non periodic changes in  $\omega$  and  $R$ . Differentiating eqn.(8), we obtain

$$\frac{dE}{dt} = \frac{\omega}{R} \frac{dV}{dt} + \frac{V}{R} \frac{d\omega}{dt} - \frac{V}{R} \frac{\omega}{R} \frac{dR}{dt} \quad (9)$$

This equation represents the influence of the three quantities  $V$ ,  $R$  and  $\omega$  upon the behaviour of the potential gradient. The above expression can be reduced to

$$\frac{1}{E} \frac{dE}{dt} = \frac{1}{V} \frac{dV}{dt} + \frac{1}{\omega} \frac{d\omega}{dt} - \frac{1}{R} \frac{dR}{dt} \quad (10)$$

The two equations show that a knowledge of the time dependence in  $E$  is not sufficient to predict changes in the other three quantities  $V$ ,  $E$  and  $\omega$ . Thus to obtain full information of the electrical circuit the measurement of electric field alone is insufficient. When two of the three electrical parameters of an electrical circuit, namely voltage, current and resistance are known the third can be deduced from Ohm's law. Under steady state conditions,

$$\frac{V}{R} = I$$

describes the relationship between the parameters of the whole circuit, in terms of a vertical column of resistance, and



$$\frac{E}{\omega} = \theta$$

describes that of an element. Therefore to get a full picture, at least two of the parameters  $V$ ,  $R$  and  $\theta$  for the column and  $E$ ,  $\omega$  and  $\theta$  for the element should be measured.

The contribution of changes in conductivity to time variations in air earth current density can be seen by differentiating eqn.(6).

$$\frac{d\theta}{dt} = \frac{1}{R} \frac{dV}{dt} - \frac{V}{R \cdot R} \frac{dR}{dt} \quad (11)$$

or

$$\frac{1}{\theta} \frac{d\theta}{dt} = \frac{1}{V} \frac{dV}{dt} - \frac{1}{R} \frac{dR}{dt} \quad (12)$$

Equations (10) and (12) show the dependence of air earth current density and potential gradient on conductivity and electrosphere potential. The influence of conductivity variations on the value of  $E$  is through variations in  $\omega$  and  $R$  and that in the value of  $\theta$  is through  $R$  variation. In other words  $\theta$  is relatively independent of local changes in conductivity whereas in the case of electric field, the local variations are more strongly pronounced because of the term  $\frac{1}{\omega} \frac{d\omega}{dt}$ .

The relationship between the global electric circuit parameters namely the electrosphere potential, the atmospheric electric field, air earth current density, columnar resistance and conductivity is clear from the discussion given above. From the relationship the following deductions about conductivity may be made.

1. The atmospheric electrical conductivity is an

independent parameter.

2. The air earth current density depends on the columnar resistance. The columnar resistance in turn depends on the conductivity of air.
3. The influence of conductivity on potential gradient is two fold; one is by changes in columnar resistance and the other is due to local variations in conductivity.

In addition, the charging of the electrosphere and earth is effected through the atmosphere above and below the thunderstorms. The charging current is dependent on the conductivity of the column of atmosphere above and below the thunderstorms.

Thus it may be said that the conductivity of air is one of the most important parameters in atmospheric electricity.

#### 1.6. CONDUCTIVITY:

The conductivity of air depends on the concentration and mobility of the ions. If a small potential difference is applied to two electrodes in air, a weak current flow is induced by the ions which flow in opposite directions to the electrodes where they deliver their charge. The current density ( $i$ ), defined as the quantity of electric charge which flows per unit time through a surface of area unity perpendicular to the direction of flow, is composed of two terms. One corresponds to the flow of positive ions and the

other to that of negative ions. Thus:

$$i = e ( \mu_+ n_+ + \mu_- n_- ) E = \sigma . E \quad (13)$$

where,  $e$  is electronic charge

Here,  $e$  should be the charge on the ion. Since almost all ions encountered in the atmosphere are singly charged, we can use the electronic charge in the expression.

$E$  is the strength of the applied field,

$n_+$  and  $n_-$  are the number densities of (the number of ions per unit volume) positive and negative ions respectively,

$\mu_+$ ,  $\mu_-$  are the mobilities of positive and negative ions. Mobility is the velocity acquired by an ion on application of an electric field of unit strength.

and

$$\sigma = e ( \mu_+ n_+ + \mu_- n_- ) \quad (14)$$

represents the total conductivity of air.

The two terms

$$\sigma_+ = e \mu_+ n_+ \quad (15)$$

and

$$\sigma_- = e \mu_- n_- \quad (16)$$

are called the polar conductivities. These expressions represent the case when there is only one type of positive ion and one type of negative ion. If there are ions of different mobilities, namely  $\mu_1, \mu_2, \dots, \mu_n$ , each having a corresponding number density  $n_1, n_2, \dots, n_n$ , then the above

expressions become

$$\sigma_+ = \sum_{j=1}^n e \mu_{+j} n_{+j}, \quad (17)$$

$$\sigma_- = \sum_{j=1}^n e \mu_{-j} n_{-j}, \quad (18)$$

and 
$$\sigma = \sum_{j=1}^n e \left[ \mu_{-j} n_{-j} + \mu_{+j} n_{+j} \right]. \quad (19)$$

Eqn.(13) is valid only when the field strength is low such that the current flow does not cause an appreciable reduction in the number of ions in the air between the plates. In other words the loss of ions due to drift towards the plates is much less than the number of ions being produced by local ionisation. If the field is increased continuously, a stage is reached when the ion production lags behind the loss and eqn.(13) becomes invalid. On further increase of the field, at a very high value a sudden rapid increase in current takes place due to impact ionisation, which initiates a self sustaining discharge.

## 1.7. MEASUREMENT OF CONDUCTIVITY -

### TECHNIQUES AND PREVIOUS WORK:

Various techniques have been employed to measure conductivity of air at different altitudes of the atmosphere. However, a marked difference can be seen between the approach

to the measurement in the upper atmosphere and that in the lower atmosphere. In the lower layers of the atmosphere all the three parameters namely conductivity ion density and ion mobility have been measured. In the upper atmosphere, ion density and mobility measurements are conducted rather than direct measurement of conductivity. It may be mentioned here that the negative polar conductivity in the region above about 70 km is mainly due to free electrons. The electrons have relatively very high mobility, and in this region of the atmosphere, the earth's magnetic field influences the motion of the charged particles. Therefore the conductivity in this region and above ceases to be purely Ohmic in nature. Hence, it is more meaningful to measure the ion and electron concentration and their variations, rather than conductivity, in this region above about 70 km.

#### 1.7.1. MEASUREMENTS IN THE UPPER ATMOSPHERE - TECHNIQUES:

The concentration and distribution of free electrons in the upper atmosphere has been investigated by ground-based technique, and also by in-situ measurements using rockets.

The instrument used for ground-based studies is the Ionosonde. It consists basically of a pulse transmitter and a receiver (Ratcliffe, 1972). The transmitter emits short pulses of a given frequency in the range of 1 - 20 MHz vertically upwards. When this radiation passes through the ionosphere the free electrons oscillate in response to the

electromagnetic wave. For a sufficiently high concentration of electrons, the radiation is reflected and received at the ground. From the time interval between transmission and reception the height at which reflection takes place is found out. The frequency at which reflection occurs depends on the electron number density, so that knowing the frequency the electron density can be calculated. Usually the frequency is swept so that the height distribution of electron density is obtained. The electron density in the D-region is relatively low and therefore this technique is insensitive for D-region measurements. Hence, in-situ measurement methods are used in the D-region.

One of the methods used for in-situ measurement of electron density is based on the principle of absorption of radio waves (Aikin et al, 1972). The technique is known as Propagation Receiver technique. In this method a CW is transmitted from ground. The transmitted signal is monitored by a rocket-borne receiver.

Another method of in-situ electron density measurement is by means of rocket-borne probes. A sensor which is widely used for the measurement of electron density is the Langmuir probe. The probe was first developed by Irving Langmuir during the nineteen twenties for laboratory studies of plasma (Subbaraya et al.1987). In this technique a metallic sensor is exposed to the medium under study and the current collected by the probe is measured as the bias voltage

applied to it is varied from a convenient negative value through zero, to a convenient positive value. From the resulting current voltage characteristic of the probe electron and ion densities are determined. The technique has been successfully used for a variety of plasma investigations.

The Langmuir probe technique was employed for ionospheric studies for the first time in 1946. After this several groups in different parts of the world developed various versions of this technique and a large amount of data on ionospheric structure has been collected.

Measurement of ion density, ion mobility and conductivity in the upper atmosphere up to about 80 km have been made by the aspiration method. Because of the high mobility of electrons and problems associated with it, the aspiration method is not used for electron density measurements. Above about 80 km it becomes difficult to use the aspiration method for ion measurements also due to the high mobility of ions.

Ion measurements in this altitude region using the aspiration method is usually conducted from two platforms; namely parachute and rocket. In parachute-borne measurement an aspiration sensor payload is dropped from the desired altitude using a rocket. The payload descends slowly with the help of the parachute and measurement is made. In rocket-borne measurement, during ascent the sensor is exposed at the desired altitude. The sensor is mounted either in the

nose cone portion of the rocket or on a boom, which is opened at the desired altitude and measurement made.

#### 1.7.2. MEASUREMENTS IN THE LOWER ATMOSPHERE - TECHNIQUES:

In the lower atmosphere, conductivity is determined approximately by dissipation measurements or precisely by the method of aspiration through a capacitor or still more precisely by evaluation measurements of the ion spectrum (Israel, 1971).

A charged conductor exposed to air suffers a specific charge loss in time which is proportional to conductivity, due to ions of opposite charge which are drawn to the conductor. In the aspiration method air is drawn through a capacitor. One of the electrodes kept at a potential drives ions in the air stream to the other electrode. The ions collected by the other electrode constitute a current which is proportional to the conductivity.

Langmuir probe and spherical probe are also used for conductivity measurement in the lower atmosphere. Spherical probe is a conducting sphere biased to a certain voltage so that ions are attracted towards it and get collected (Beig et al 1989). The polarity and magnitude of the biasing voltage depends on the region of measurement and the polar conductivity measured.

The antenna method offers the advantage of measuring



conductivity, electric field and current with the same sensor (Ogawa, 1973). This works on a principle similar to the relaxation technique. Potential difference between two antennas separated along the direction of the field is measured. The measured potential difference is proportional to the field. If the antennas are shorted and opened before measurement, the potential difference measured rises exponentially. From the time constant conductivity is calculated.

Probably because of the simplicity of operation the relaxation method is widely used for the measurement of conductivity, from balloon platforms. Probes of different geometry, say sphere or plate and in different configurations have been used for balloon measurements (for instance, Iversen et al 1985 and Holzworth et al 1986).

Compared to other probes the aspiration analyzer, namely the Gerdien condenser, has the advantage that it can measure ion density, mobility and conductivity simultaneously. Therefore whenever all these parameters are to be measured the Gerdien condenser is used. On balloon and parachute this may be operated either in self-aspiration mode or forced aspiration mode. A detailed description of the technique is given in chapter-2.

### 1.7.3. PREVIOUS WORK :

Before going specifically into the discussion of

previous work on conductivity measurements, a look into the variability of atmospheric electric circuit parameters, its causes and effects will be useful. Such an discussion by Markson (1978) is given below.

The paper clearly illustrates how an increase in intensity of ionising radiation can decrease the charging resistance over thunderstorm. The possibility of such a decrease is justified by the fact that most of the variations in ionising radiation happen above 15 km altitude. A decrease in charging resistor causes an increase in the ionospheric potential. This results in an increase in field in the fair weather parts of the world. Further, the possible effects of a change in the field on cloud electrification, thermodynamics of troposphere and precipitation are discussed. The suggested variations in the number of thunderstorms and changes in thermal energy are supported by Muir (1979 a,b).

A change in ionisation can be brought about by many phenomena. Galactic cosmic rays are known to be modulated by solar activity. Over a short term this is seen as 'Forbush decrease' following solar flares. In mid to high geomagnetic latitudes, following magnetic storms Bremsstrahlung X-rays affect ionisation down to 12 km altitude. A large decrease in vertical electric field occurring simultaneously with a solar proton event followed by a large increase in solar X-radiation intensity has also been observed.

Other solar related events reported in the paper are

an increase in lightning frequency, thunderstorm frequency as well as electric field variations in the arctic and antarctic with solar sector crossings.

Before concluding this section a few interesting findings reported relatively recent are worth mentioning. One is the detection of current and field pulses in the ionosphere by Kelly et al. (1985) from his rocket experiments. Holzworth (1991 b) has reported the occurrence of electric field pulse. Also it was reported that component of the field pulse parallel to the geomagnetic field line occurred significantly before the whistler. This was aptly called a pre-cursor pulse. A pulse was recorded in the search coil magnetometer coincident with the pre-cursor pulse also. Another is the observation of lightning induced electron precipitation into the ionosphere by Goldberg et al. (1986, 1987). These observations and the appearance of intermittent large fields near 60km (Goldberg et al., 1984) raises questions on the role of ionosphere on atmospheric electrodynamics.

#### 1.7.3.1 Upper atmospheric measurements:

A large volume of data on electron density in the upper atmosphere has been collected by radio wave absorption and in-situ measurements. The number of in-situ measurements from Thumba, an equatorial rocket launching station itself is large. Subbaraya et al. (1983) reports of a modified Langmuir probe and results from twenty five rocket experiments using

this probe during the period 1966 to 1978 from Thumba. Measurements conducted by this group have yielded electron density profiles from 60 km onwards, during day, night and twilight hours. Subbaraya et al. (1983) has given a reference electron density profile for an equatorial station, obtained by averaging results from twelve experiments. The comprehensive experiment conducted by Aikin et al. (1972) which consisted of three rocket flights was also from Thumba. In this experiment simultaneous measurement of D-region ionisation sources and electron and ion densities were made in one day. Electron density was measured by nose tip probe and propagation receiver, positive ion density by Gerdien condenser, positive ion composition by quadrupole ion mass spectrometer and investigation of ionisation sources by ion chambers and proportional counters. The results showed that the possible production sources of D-region are dominated by X-rays, photo ionisation of NO and cosmic rays. D-region electron and positive ion density profiles also have been obtained in this experiment. An asymmetry about noon was seen in the electron density profiles obtained.

Regarding upper atmospheric conductivity measurements, Bordeau et al (1959) reported the first rocket-borne Gerdien condenser measurement of polar conductivities from 35 km to 80 km. The sensor was operated in the relaxation mode. The measured negative polar conductivity from 35 to 50 km was found to be in good

agreement with theoretically predicted values. Also the polar conductivities measured above 50 km were found to be less than the predicted values.

In 1970 Widdel et al. (1970) reported probably the first parachute-borne measurement of positive ion density and mobility between 39 and 70 km. Also it seems that this was the first time the Gerdien condenser was operated with a driving sweep voltage. Rose et al. (1971) and Rose and Widdel (1972), using the same technique, conducted parachute-borne positive and negative ion measurement from 40 to 70 km and 22 to 85 km. This group reports of having detected two types of ions above 60 km. An important finding reported in the last two papers is about the ion loss caused by the introduction of grid at the inlet and outlet of the Gerdien condenser. These grids are introduced to reduce field fringing at the inlet and outlet. Widdel et al. (1976, 1977 and 1979) reports a few more parachute-borne measurements. One of the measurements (Widdel et al. 1977) has given mobility values from 10 km to 74 km. Some problems associated with materials used for electrodes are discussed in (Widdel et al. 1976). The parachute-borne measurement of Maynard et al. (1984) have yielded conductivity profile from about 20 km to 120 km using Gerdien condenser and blunt probe. From the three measurements done by him within a month, he observed the upper stratospheric conductivity to vary by almost an order of magnitude. Mitchell et al. (1977, 1983 and 1985) has used

Gerdien condenser and blunt probe on a parachute to obtain polar conductivities, ion densities and ion mobilities from about 10 km to 80 km, during a solar eclipse and sunrise conditions. Mitchell et al. (1985) describes a measurement on the previous day of eclipse. Here a minimum is seen in the positive ion density profile at about 62 km.

Measurement of positive ion density reported by Conley (1974) discusses certain significant aspects of rocket-borne Gerdien condenser measurement. This is an experiment in which flow calibration of the Gerdien condenser was done in a wind tunnel where the flight environment could be simulated. Various other problems encountered in rocket-borne Gerdien condenser measurements are discussed in detail in this paper. The measurement by Farrokh (1975) is also of similar type as the last one. Aerodynamic instrument calibration has been discussed by Conley et al. (1983) also. In this paper they also discuss techniques for analysis of Gerdien condenser data. The experiment consisted of two rocket flights, one during eclipse and one after eclipse. Positive and negative ion concentration and mobility measurements were conducted in these flights. Possibility of multiply charged ions below about 60 km is also suggested in this paper. Rocket-borne Gerdien condenser measurement has been done by Takagi et al. (1980) also. Here two sensors were used for bipolar measurement of ion density and mobility. Both positive and negative ion mobilities from 60 to 90 km and

ion densities were obtained from this experiment.

All the experiments mentioned here were aimed at measuring conductivity, ion density and mobility in the upper atmosphere. The mobility information along with mass dispersion curve of Mitchell & Ridler, Kilpatric and Dotan (Meyerott, et al., 1980) may be used for obtaining the mass of the ion. To get a picture of the types of ions the cryo pumped quadrupole mass spectrometer measurements of Narcisi et al. (1970) is helpful. The report describes laboratory studies of cluster ions and results of 23 ionospheric measurements.

#### 1.7.3.2. Lower atmospheric measurements:

The first measurement of conductivity profile was made by Gerdien in 1905 (Israel, 1971). Later Gish and Sherman (Israel, 1971) measured conductivity up to about 22 km in which the conductivity showed a decrease with altitude above 18 km. Further in this measurement the ratio of  $\sigma_+$  to  $\sigma_-$  was found to be 0.78 throughout the altitude range. Woessner, et al. (1957) measured polar conductivities with two Gerdien condensers from 3 to 28 km. The Gerdien condensers were operated in relaxation mode. From a number of successful measurements he found  $\sigma_-$  to be greater than  $\sigma_+$ . Also considerable variation in polar conductivities were observed.

Another interesting set of measurements were made by Rossmann (Israel, 1971). He conducted the measurements with

the help of gliders. The 85 measurements made by him gave very good picture of the variation of conductivity in the troposphere and close to ground. The influence of meteorological parameters on conductivity is also seen in these measurements. The experiments conducted by Callahan, Sagalyn and Faucher (Israel, 1971) show clearly the change in conductivity profile within the exchange layer. Similar observations about the influence of exchange layer were made by Mani et al. (1962 & 1971), Anna Mani et al. (1965) and Srivastava et al. (1972). Also surface measurements by Kamra et al. (1982) showed very high values of negative space charge at night.

The balloon-borne Gerdien condenser conductivity and ion density measurement of Paltridge (1965) is an important one from the experimental point of view. This seems to be the first force-aspirated balloon-borne measurement. The sensor operated in the self aspiration mode during ascent and at float (30.5 km) air was drawn through the sensor with the help of a fan. Many of the problems encountered in Gerdien condenser balloon measurements, especially those due to flow are discussed in this paper. A similar instrument as that of Paltridge was used by Gras (1975) for stratospheric conductivity measurement.

Measurement of stratospheric conductivity using relaxation probe are many. Iversen et al. (1985), Byrne et al. (1988), Holzworth et al. (1986) and Holzworth (1991 a) are



some of them. Some controversy exists for the relation between  $\tau$ , the time constant measured and the atmospheric resistivity. Iversen et al. considers that the resistivity is equal to  $\tau/\epsilon_0$  ( $\epsilon_0$  is the dielectric constant), whereas Holzworth considers it to be equal to  $\tau/2\epsilon_0$  arguing that when charging takes place probes collect ions of one sign only (Iversen et al. 1985). Byrne et al., whose measurement covers three latitudes, suggests that the technique is useful only above 10 km. However, in the report on Atmospheric electrical measurements workshop at Wyoming, Rosen et al (1982) observed that the conductivity measured using the relaxation technique is half that measured by other techniques.

Another important work from the point of view of development of technique was done by the group from the University of Wyoming. This group has done conductivity, ion density and mobility measurement using self aspirated and force aspirated Gerdien condensers (Rosen et al. 1981, 1982, 1983 and Morita 1981). Forced aspiration was accomplished with a lobe pump. Comparison of the self aspirated and force aspirated measurements shows the remarkable advantage of the latter. In the workshop mentioned above, ionisation measurements were done by Rosen et al. and Morita. The former used a thin film, ambient pressure chamber and the latter used a sealed thin walled Aluminium chamber. The results were found to compare well with each other.

Regarding temporal variation of stratospheric

conductivity the contribution by Holzworth et al. (1986 & 1991 a) is significant. From the former measurement, the polar conductivities were found to vary independently and almost by a factor of 2. The profile of the temporal variation was found to be different from that of the DC electric field. The measurement was done during disturbed weather and it was found that in 7 out of 9 thunderstorms the conductivity of atmosphere over thunder storm increased. In the latter measurement the conductivity was found to vary with time at all altitudes between 11 and 28 km. Another observation in this paper is the reduction in conductivity by 20 % (for an ascent rate of 8 km/hr) when the measurement is done in the wake of the rising balloon, irrespective of the technique of measurement. Therefore it is suggested that the measured conductivity value be increased by 25% . The measurements by Hua Hu et al. (1989) also shows variation in conductivity over thunder storms.

Ion composition measurements were done by Arijs et al. (1983) and obtained positive ion measurements between 20 and 33 km only.

In India, apart from the early workers, simultaneous measurement of vertical electric field and current were done by Udare et al. (1991) from 17 to 32 km using the antenna technique. Results from two flights conducted in different seasons showed nearly coincident field profile. However, the deduced conductivity showed considerable difference.

Conductivity measurements were done by Beig et al. (1988 & 1989) using spherical probe. They obtained conductivity measurements from 20 to 34 km. Gupta et al. (1987) used relaxation technique in their measurements. Garg, et al. (1989) modified the Langmuir probe for stratospheric measurements and obtained negative polar conductivity from about 8 km to 34 km.

A review by Goldberg (1984) of the developments in the field of Atmospheric electrodynamics points to some of the interesting findings in the field. In the light of reports about the existence of large  $V_m^{-1}$  order fields in the upper stratosphere and mesosphere, he suggests that investigation about the origin and the effect of such fields on the electric circuit should be done. Such investigations on middle atmosphere electrodynamics may throw light into the coupling process. Similarly, Holzworth (1991,b) discusses the studies in Atmospheric electrodynamics in the US between 1987 and 1990. He supports the view of Goldberg et al.(1987) and many others about the point that conductivity is the key to determining the extent of electrodynamic coupling between ionosphere and lower layers of atmosphere. Therefore Holzworth is of the opinion that every new measurement of conductivity profile during the period of review has added something new to the investigation of electrodynamics.

Before concluding this section, model studies also are to be mentioned. The models are useful not only for other

model studies but also for designing experiments and evaluating experimental results. The model by Deshpande, et al.<sup>(1985)</sup> gives the middle atmospheric ion production rate over India from 5 km to 110 km. Ion production rate for different constituents, for cosmic rays and total ion production rates are given in this model. Production rates given in the model cover solar zenith angles from 0 to 90 degrees for different solar activity conditions including flare conditions. Prasad, et al.(1982) gives the IRI models of electron densities between 60 and 100 km, for eight stations over the Indian subcontinent. Jayati Datta et al.<sup>(1984)</sup> in their model on cosmic ray ion production rate discusses about the lack of consistent experimental data for comparison. Ion production rate for low latitudes between 10 to 100 km are given in this model.

#### 1.8. PRESENT WORK:

Four balloon experiments and four rocket experiments were conducted during the present work for the measurement of ion density, mobility and conductivity. The Gerdien condenser sensor was used for the measurement. All the experiments were integrated experiments, i.e. atleast two payloads were flown in all flights. This has imposed certain constraints for rocket-borne Gerdien condenser measurements. In all rocket experiments the other payload flown with the Gerdien condenser was an optical payload, which required a stable and predicted trajectory. Removal of nose cone or tip required for exposing

the Gerdien condenser could not be done before 45 to 50km altitude because of the apprehension of misbehaviour of the rocket. Therefore rocket measurements could be done only above about 50 km.

#### 1.8.1. TECHNIQUE:

As mentioned earlier Gerdien condenser is a sensor which can measure all the three parameters simultaneously. Also it can be used for ion measurements from ground to D-region. Therefore the Gerdien condenser was used in the present work for upper and lower atmospheric measurements.

---

## CHAPTER- 2

### TECHNIQUE OF MEASUREMENT

For the study described here, measurements of electrical conductivities, ion densities and ion mobilities have been carried out using the Gerdien condenser technique. In this chapter, the principle and theory of operation of this technique, the probable sources of uncertainties and the practical considerations for making measurements with this technique are discussed.

#### 2.1. PRINCIPLE :

The Gerdien condenser is a cylindrical capacitor consisting of two concentric cylinders. Named after H.Gerdien (1905), this instrument has been used for the measurement of electrical polar conductivity to start with and later extended for the measurement of ion density and ion mobility.

In the operation of the instrument, a potential difference is maintained between the cylinders and air is allowed to flow between them. Ions in the air stream are driven to and are collected at either cylinder depending on the sign of charge. Ions thus collected constitute a current.

This basic operation of the Gerdien condenser is shown in Figure 2.1. By varying this potential difference, it can be seen that the collector current increases with the potential difference, up to a certain value. Above this value, with further increase in potential difference, the collector current does not increase, but remains steady. Then the condenser is said to be saturated, that is all the ions entering the condenser get collected. In principle, therefore, the current - voltage characteristic of the condenser will be as shown in Figure 2.2. From this current - voltage characteristic, conductivity, ion density and ion mobility can be derived, as shall be seen here.

In a very commonly used configuration a voltage is applied to the outer electrode, with reference to the central electrode, and the current at the central electrode due to the collection of ions is measured. Then the inner electrode is called the collector and the outer one the driving electrode. It is possible to use the outer electrode as the collector and the inner one as the driving electrode also. Further, the same electrode may be used as the driving electrode and collector, in which case the other electrode is grounded.

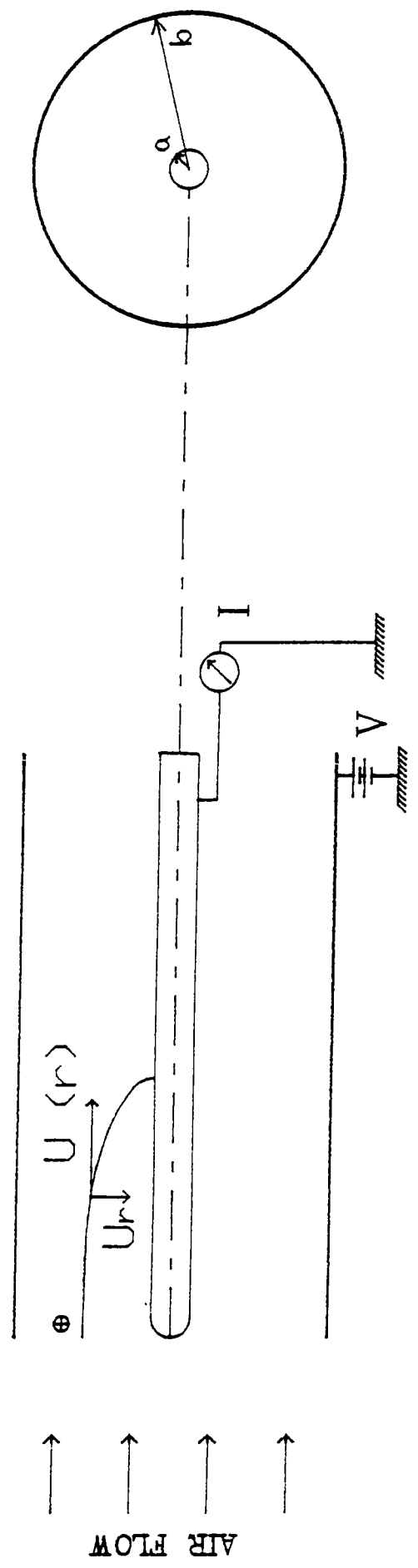


FIGURE 2.1. Cross sectional view of a Gerdien condenser (a cylindrical capacitor) in plan and elevation. Here the inner cylinder is used as the collector and the outer one as the driving electrode.



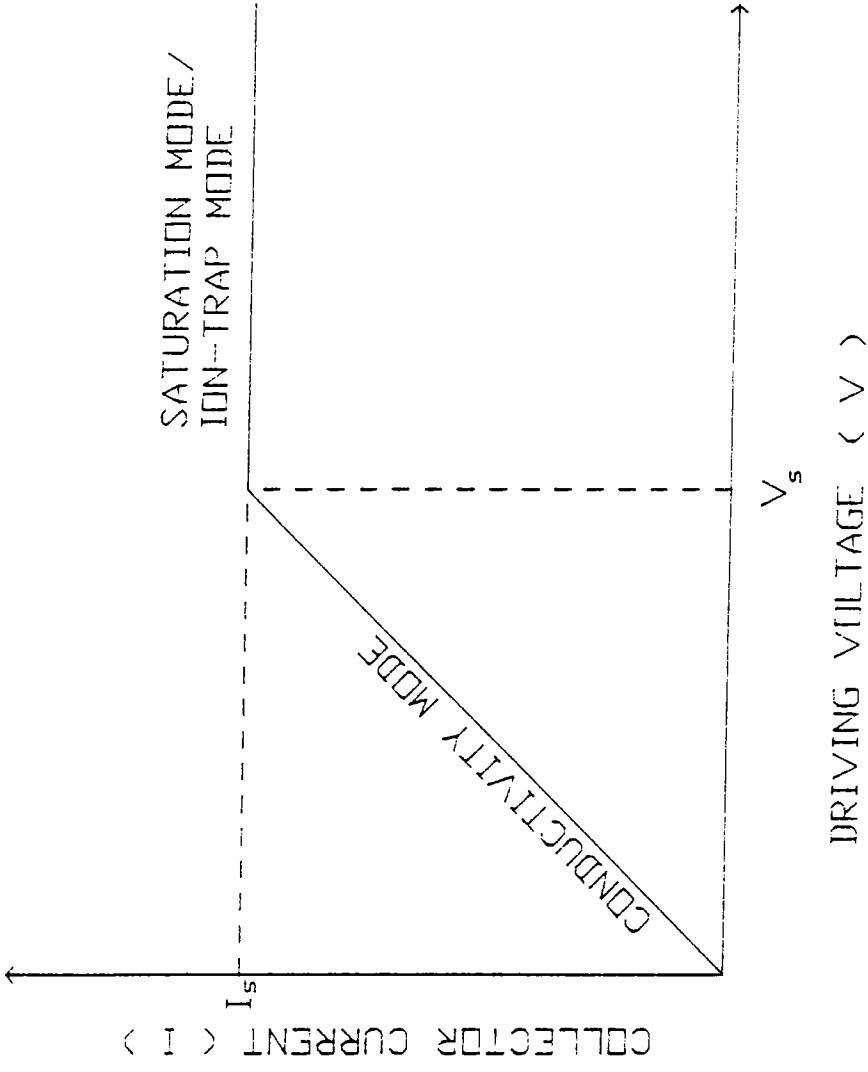


FIGURE 2.2. A typical current-voltage characteristic of a Gerdien condenser showing the different operational regions, such as the conductivity region and the ion-trap region.

## 2.2 THEORY OF OPERATION :

### 2.2.1. CURRENT COLLECTION :

Before saturation, apart from electric field, diffusion and convection also contribute to the collection of ions at the collector. Then the equation for current collection at a point is

$$J = n e U' + e D \nabla n + \mu n e \nabla \phi \quad (1)$$

where  $J$  is the current density,

$n$  and  $\mu$  are the number density and mobility of the type of ion considered,

$\phi$  is the electric potential,

$U'$  is the convection velocity,

$D$  is the coefficient of diffusion of ions considered,

and

$e$  is the elementary charge.

The three terms on the right hand side of eqn.(1) represent the contribution of convection, diffusion and conduction respectively to the collector current.

In the classical operation of the condenser, air flow inside the instrument is considered parallel to the axis of the collector and perpendicular to the drift of ions to the collector. Under this condition the convection term can be neglected.

Of the remaining terms the diffusion term can be

seen to be negligible compared to the convection term using Einstein's relation

$$\frac{D}{\mu} = \frac{k T}{e} \quad (2)$$

where  $T$  is the temperature and  $k$  is the Boltzmann's constant. The right hand side of the above expression is of the order of 0.01 volts so that for probe potentials much greater than this the diffusion term can be neglected.

Therefore eqn.(1) becomes

$$J = \mu n e \nabla \phi \quad (3)$$

In arriving at the above expression, it is assumed that the Gerdien condenser is operating in a collision-controlled regime. The collision-controlled regime occurs when the ratio of mean free path to the diameter of the outer electrode is equal to or greater than 0.01. Hoult (1965) and Sonin (1967) have shown that eqn.(3) is valid for a wide class of probes. The probes used for measurements reported here also come under this.

#### 2.2.2. EVALUATION OF $\nabla \phi$ :

Eqn.(3) is the general expression for current density. Here the potential gradient  $\nabla \phi$  has to be determined to obtain the collector current. To determine the potential

gradient, the effect of space charge has to be considered. Space charge forms if charged particles of one polarity are collected more quickly causing a distortion in the applied electric field. In order to estimate the magnitude of space charge that can affect the measurement, we make a simplifying assumption that one type of charge density remains constant throughout the chamber. Then the variation of the field inside the condenser can be estimated by solving Poisson's equation. Poisson's equation for Gerdien condenser for constant charge density ( $n^+$ ) can be written as

$$\frac{d^2\phi}{dr^2} + \frac{1}{r} \frac{d\phi}{dr} = \frac{-n^+ e}{\epsilon_0} \quad (4)$$

where  $r$  is the radial distance from the axis and  $\epsilon_0$  is the free space permittivity. The general solution of eqn.(4) for constant positive charge density is

$$\frac{d\phi}{dr} = \frac{-n^+ e r}{2\epsilon_0} + \frac{B}{r} \quad (5)$$

and 
$$\phi = \frac{-n^+ e r^2}{4\epsilon_0} + B \ln r + c \quad (6)$$

where  $B$  and  $c$  are constants of integration. By applying boundary condition that  $\phi = 0$  at  $r = a$ , the radius of inner electrode and that  $\phi = V$  at  $r = b$ , the radius of outer electrode  $B$  and  $c$  are evaluated.

$$B = \frac{V}{\ln(b/a)} + \frac{n^+ e}{4\epsilon_0} \frac{(b^2 - a^2)}{\ln(b/a)} \quad (7)$$

$$c = -B \ln a + \frac{n^+ e a^2}{4\epsilon_0} \quad (8)$$

Substituting in (5) and (6), we get

$$\frac{d\phi}{dr} = \frac{V}{r \ln(b/a)} - \frac{n^+ e}{2\epsilon_0} \left[ r - \frac{(b^2 - a^2)}{2r \ln(b/a)} \right] \quad (9)$$

and

$$\phi = \frac{V \ln(r/a)}{\ln(b/a)} + \frac{n^+ e}{4\epsilon_0} \left[ \frac{(b^2 - a^2) \ln(r/a)}{\ln(b/a)} \right] - (r^2 - a^2) \quad (10)$$

Similar relationships apply when the charge is negative.

In eqn.(9) the first term on the right hand side gives the distribution of electric field within the Gerdien condenser in the absence of any space charge. The second term gives the effects of space charge on the distribution. To evaluate this effect, the electric field distribution for different space charge densities, namely, 0,  $10^{10} \text{ m}^{-3}$ ,  $10^{11} \text{ m}^{-3}$  and  $10^{12} \text{ m}^{-3}$  have been calculated for a typical Gerdien condenser used here. The results are shown in Figure 2.3. It can be noticed that up to a concentration of  $10^{11} \text{ m}^{-3}$  the effect of space charge on electric field distribution is negligible. But charge densities of  $10^{12} \text{ m}^{-3}$  distort the field

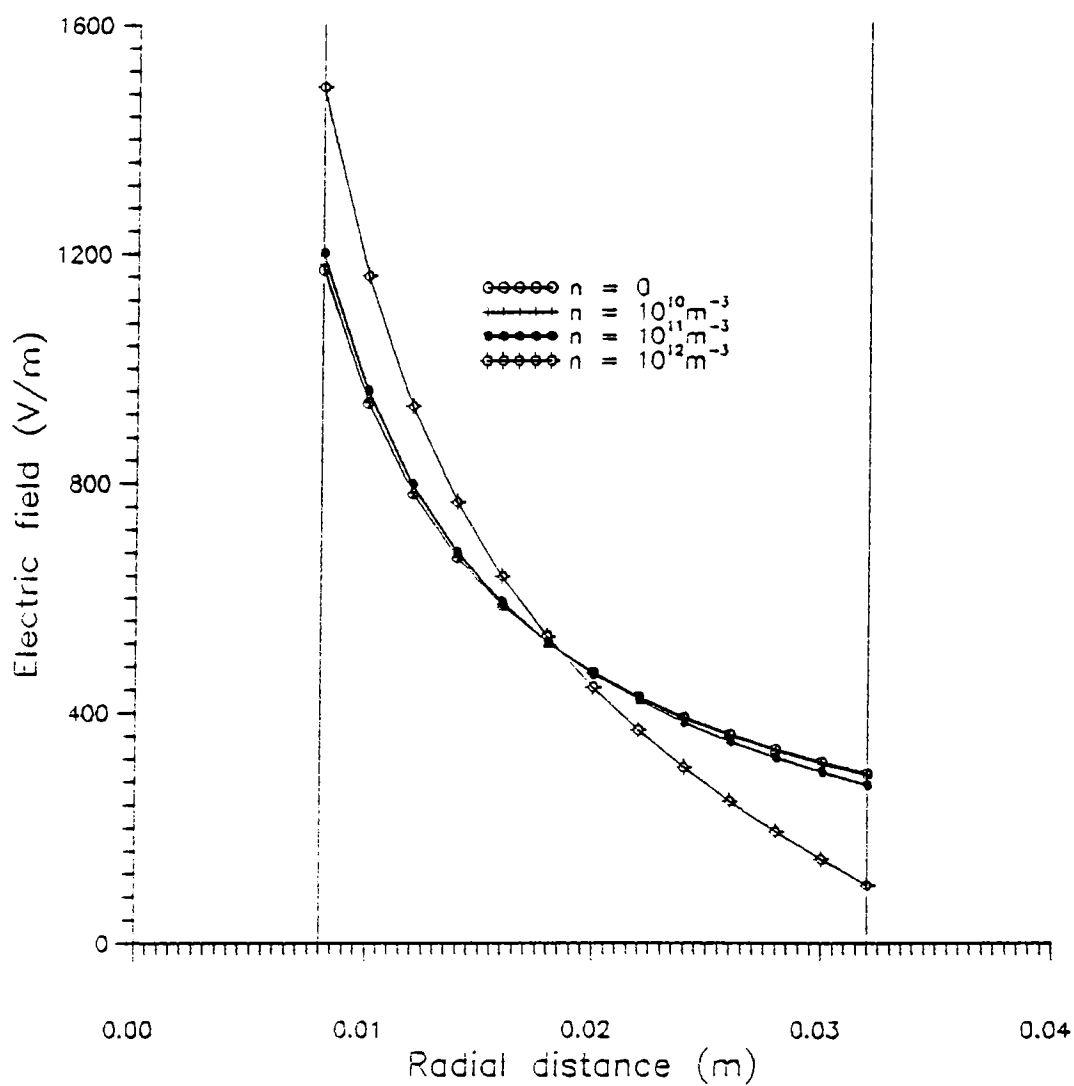


FIGURE 2.3. Variation of electric field in a typical Gerdien condenser for different charge densities. A voltage of 13 V is applied to the driving electrode of 0.032 m radius. The collector is of 0.008 m radius. It can be noted that charge densities upto  $10^{11} \text{ m}^{-3}$  do not affect the electric field distribution appreciably.

appreciably. This order of concentration is not normally found in the region under consideration here. Therefore for charge densities of  $10^{14} \text{ m}^{-3}$  or less we can neglect the field distortion due to space charge. The second term in eqn.(9) can then be omitted and the eqn.(9) reduces to,

$$\frac{d\phi}{dr} = \frac{V}{r \ln(b/a)} \quad (11)$$

Substituting for  $\nabla\phi$  in eqn. (3) (since the variation in  $\phi$  is only with  $r$ , due to cylindrical symmetry), we obtain for the current density at the collector:

$$J = \frac{\mu n e V}{r \ln(b/a)} \quad (12)$$

### 2.2.3. EXPRESSIONS FOR CONDUCTIVITY, ION DENSITY AND MOBILITY :

#### 2.2.3.1. Conductivity ( $\sigma$ ) :

The current for unit length of the probe is  $2\pi r J$  and the total current to the probe is

$$I = 2 \pi r J L$$

Substituting for  $J$  from eqn.(12)

$$\begin{aligned} I &= \frac{2 \pi r L \mu n e V}{r \ln(b/a)} \\ &= \frac{\mu n e V C}{\epsilon_0} \end{aligned} \quad (13)$$

where  $L$  is the length of the collector and

$$C = \frac{2\pi\epsilon_0 L}{\ln(b/a)}$$

is the capacitance of the cylindrical condenser. Now,

$$\sigma = n e \mu \quad (14)$$

is the conductivity of the medium. Therefore we can write

$$I = \frac{\sigma C V}{\epsilon_0} \quad (15)$$

or

$$\sigma = \frac{\epsilon_0}{C} \left[ \frac{I}{V} \right] \quad (16)$$

Eqn.(15) describes the current-voltage relationship of the Gerdien condenser. If there is only one type of charged species, eqn.(15) shows that the current is proportional to the driving voltage. This is depicted as conductivity mode in Figure 2.2. For a given condenser the above proportionality is valid for voltages that are low enough so that only part of the ions in the air are collected. When this condition is satisfied, knowing C and measuring collector current I for an applied voltage V or the slope of I-V characteristic the conductivity  $\sigma$  can be calculated from eqn.(16).

#### 2.2.3.2. Ion density (n):

If the applied voltage is sufficiently high, so that all the ions that enter the condenser are collected, a further increase in applied voltage does not result in an increase in collector current. The condenser is then said to be saturated and the corresponding collector current is known as saturation



current. The saturation mode of the Gerdien condenser is depicted in Figure 2.2. An expression for saturation current can be obtained as follows.

The quantity of air flowing through the condenser per unit time, i.e. the volume flow rate, is

$$Q = U A$$

where  $U$  is the speed of air flow and

$$A = \pi (b^2 - a^2)$$

is the area of cross section, of the condenser. Assuming all the ions to be singly charged, the saturation current

$$I_s = n e Q \quad (17)$$

$$= n e U A$$

$$= n e U \pi (b^2 - a^2) \quad (18)$$

and  $\therefore n = \frac{I_s}{e U \pi (b^2 - a^2)} \quad (19)$

Thus by knowing the speed of air flow and measuring  $I_s$ ,  $n$  can be calculated.

### 2.2.3.3. Ion mobility ( $\mu$ ):

Ion mobility can indirectly be obtained from eqn.(14) when  $n$  and  $\sigma$  are known. The mobility can directly be obtained by measuring the saturation voltage also. Saturation voltage is that voltage at which the collector current just saturates. An expression relating saturation voltage  $V_s$  and  $\mu$

can be derived as given below.

Consider an ion which enters the condenser at a point distant  $r$  away from the axis. It has a velocity  $U(r)$  in the direction parallel to the axis. It acquires a drift velocity  $U_r$  perpendicular to the axis, given by

$$U_r = -\mu \frac{d\phi}{dr}$$

Then in a short time interval  $dt$ , the ion travels a distance  $dr$  radially and distance  $dx$  axially. Then,

$$dt = \frac{dr}{U_r} = \frac{dx}{U(r)}$$

$$dx = \frac{dr U(r)}{U_r} = \frac{dr U(r)}{-\mu d\phi/dr}$$

Substituting  $d\phi/dr$  from eqn.(11) and integrating over  $r$  from  $r'$  to  $r$ , we obtain

$$l = \int_{r'}^r \frac{-U(r)}{\mu V} \ln(b/a) r dr$$

$$= \frac{\ln(b/a)}{\mu V} \int_r^{r'} U(r) r dr$$

Here  $l$  is the distance through which the ion moves axially while it travels radially from  $r'$  to  $r$ . Now consider a particle entering the condenser at a point close to the driving electrode. The axial distance it will travel by the time it gets absorbed is

$$L = \frac{\ln(b/a)}{\mu V} \int_a^b U(r) r dr$$

In other words if this ion is to be collected then for a driving voltage  $V$ , the length of the condenser should at least be  $L$ . Now if it is assumed that the speed of air flow

is constant across the radius of the condenser then the above integral is equal to  $1/2\pi$  times the volume flow rate. Thus we obtain

$$L = \frac{\ln(b/a) U (b^2 - a^2)}{2 \mu V} \quad (20)$$

Thus for a condenser of dimensions  $a$ ,  $b$  and  $L$  the saturation voltage is given by

$$V_s = \frac{U (b^2 - a^2) \ln(b/a)}{2 L \mu} \quad (21)$$

and therefore mobility,

$$\mu = \frac{U (b^2 - a^2) \ln(b/a)}{2 L V_s} \quad (22)$$

Ion mobility can be calculated from the above expression if the saturation voltage is measured.

Therefore to measure  $n$ ,  $\mu$  and  $\sigma$  together the current-voltage characteristic of the probe is obtained. The various regimes of the probe are indicated in the typical I-V characteristic of a Gerdien condenser in Figure 2.2.

The current-voltage characteristic will be same if the outer cylinder is used as the collector. The condenser operates in a similar manner if the electric field is reversed and negative particles are collected. The saturation current  $I_s$  will then be proportional to  $U(n_0 + n)$ , where  $n_0$  is the electron density.

### 2.3. SOURCES OF ERROR :

The theoretical expressions derived above assume an

ideal state. In actual use several deviations from the ideal state are likely to occur. They have to be considered for effective use of the instrument.

### 2.3.1.ELECTRICAL CONSIDERATIONS :

#### 2.3.1.1.Edge effect:

The electric field inside the Gerdien condenser is assumed to be independent of axial distance, as given by eqn.(11). This is true only for an infinitely long condenser. For a condenser of finite length, the electric field distribution gets modified at the ends. This is called the edge effect. At the ends of the condenser, some field lines originating at the outer surface of the driving electrode terminate at the collector. Because of this, some ions which are not present in the volume of air being sampled are also pulled in. This tends to increase the effective area of cross section for ion collection. When a third cylinder of same length as the driving electrode is used as shield, over the driving electrode, the problem of increase in effective area is eliminated. However, even after this, at the ends of the condenser all electric field lines originating at the driving electrode do not end at the collector. Some of the field lines curve outward and terminate at some point outside the condenser. Because of this, the effective area of the condenser, for ion collection, becomes smaller since some

ions are diverted and deposited on the outer shell escaping measurement. It has been shown by Schmeer et al. (1962) that for driving voltages much higher than saturation voltage the current decreases as a result of edge effect. Thus, reduction of edge effect is important.

Also, the ambient mobility varies with ambient density as

$$\mu_a = \frac{\rho_o \mu_o}{\rho_a} \quad (23)$$

where  $\mu_a$  = ambient mobility

$\mu_o$  = mobility at S.T.P

$\rho_o$  = density at S.T.P and

$\rho_a$  = ambient density.

Therefore, the mobility of ions is low at low altitudes and hence relatively large stray fields are necessary to influence the ions. Therefore the edge effect is not so pronounced at low altitudes. At higher altitudes mobility increases and smaller stray fields are sufficient to divert the ions. Therefore it becomes necessary to reduce the edge effect especially for both balloon and rocket-borne measurements.

In order to reduce edge effect Jespersen et al. (1964) suggested the use of grounded wire meshes at both ends of the condenser. However Rose and Widdel (1972) reported that the use of a wire mesh of 95% transparency could reduce ion collection by up to 50%. They instead suggested the use of grounded guard rings at both ends. Most of the

later experimenters have used this system in their instruments. The Gerdien condenser used here had both the shield and guard rings to reduce the edge effect. Qualitative sketches showing edge effect without and with guard rings are shown in Figure 2.4. a & b.

### 2.3.1.2. Electric field :

Another factor to be considered is the effect of electric field intensity on the behaviour of ions. When ions in the air are influenced by an electric field, they gain energy from the field between collisions with molecules of air and are accelerated in the direction of field. The energy gained thus is given by  $eE\lambda$ , where  $E$  is the intensity of electric field and  $\lambda$  is the ion-neutral mean free path. When this energy is much less than the thermal energy of air molecules, which is given by  $kT$ , then it is considered to be a low field case. When  $eE\lambda \gg kT$  it is said to be a high field case. The above inequalities can be rewritten in terms of electric field and pressure as

for the low field case,

$$E / p \ll 250 \text{ V m}^{-1} (\text{mm of Hg})^{-1}$$

and for the high field case

$$E / p \gg 250 \text{ V m}^{-1} (\text{mm of Hg})^{-1}$$

where  $p$  is the pressure. In a low field situation the mobility of the ion is known to be independent of the field  $E$ . This situation may continue well into the region of the high field case. The exact point at which the mobility begins to

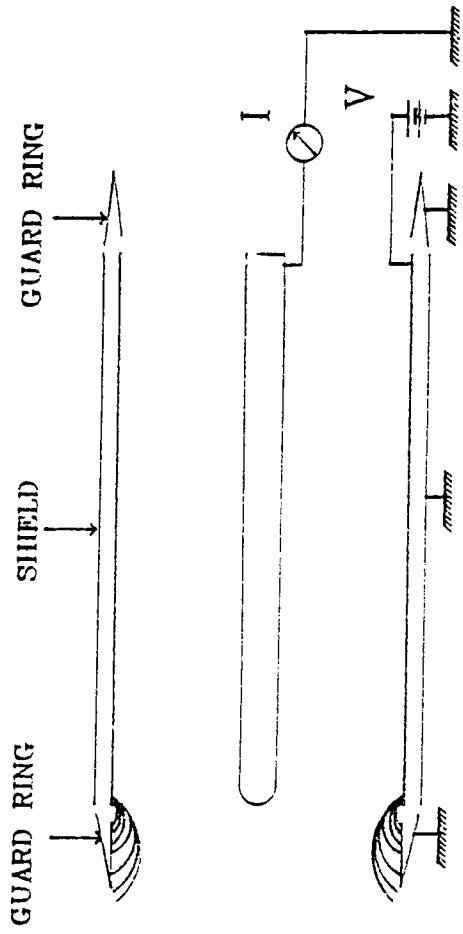


FIGURE 2.4(a). The fringing of field lines at the inlet of the condenser. This is called edge effect.

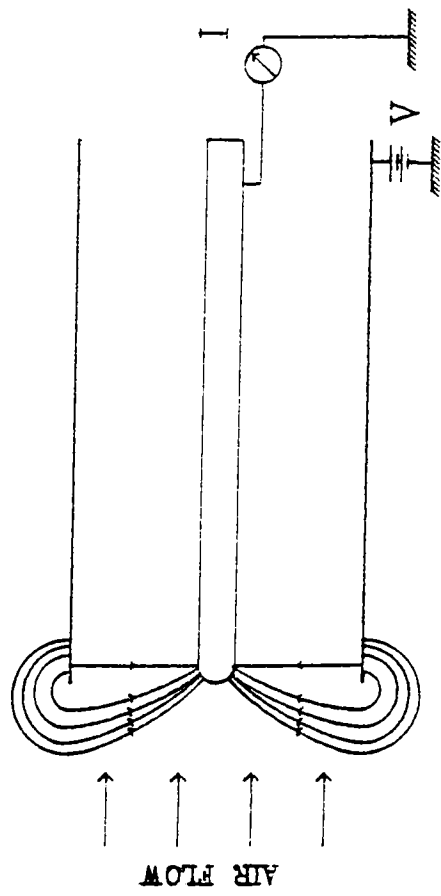


FIGURE 2.4(b). Incorporation of the shield and guard rings is, shown. This reduces edge effect.

be dependent on the magnitude of the field depends on the type of ions and the kind of gases, and apparently is dictated by the strength of the forces acting between the molecules and the ions. At still higher  $E/p$  values the mobility becomes proportional to  $E^{1/2}$ .

Figures 2.5 a & 2.5 b show the  $E/p$  variation of Gerdien condensers used in balloon and rocket experiments respectively. In the case of balloon-borne sensors it can be seen that the  $E/p$  value is not exceeded for all sensors at 1 V and peak applied voltages, in the region of measurement. Therefore, in the case of balloon experiments, the applied electric field is in the low field regime and so the mobility measurement in all experiments can be considered to be independent of the electric field strength.

In the case of rocket measurements, it can be seen that  $E/p$  value exceeds  $250 \text{ Vm}^{-1}$  per mm of Hg, for an applied potential of 1 V at about 55 km; and for an applied voltage of 13V in the complete region of measurement. In all the experiments a linear sweep voltage was used as the driving potential. The sweeping voltage changes the  $E/p$  from low field to high field in the rocket experiments. Here the change from low field to high field is not important, but the important consideration is whether the mobility is constant over the range of applied electric field. A linear current-voltage curve is indicative of constant mobility. Figure 2.6 shows the driving voltage and collector current



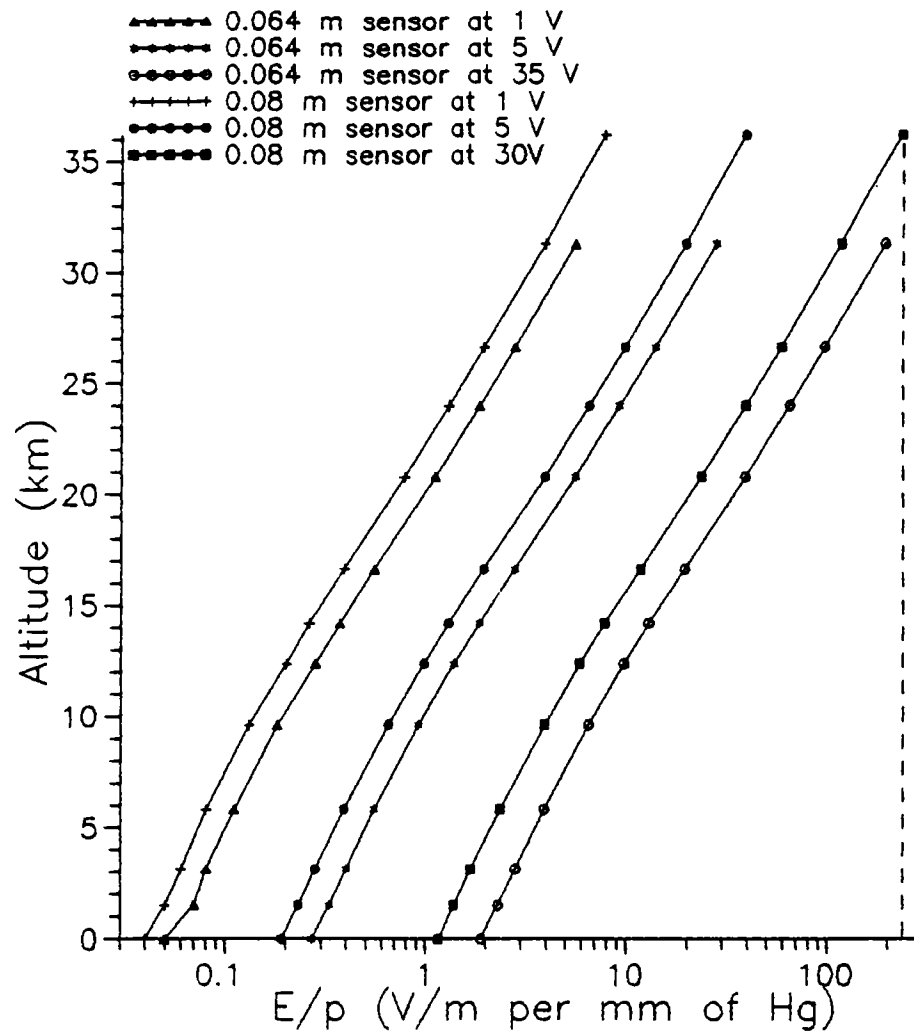


FIGURE 2.5 a. Variation of  $E/p$  with altitude in balloon-borne condensers, shown for the different peak voltages. It can be seen that the value of  $E/p$  does not exceed the limit of  $250 \text{ Vm}^{-1}$  per mm of Hg.

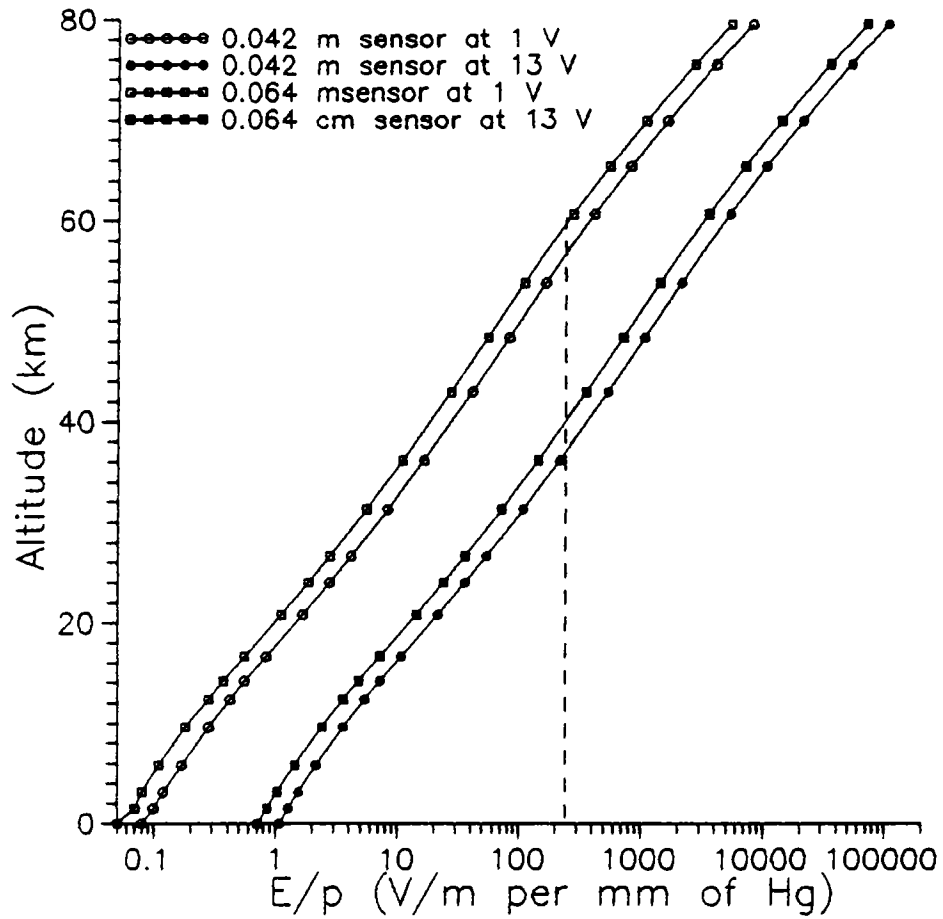


FIGURE 2.5.b Variation of  $E/p$  with altitude for the rocket sensors. The value exceeds  $250 \text{ Vm}^{-1}$  per mm of Hg in the entire range measurement.

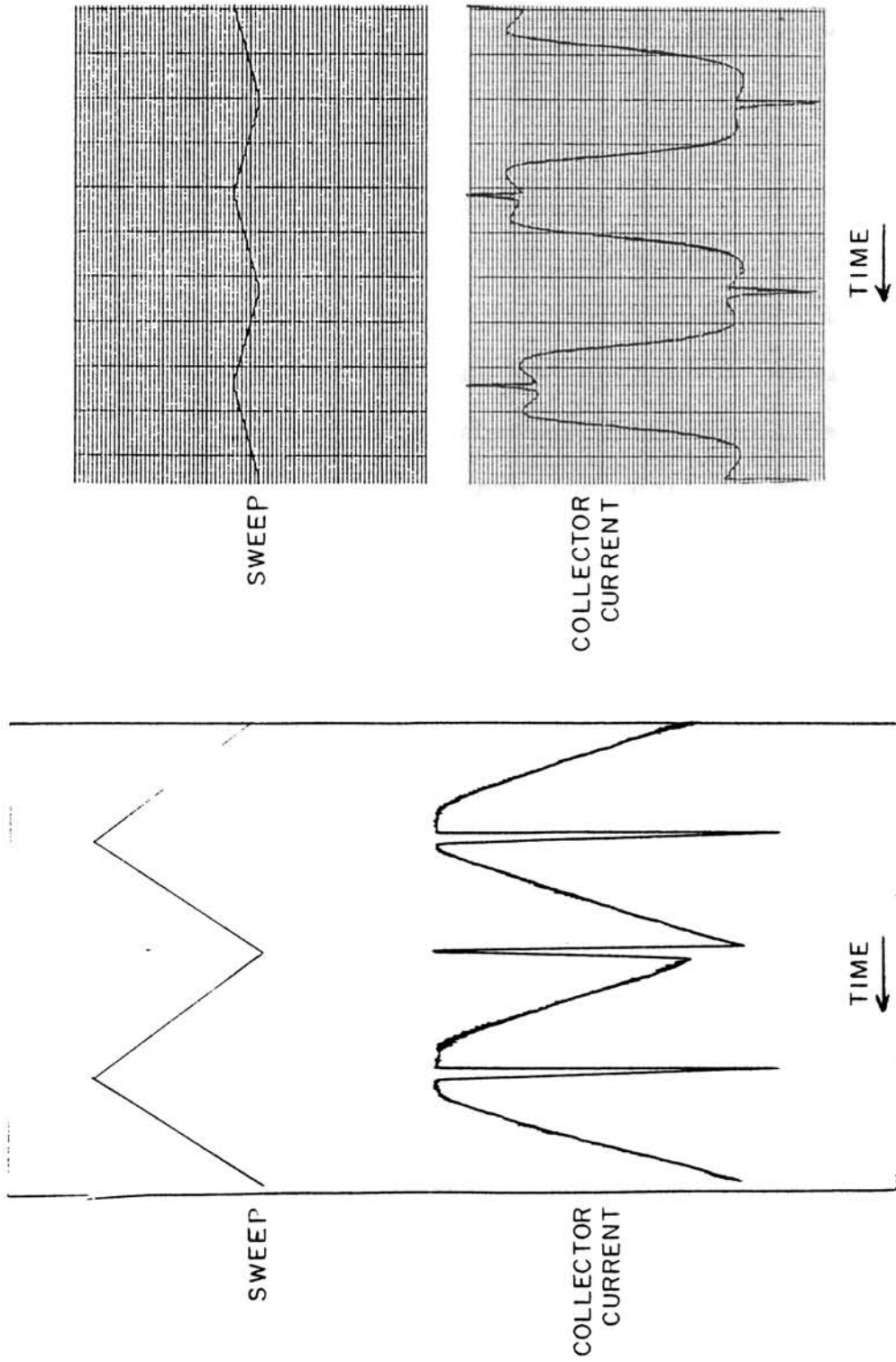


FIGURE 2.6 Reproduced data samples from rocket and balloon experiments. The spikes seen in the amplifier outputs are due to change of slope of driving voltage. Rocket data sample (left) is for unipolar measurement and balloon data sample (right) is for bipolar measurement.

wave forms obtained from rocket and balloon experiments. It can be seen that the current varies linearly with the driving voltage.

#### 2.3.1.3. Photo electron production :

A third factor to be considered is the effect of photo electrons produced by solar ultra violet radiation. Most of the radiation that is energetic enough to generate photo electrons are absorbed by the atmosphere above about 60km altitude. Hence this is not a serious problem in balloon-borne measurements which rarely go above 35 to 40km. However it becomes important in rocket experiments which go above 60km. If photo electrons are produced from the driving electrode or the collector, they can add to the collector current when the driving electrode becomes negative. One of the ways to prevent this is to ensure that the solar ultraviolet radiation does not directly fall on any part inside the sensor. Coating the electrodes with a material having high ionisation energy is also helpful.

#### 2.3.2. FLOW CONSIDERATIONS :

In the classical theory of the Gerdien condenser, the flow is assumed to be laminar, which means the Reynolds' number should be less than a critical value. For two very long axial cylinders this value is 2000, but the exact figure for a given condenser will have to be determined

experimentally. Since the situation is different in rocket-borne and balloon-borne condensers, we shall discuss them separately.

The influence of flow profile on measurements using balloon-borne condensers was investigated in detail by Paltridge(1965). He found that available theories dealt with fully developed flow, i.e. when the pipe is sufficiently long for the flow to develop fully its characteristics. In the case of a Gerdien condenser, the pipe is short and the type of flow corresponds roughly to that at the inlet region of a long pipe. The theory here becomes very complicated. From wind tunnel investigations of short tubes, it has been seen that two general patterns can be identified depending on the Reynolds' number. At Reynolds' numbers of 8000 and above, the velocity profile remains constant across both inlet and outlet of the tube. A turbulent layer starts to develop but does not have enough time to grow to any considerable distance away from the wall. The flow pattern is almost unaltered by the presence of the tube. For Reynolds' numbers less than 8000, the boundary layer remains laminar, but at the exit it extends to a considerable distance away from the wall. At very low Reynolds' numbers, the velocity profile at the exit assumes parabolic shape characteristic of fully developed laminar flow. Viscous energy losses are high and the actual flow rate will be heavily dependent on the Reynolds' number and the length of the tube.

For a typical balloon-borne instrument, the Reynolds' number varies considerably, from very high values near ground to very low values at float altitude. Paltridge calibrated his instrument for the range of Reynolds' numbers encountered by his instrument. He found that the flow rate remained more or less constant up to an altitude of about 12km, but began to reduce thereafter reaching about 50% of the expected value at around 25km altitude. Even below 12km the flow rate was about 10% less than expected. He also showed that conductivity measurements, which normally do not depend on the flow rate, are affected if the velocity profile across the condenser alters from one point to another. In his instrument he found the effect to be pronounced around 20km.

Rosen and Hofmann (1981) suspected that even with the correction for Reynolds' number the results did not give a true picture of the ion density and mobility profiles. They therefore used a pump to draw air through the condenser. They found that unexpected fluctuations in the ion density profile and a decrease in reduced mobility with altitude, seen when self aspirated condensers are used, disappeared when the pump is used.

Of the four balloon experiments described here, two were conducted with self-aspirated sensors and the other two with force-aspirated ones. Figure 2.7 shows the variation with altitude of Reynolds' number for the balloon-borne self-aspirated sensors, for maximum and minimum velocities

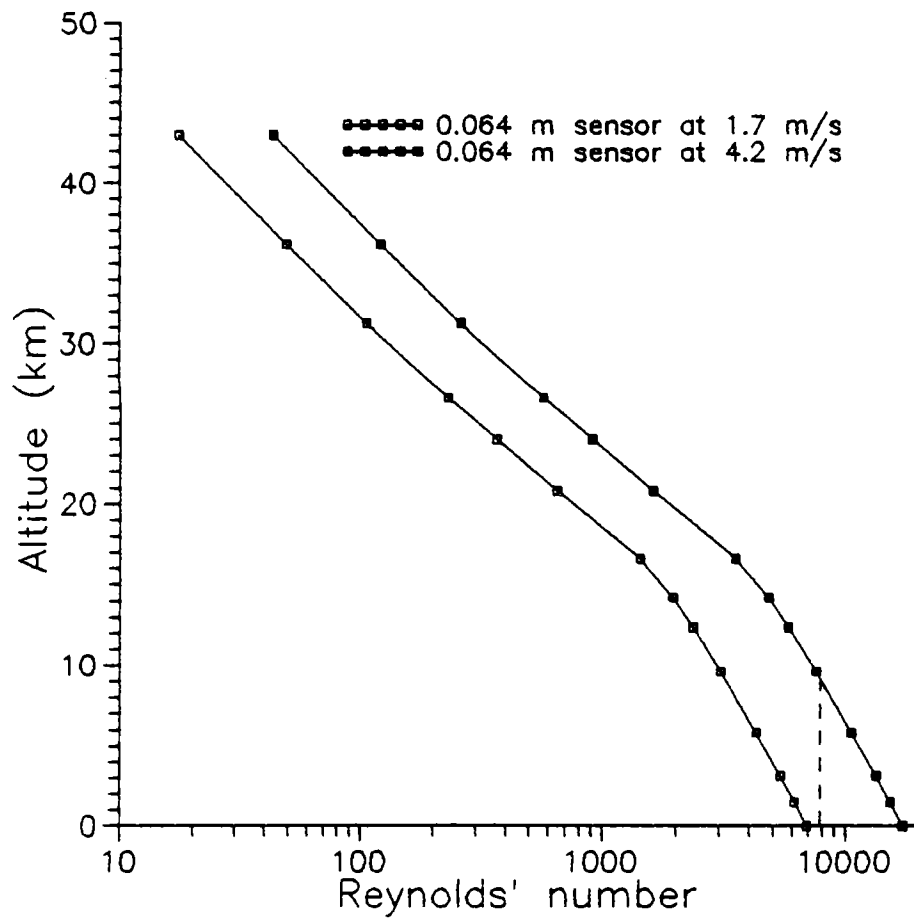


FIGURE 2.7. Variation of Reynolds' number with altitude for the self aspirated balloon-borne sensors. The Reynolds' number is less than the critical value above 8 km.

encountered during flight. It is seen from the figure that for self-aspirated sensors, above about 9km, the Reynolds' number is less than 8000 for the highest ascent rate. In both self aspirated measurements the data could be obtained only above about 10km altitude.

In the case of rocket-borne condenser where the instrument is mounted on the rocket itself the problem is that of supersonic flow. All sounding rockets have supersonic velocities in the region of measurement, which is normally above 40 to 50km. At these velocities, a shock wave is formed at the front end. Now the dynamics of the system is governed by the following expression:

$$\frac{dU}{U} (1-M^2) = - \frac{dA}{A}$$

where  $A$  is the area of inlet of the cylinder and  $M$  is the Mach number. For subsonic flow,  $M < 1$  and  $U$  decreases when  $A$  increases. But when the flow is supersonic  $M > 1$  and  $U$  decreases with decrease in  $A$ . If  $M$  approaches unity at any time during the flow, then a phenomenon called choking takes place. Thus the actual rate of flow depends to a great extent on the type of flow present. A theoretical computation is possible when the inner electrode has a negligible boundary region. However this may not be true at all attitudes. Thus only an experimental calibration can be done on the instrument. Conley (1974) carried out such a calibration of



his instrument using a wind tunnel where the conditions in the altitude region from 40 to 85 km could be simulated. He found that the flow rate does decrease with altitude beyond a certain height which is dependent on the Mach number. The mass flow efficiency, defined as the ratio of actual flow rate to the flow rate expected from geometry, remained at unity up to an altitude of 71 km at Mach 3 and up to 56 km at Mach 2. Beyond this it decreased uniformly with altitude to values as low as about 0.3 at 85 km. Flow rate calibration thus is important in rocket-borne measurements. However it is difficult to obtain facilities for doing this calibration since a supersonic wind tunnel with environmental control facility is needed.

#### 2.4. OPERATION:

##### 2.4.1. AIR FLOW:

As mentioned in section 2.1, air flow through the Gerdien condenser is needed when it is in operation. Air flow through the sensor is accomplished either by self aspiration or by forced aspiration. In self aspiration the air flow is achieved by moving the sensor, as in the case of rocket-borne or balloon-borne Gerdien condenser. In forced aspiration a fan or pump is used to draw air through the condenser.

In rocket-borne measurements supersonic velocities and very low pressures are encountered. In the case of high altitude parachute measurements also the condenser operates in

very low atmospheric pressures. In such cases self aspiration is employed for generating air flow. In balloon-borne measurements also self aspiration may be employed. There are some problems encountered in balloon-borne self aspirated measurements which are discussed in a later section dealing with the balloon measurements. An air pump which can operate down to a few millibars of atmospheric pressure can be used for forced aspirated operation of the Gerdien condenser on balloons. Forced aspiration can significantly improve the quality of data, as observed by Rosen and Hofmann (1981). The present work confirms this. For ground based measurements any pump or fan may be used to generate air flow; the capacity of the pump or fan being decided by the sensitivity of the current amplifier used for measuring collector current.

#### 2.4.2. DRIVING VOLTAGE:

The I-V characteristic in Figure 2.2. shows the conductivity and ion-trap (saturation) modes of operation of a Gerdien condenser. It can be seen from the figure that, by proper selection of driving voltage, the Gerdien condenser may be operated in any one of the modes. When the applied voltage is less than the saturation voltage, the condenser operates in the conductivity mode and the current-voltage relationship is governed by eqn.(15). It may be noted here that the collector current is then independent of the air flow rate. In other words, when the velocity of air flow increases, even though

more ions enter the condenser, the same number of ions only get collected, since the driving voltage remains unchanged. Similarly for a reduction in the quantity of air flow even though the total number of ions entering the condenser reduces, because of the reduction in velocity same number of ions get collected. In practice, for conductivity mode of operation the driving voltage is kept well below  $V_s$  so that even a large reduction in air flow speed will not cause the operating point to shift into ion-trap mode.

In ion-trap mode of operation, as suggested by the name itself, all ions entering the condenser get collected. This happens when the applied voltage is greater than the saturation voltage. Ion concentration measurements are made by operating the condenser in the ion-trap mode. Here also, proper selection of driving voltage is important. At high altitudes, where ion mobility is large, driving voltages far in excess of  $V_s$  can lead to large errors in ion concentration measurements due to the effect of fringing fields. Further, a very high voltage can also cause voltage breakdown at high altitudes. Therefore when ion density profiles are measured using a constant driving voltage, the voltage is switched to a lower value at higher altitudes.

Simultaneous measurement of conductivity, ion density and mobility is made by applying a time varying voltage to the driving electrode. This also offers the advantage of obtaining the characteristic of the Gerdien

condenser for each sample of measurement so that errors due to noise and amplifier drift are minimized. A triangular sweep varying from zero to a value greater than  $V_s$  is well suited for this purpose since the voltage varies linearly with time. However, a varying driving voltage generates a displacement current in the condenser, which is proportional to the rate of change of voltage. This gets added to the measured collector current, and hence has to be compensated for. When a triangular sweep is used as the driving voltage, the displacement current appears as a square wave at the output of the current measurement circuit. This has to be eliminated from the output. When the square wave is eliminated by a suitable technique, the I-V characteristic is obtained, as shown in Figure 2.6. As mentioned earlier, to calculate conductivity, the slope of the output is taken rather than a spot value so that error due to noise is minimized. By estimating  $V_s$ , the ion mobility and from the saturation current the ion density are also calculated.

## 2.5. THE SENSOR ; PRACTICAL CONSIDERATIONS:

### 2.5.1. ASSEMBLY:

Sectional view of a typical Gerdien condenser is shown in Figure 2.8. The outermost cylinder is the shield. The driving electrode slips into this shield and is insulated from it by hylam rings. Both ends of the shield are threaded and two threaded, bevelled end rings fit at the ends. These

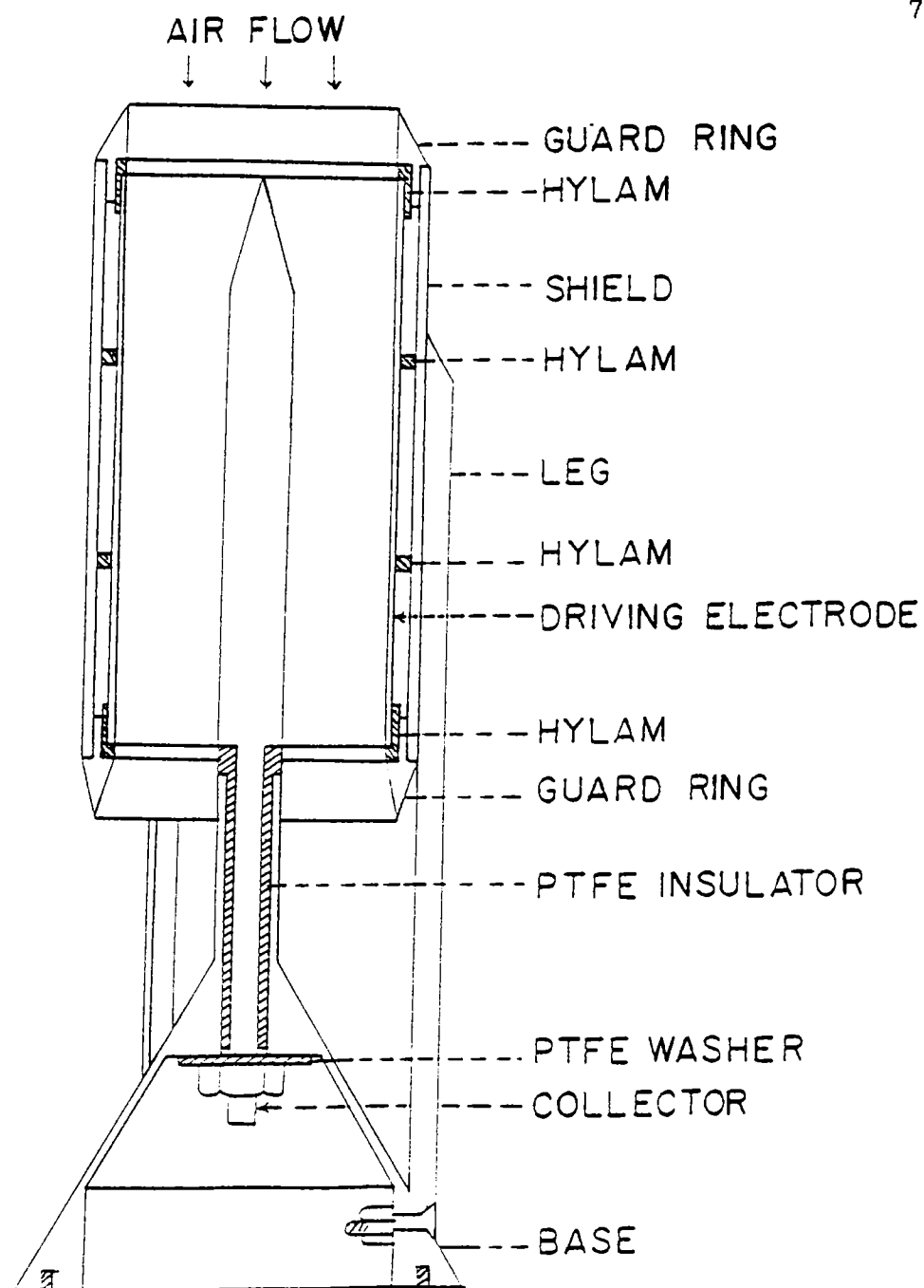


FIGURE 2.8. A TYPICAL GERDIEN CONDENSER FOR ROCKET-BORNE MEASUREMENTS. THE DETAILS OF THE DIFFERENT FIXTURES ARE SHOWN CLEARLY.

end rings are tightened to secure the driving electrode in position. Two hylam rings at both ends of the driving electrode insulate it from the end rings. Electrical connection to the driving electrode is accomplished through a 10 mm port on the shield. The assembly is supported by three legs and the legs are fastened to the base. A tube extending from the base supports the collector. The stepped lower portion of the collector slips through the tube and is insulated from it by a P.T.F.E.(Teflon) sheath of 2 mm thickness. The lower end of the collector rod is threaded and it is fastened to the base with a nut and a P.T.F.E. washer. The base is hollow and electrical connection to the collector is made at the lower end of the collector rod. The end rings, shield, legs and the base are electrically grounded through the rocket body or the gondola which ever is the case. The base and the tip of the collector are suitably shaped to facilitate free air flow.

#### 2.5.2. MATERIAL:

The shield, the end rings and the base are made of Aluminium and the legs are made of mild steel. The electrodes are made of brass and electroplated with Nickel. Aluminium is used because it is light in weight, is easy for fabrication and it does not require a protective coating for normal use. Aluminium always has an oxide coating over the surface. Because of the oxide coating Aluminium cannot be used for the

electrodes since they cause a level shift in the output due to contact resistance between air and the electrode (Widdel et. al. 1976). Brass electrodes, electroplated with Nickel provides a polished corrosion free surface. Legs are made of mild steel so that they can withstand the severe shock and vibration that the pay load will be subjected to during launch and powered flight.

Two types of material have been used for insulation in the sensor of which hylam is a relatively poor quality insulator. Insulation of this quality is sufficient for the driving electrode since it is usually driven by a low impedance source and so leakages of the order of even a fraction of a milliampere can be tolerated. Virgin P.T.F.E. is a high quality insulator and it is essential that the collector is insulated by such a material, since leakages of the order of even  $10^{-14}$  ampere cannot be tolerated. P.T.F.E. also has the advantage that its surface can be polished and cleaned to minimize surface leakage. There is one disadvantage with P.T.F.E. which becomes important in a vibration environment. In a vibration environment, P.T.F.E. causes the production of what is known as triboelectric noise (Harris and Crede, 1976). The amplitude of the noise can sometimes be as high as the signal itself. In the Gerdien condensers used in the experiments described here, collector rods are insulated from their supports by means of P.T.F.E.tubes(sheaths). Production of noise in these Gerdien

condensers is the result of the separation of triboelectric charges when the P.T.F.E. tube momentarily loses contact at some point with the collector. When this happens, one polarity of charges are left on the surface of P.T.F.E., where they are trapped by the low conductivity of the P.T.F.E. surface. The excess opposite charges left on the collector are neutralized by a transfer of charges between the collector and ground through the terminating impedance. The transfer produces a pulse at the input of the first amplifier. On reestablishment of collector-P.T.F.E. contact the excess charge on the surface of P.T.F.E. is again neutralized by charge redistribution, resulting in a pulse of opposite polarity at the amplifier.

The triboelectric noise can be reduced to negligible levels by increasing the surface conduction of the P.T.F.E. tube. Graphite coated tubes may be used for this purpose. If such tubes are not readily available the graphite coating has to be done manually. Care has to be taken to see that the ends of the sheath are free of graphite powder. The graphite layer thus formed, being conductive, prevents charges from getting trapped, thereby reducing noise.

Triboelectric noise is also produced by P.T.F.E. co-axial cables when they are used to link the sensor to the electrometer amplifier. Here again the solution is either to use a graphite coated co-axial cable or coat graphite on a cable. This can be done by carefully removing the sheath of



the cable, applying a graphite-alcohol colloid over the braided shield and then putting back the sheath. It is possible to do such a coating on RG-178 cables of small length, of up to 2 meters which are used in the experiments.

Triboelectric noise has not been a problem in the rocket experiments since in all experiments the sensors were exposed long after the motor burn-out. In balloon experiments precautions were taken to eliminate the triboelectric noise in the manner described above.

#### 2.6. SUMMARY:

As has been seen, the Gerdien condenser technique can be used to measure the conductivities alone, the ion densities alone or the conductivities, ion densities and ion mobilities simultaneously by a proper choice of the driving voltage. In the experiments described here, simultaneous measurements of  $\sigma$ ,  $n$  and  $\mu$  of both positive and negative ions were done.

---

## CHAPTER - 3

### UPPER ATMOSPHERIC MEASUREMENTS

This chapter deals with upper atmospheric measurements. The measurements were conducted using rockets flown from Thumba Equatorial Rocket Launching Station (TERLS), Thiruvananthapuram, India (Geog. Lat:  $8.54^{\circ}$ , Long:  $76.86^{\circ}$ ). The experimental details and the results obtained from these rocket experiments are discussed. The chapter is divided into two sections. The first section deals with the experimental details and the second one with the results.

#### 3.1. THE PAYLOAD:

Five rocket experiments were done using the Gerdien condenser technique. The first two payloads were instrumented to measure positive ion densities and their mobilities. The later three payloads measured both positive and negative ion densities and their mobilities. In these payloads, in-flight calibration also was incorporated. Figure.3.1 shows the block diagram of the payload. The part of the diagram shown in dashed lines indicate the modifications incorporated in the payload from third flight onwards.

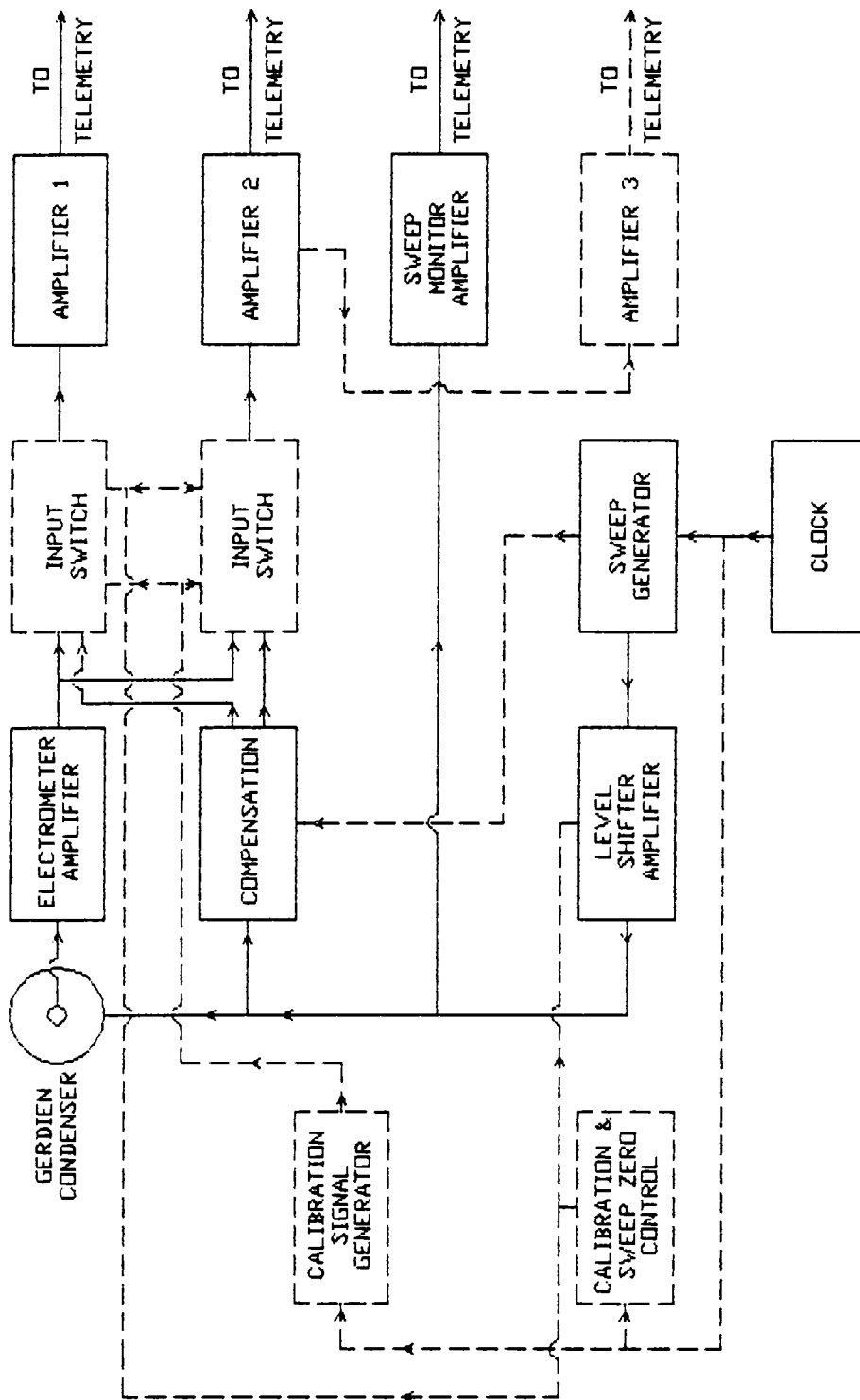


FIGURE 3.1. Functional block diagram of a Gerdien condenser payload. The part of the diagram in dashed lines indicate the modifications incorporated in the payload from third flight onwards.

The blocks are discussed in detail here.

### 3.1.1. THE GERDIEN CONDENSER SENSOR:

Two major constraints in designing the rocket sensor are the limitation in dimension enforced by the type of rocket and the total payload weight that can be flown. Another design constraint is the large shock during take off and the severe vibration during powered flight of the rocket. The sensor has to be designed and fabricated in such a way that it withstands the shock and vibration of the rocket on which it will be flown. The first two experiments were flown on M100-B rockets and the later ones on Rohini-300. The dimensions of the sensors flown in these two types were slightly different to suit each of these rockets. The details of the dimensions are given later. Here, we describe the general design of a typical rocket sensor.

Figure 3.2. shows the sensor at various stages of fabrication. The sensor consists of a driving electrode, a shield, end rings, legs to support the driving electrode assembly, a base, a collector, and a set of insulators.

The driving electrode is a brass tube electroplated with nickel. This driving electrode is held inside the shield with the help of insulating hylam rings such that the shield protrudes at both ends. The shield is made of an Aluminium tube slightly larger in diameter and longer in length than the driving electrode. Both ends of the shield are threaded and two threaded, bevelled rings fit at the ends. These end rings

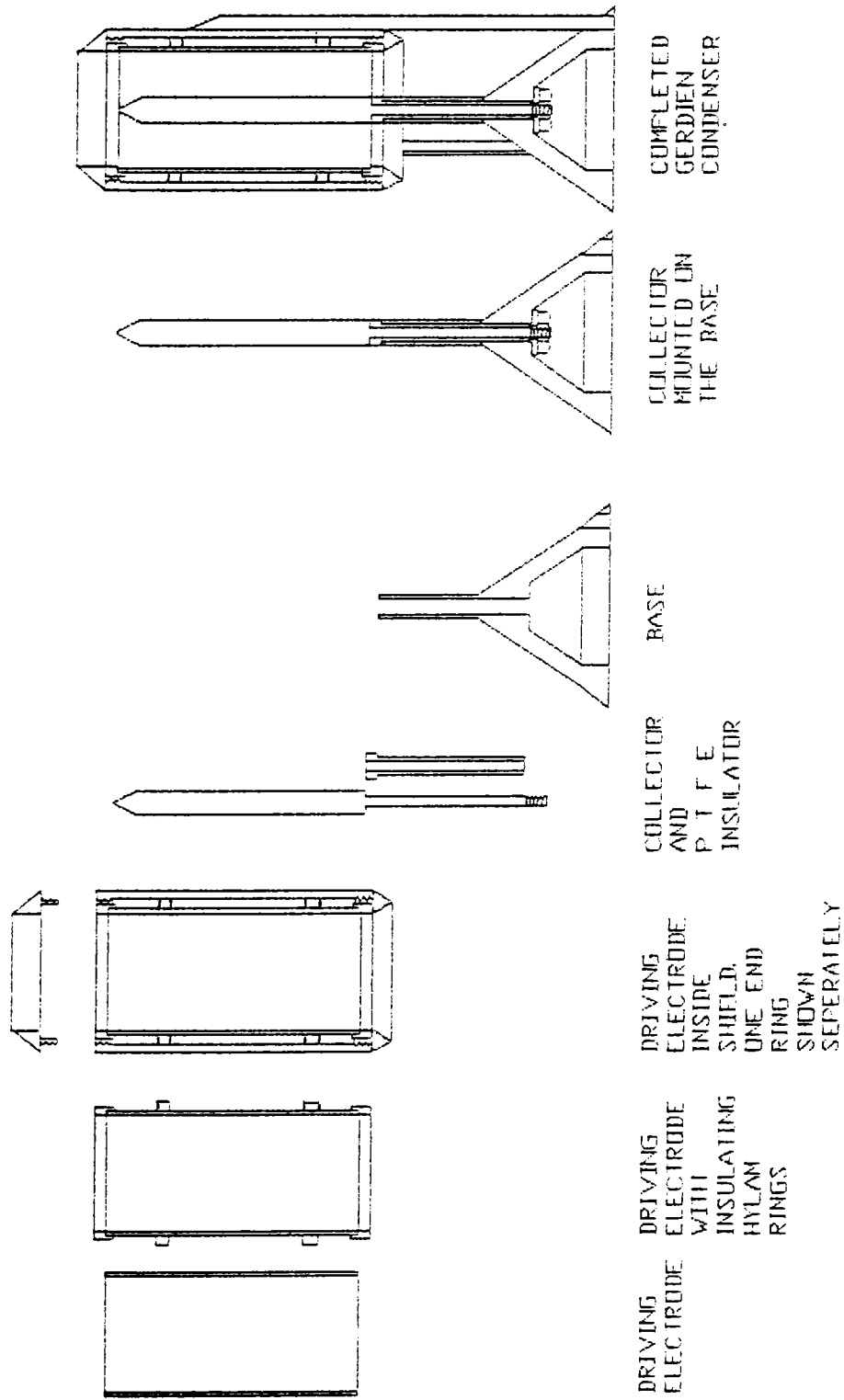


FIGURE 3.2. Assembly of a rocket-borne Gerdien condenser. Starting from the driving electrode, different stages of assembly are depicted. At the end a completely assembled sensor is also shown.

function as guard rings. The end rings and the insulating hylam rings at the ends of the driving electrode are made such that when the end rings are tightened the driving electrode is secured in position. Also the inner diameter of end rings and the hylam rings at the ends are such that the air flow through the sensor is smooth. Electrical connection to the driving electrode is accomplished through a 10 mm port on the shield.

The driving electrode and shield assembly are supported by three legs made of mild steel. The legs are fastened to the shield using screws and nuts in such a way that the insulation between the shield and the driving electrode is not affected. The lower end of the legs slip into three slots in the base and are fastened using screws and nuts. Also, the legs are made in such a way that on completion of assembly of the sensor, the ends of both driving electrode and collector are exactly at the same level.

A tube extending from the base supports the collector. The collector rod is made of brass and electroplated with nickel. The collector rod has a thick upper portion and a stepped thin lower portion. The upper thick portion is fabricated in two steps. First the rod is machined and then some material is removed from inside by drilling. Then the tip is made and brazed onto the collector rod. This material removal not only helps in reducing weight but also minimizes the chances of vibration failure. The stepped lower portion of the collector slips through a tube

extending from the base and is insulated from it by a P.T.F.E (Teflon) sheath of 2 mm thickness. The shape of the P.T.F.E. sheath is shown in the figure. The exposed part of the P.T.F.E. sheath, the support tube for the collector and the collector rod have exactly the same outer diameter to facilitate smooth air flow. The lower end of the collector rod is threaded and it is fastened to the base with a nut and a P.T.F.E washer. The length of the P.T.F.E. sheath is such that it does not touch the P.T.F.E. washer. The base is hollow and electrical connection to the collector is done at the lower end of the collector rod. The rocket body and flight decks are at power supply ground potential and so the end rings, shield, legs and the base get grounded when the sensor is mounted on the rocket deck. The base and the tip of the collector are suitably shaped to facilitate free air flow.

The diameter of the driving electrode is the first parameter considered in designing the sensor. For a given velocity of ascent of the rocket the collector current is proportional to the area of cross section of the sensor. Therefore it is desirable to have a driving electrode of largest possible diameter from the point of view of collector current output. The driving electrode diameter is limited by the space available in the rocket in which the sensor is flown. For example in M-100B rocket, the sensor could be mounted only in the steeple portion of the rocket and the maximum available space was of 70mm in diameter. Similarly in

RH-300 rocket there was a limitation on size imposed by legs supporting the nose cone ejection pyrojack. Taking this upper limit on the outermost diameter of the sensor into consideration, the thickness of the legs, diameter of the shield, thickness of hylam insulators and diameter of the driving electrode are decided.

The next design parameter is the length  $L$  of the condenser.

An expression for  $L$  is given by eqn.(20) in Chapter 2, which is reproduced here for the sake of convenience.

$$L = \frac{U (b^2 - a^2) \ln (b/a)}{2 \mu V_s} \quad (20)$$

For a given value of  $V_s$  and a range of values of  $U$  and  $\mu$  the length  $L$  required for operation of the condenser in saturation mode can be calculated. The collector diameter  $a$  is initially chosen arbitrarily, taking mechanical strength required into consideration, to calculate the value of  $L$ . If required the collector diameter is later changed and design of  $L$  redone.

In all the experiments a triangular sweep was applied to the driving electrode. Here the peak value is taken as  $V_s$  for calculation of  $L$ , so that the condenser saturates at the peak value. The peak value of sweep depends on the power supply and electronics. Taking into consideration the available on-board power supply voltages and



the type of electronics used the saturation voltage  $V_s$  is decided. For example, in the case of the first experiment analogue devices with a maximum supply rating of  $\pm 18$  V were used in the payload. Therefore, with allowances for safety the payload was designed for  $\pm 15$  V operation and so a sweep generator giving +13 V peak sweep was developed and fabricated.

Regarding  $U$ , the rocket velocity was known to vary from  $1000 \text{ ms}^{-1}$  to  $500 \text{ ms}^{-1}$ . Here the upper limit on velocity is taken for calculation of  $L$  so that the condenser saturates at all speeds of air flow.

The lowest value of  $\mu$  reported by Conley (1974), Rose\* Widdel (1972) and others were taken to calculate  $L$ . It may be mentioned here that some allowance is given for the value of  $\mu$  substituted to ensure saturation of the condenser even if lower mobility ions are encountered during the experiment.

Substituting these values of  $\mu$ ,  $U$  and  $V_s$ , the length  $L$  of the condenser is calculated.

Table 3.1 shows the dimensions and peak sweep voltages of typical sensors used in M100-B and RH-300 rockets.

TABLE - 3.1  
 Dimensions, peak sweep voltage and collector current  
 of typical sensors used in M100-B and RH 300 rockets.

| Type of rocket. | Driving electrode diameter.<br>(m) | Collector diameter<br>(m) | Length of condenser<br>(m) | Sweep voltage.<br>(V) | Collector current range<br>(nA) |
|-----------------|------------------------------------|---------------------------|----------------------------|-----------------------|---------------------------------|
| M100-B          | 0.042                              | 0.01                      | 0.107                      | 13                    | 0.01 to 1.0                     |
| RH-300          | 0.064                              | 0.016                     | 0.131                      | 12                    | 0.02 to 2.5                     |

### 3.1.2. THE SWEEP GENERATOR:

The sweep generator provides driving voltage to the Gerdien condenser. The functional block diagram and circuit diagram of the sweep generator are shown in Figure.3.3 a & b. An integrator, Schmitt trigger and an inverter connected in closed loop provide a triangular wave of  $\pm 2.5$  V amplitude and a clock output. The clock output was not used in the first two flights, but was used in the later flights for synchronous control of in-flight calibration and sweep zero check. The triangular wave output is amplified and level shifted in the level shifter amplifier to obtain the desired driving voltage. Unipolar sweep used in the first two flights and bipolar sweep used in later flights were derived in this way. For data analysis it is necessary that driving voltage also is

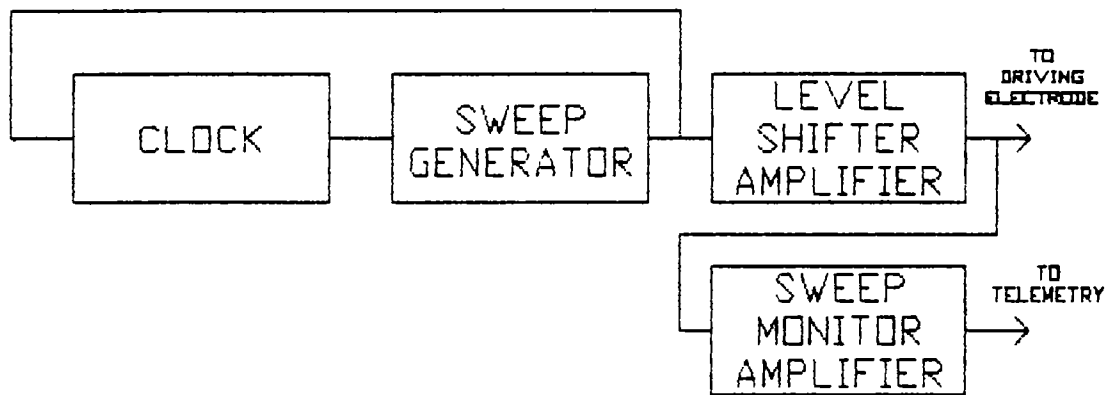


FIGURE 3.3. a. Sweep generator, block diagram.

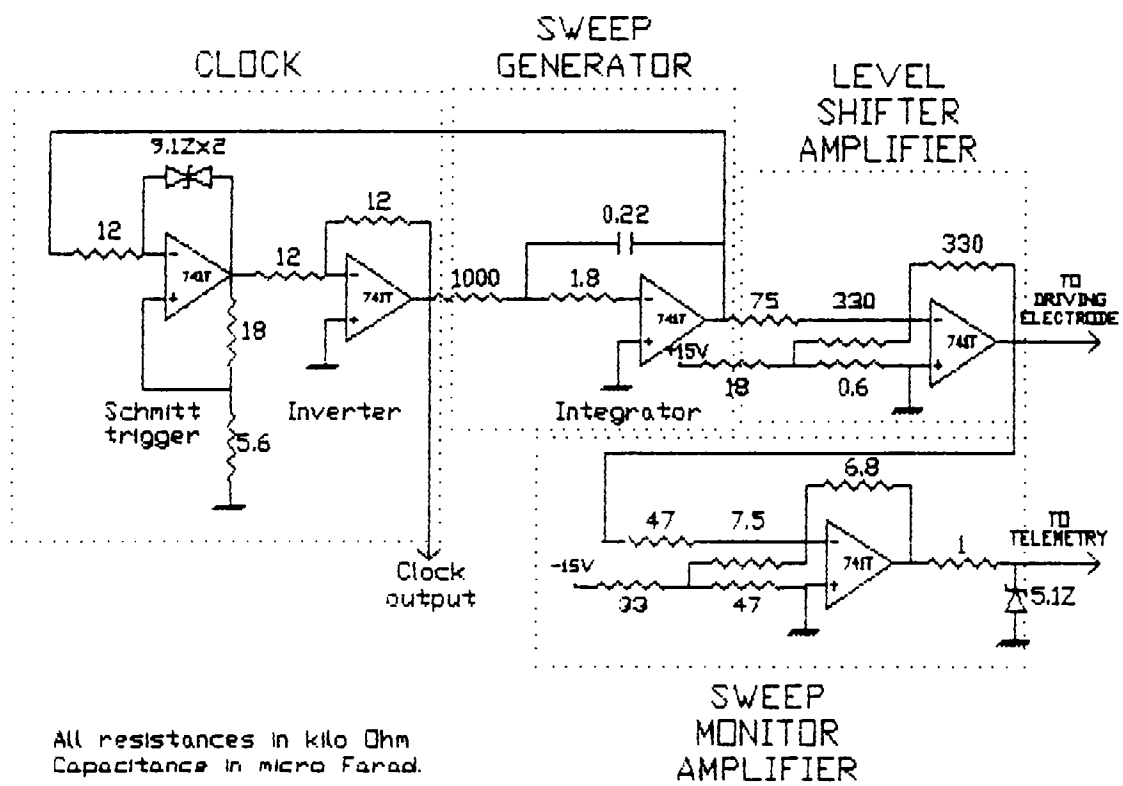


FIGURE 3.3 b Sweep generator, circuit diagram.

telemetered. The telemetry input voltage range is from 0 to 5V and so the driving voltage wave form is attenuated to a range of about 0 to 4 V (the exact value changes from flight to flight) by the sweep monitor amplifier and fed to sweep monitoring channel of telemetry.

The frequency of the sweep is set by the the resistance and capacitance of the integrator. Depending on the number of samples required for every kilometer of altitude the frequency of sweep is decided. For example in the first flight a sweep of about 5 Hz was used. With a maximum rocket velocity of 1 km/s the sweep of 2 Hz yields four data points for every kilometer of altitude.

The sweep applied to the sensor produces a square wave at the output of the electrometer amplifier due to displacement current. This is compensated by adding a similar inverted square wave to the current measurement system. In the first two experiments the sweep was fed to an R-C circuit to generate the square wave required for compensation. In the later experiments a square wave available in the sweep generator was used instead. This method of compensation was found to be more stable.

### 3.1.3. THE CURRENT MEASUREMENT SYSTEM:

Figure.3.4 a & b shows the block diagram and circuit diagram of the system used for measuring collector current in the first two experiments. The heart of the system is an

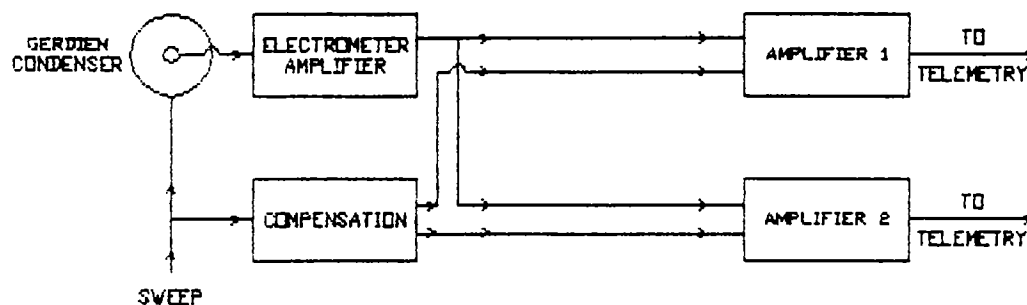


FIGURE 3.4.a. The system used for collector current measurement in a rocket payload; block diagram.

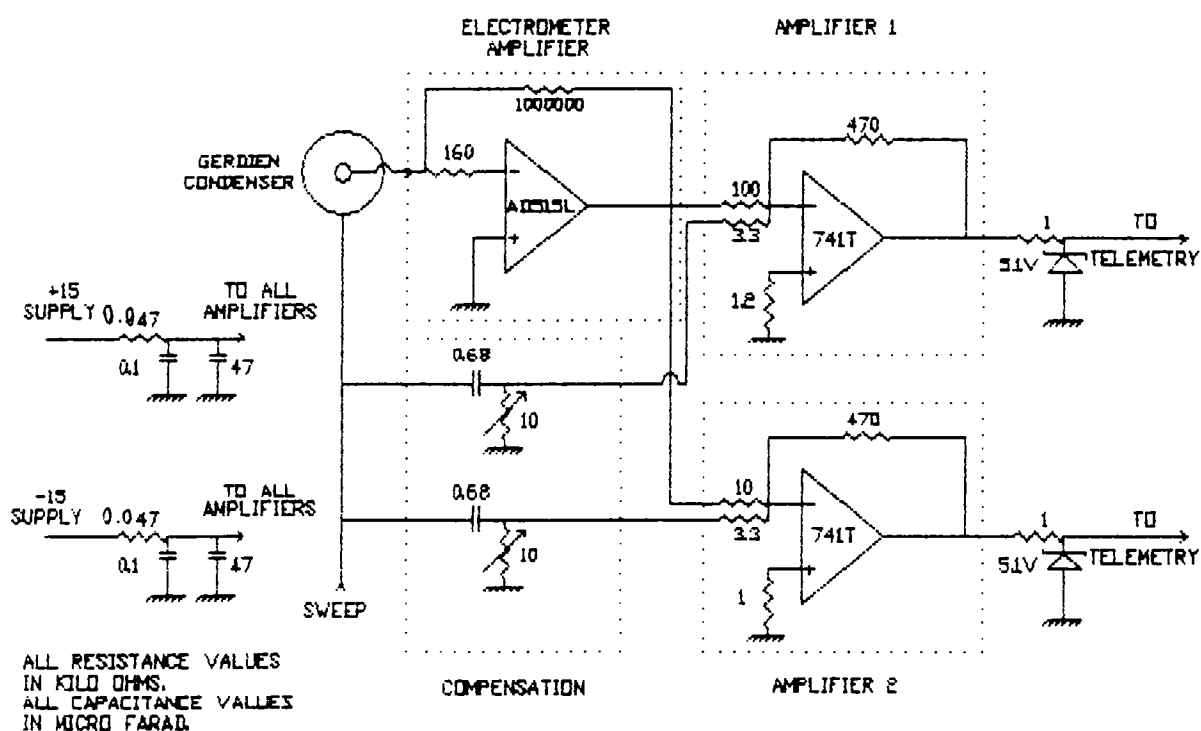


FIGURE 3.4.b. Circuit diagram of the system used for collector current measurement.

electrometer amplifier constructed with an AD 515L operational amplifier, which converts the collector current to voltage. For each rocket experiment, from the known range of ion density values, the expected collector current range was calculated and it was found that current of the order of a fraction of a nA could be expected. Therefore an electrometer amplifier of 1 V/nA sensitivity was designed and fabricated for all the rocket experiments.

The output of the electrometer is fed to two independent amplifiers designated amplifiers 1 & 2 wired around operational amplifiers. The compensation for displacement current is done at these amplifiers. The square wave signal for compensation is fed to two preset potentiometers at the summing input of each amplifier. These potentiometers control the amplitude of compensation signal fed to the amplifiers. During fabrication and testing these potentiometers are adjusted so that the signal due to displacement current gets annulled.

The amplifiers provide two overlapping ranges of current measurement. The current measurement system used in the later flights were slightly different from the first two. In the third flight the output of amplifier 2 was fed to a third amplifier (inverting, unity gain) to obtain negative ion data. Negative and positive ion data were obtained in the fourth and fifth experiments by level shifting the amplifier outputs such that at the telemetry inputs the voltage was 2.25

volts for zero collector current. This was needed because the rocket telemetry would accept input voltages from 0 to 5 V only.

With this telemetry input range the overall sensitivity and range of measurement for each experiment is determined by the dimensions of the sensor, speed of air flow, the electrometer amplifier sensitivity and gain of amplifiers. Therefore, taking all these factors into consideration the gain of amplifiers for each experiment is decided.

The payloads of third, fourth and fifth experiments contained a system for sweep zero check and in-flight calibration. Sweep zero check is done by grounding the driving electrode after disconnecting the sweep for a few hundred milliseconds. Sweep zero check helps not only in estimating contact potentials if any but also serves in estimating the reference value of all outputs of the current measurement system when the collector current is zero. Followed by the sweep zero check, the amplifiers are disconnected from the electrometer amplifier and a calibration signal derived from a reference source is fed to the amplifiers. The calibration period also is of the order of a few hundred milliseconds. The whole process is repeated at an interval of approximately 30 seconds. The clock output of the sweep generator is used to control the process as mentioned earlier so that the calibration and sweep zero check were done synchronous with the sweep.



#### 3.1.4.CALIBRATION AND TESTING:

The current measurement system was calibrated with a Keithley picoampere current source (calibrated against N.B.S., U.S.A). The calibration was done along with the cable connecting the sensor to the electrometer amplifier. Further the attenuation factor and phase relationship of the output of the sweep monitor amplifier to the sweep applied to the sensor is noted.

After fabrication, the payload was calibrated and tested at various temperatures from  $-10^{\circ}\text{C}$  to  $70^{\circ}\text{C}$  for satisfactory performance. The payload was then integrated with other systems in the rocket and checked for proper functioning. Vibration, shock and acceleration checks were then conducted on the integrated payload.

By the time the third flight was conducted a set of mandatory tests known as GATE tests to evaluate the flight worthiness of scientific payloads had come into operation. The GATE test is meant to weed out weaklings and serves the purpose of early detection of inherent weakness. A typical GATE test report is given in TABLE 3.2.

TABLE 3.2.  
GATE TEST REPORT  
THIRD FLIGHT

| Type of test   | Parameter measured.             | Expected value.  | Obtained value   | Remarks          |
|--|---------------------------------|------------------|------------------|------------------|
| I. 70°C,<br>8 hr un-<br>powered,<br>1hr<br>powered.    | a. Calibration:                 |                  |                  | Accept-<br>able. |
|  | 1. 2 gain cal.<br>output        | 1.8 V,<br>3.6 V. | 1.9 V,<br>3.7 V. |                  |
|  | 2 10 gain cal.<br>output        | 0.9 V,<br>1.8 V. | 1.1 V,<br>2.0 V. |                  |
|  | b. Sweep zero-<br>outputs       |                  |                  | Accept-<br>able. |
|  | 1. E M<br>Amplifier             | 50 mV            | 50 mV            |                  |
|  | 2. 2 gain<br>amplifier          | -50 mV           | -40 mV           |                  |
|  | 3. 10 gain<br>amplifier         | -250 mV          | -210 mV          |                  |
|  | 4. Negative output<br>amplifier | 250 mV           | 200 mV           |                  |
|  | 5. Sweep<br>monitor             | 2 V              | 2 V              |                  |
|  | c. Sweep                        |                  |                  | Accept-<br>able. |
|  | 1. Sweep<br>voltage             | +13V, -12V       | +13V, -12V       |                  |
|  | 2. Sweep<br>period              | 480 m s          | 480 ms           |                  |
|  | 3. Sweep<br>monitor<br>output   | 0 to 3.8V        | 0 to 3.8V        |                  |
| II. 10°C,<br>1 hr. un-<br>powered,<br>10 mt<br>powered | a. Calibration:                 |                  |                  | Accept-<br>able. |
|  | 1. 2 gain cal.<br>output        | 1.8 V,<br>3.6 V. | 1.8 V,<br>3.6 V. |                  |
|  | 2 10 gain cal.<br>output        | 0.9 V,<br>1.8 V. | 0.9 V,<br>1.8 V. |                  |
|  |                                 |                  |                  |                  |

| Type of test   | Parameter measured.            | Expected value.  | Obtained value   | Remarks          |  |
|--|--------------------------------|------------------|------------------|------------------|--|
| III.<br>96 hr<br>Burn-in,<br>room<br>temp.,<br>powered | b.Sweep zero-<br>outputs       |                  |                  |                  |  |
|  | 1.E M<br>Amplifier             | 15 mV            | 15 mV            | Accept-<br>able. |  |
|  | 2.2 gain<br>amplifier          | 20 mV            | 20 mV            |                  |  |
|  | 3.10 gain<br>amplifier         | 100 mV           | 90 mV            |                  |  |
|  | 4.Negative output<br>amplifier | -100 mV          | -110 mV          |                  |  |
|  | 5.Sweep<br>monitor             | 2 V              | 2 V              |                  |  |
|  | c.Sweep                        |                  |                  |                  |  |
|  | 1.Sweep<br>voltage             | +13V, -12V       | +13V, -12V       | Accept-<br>able. |  |
|  | 2.Sweep<br>period              | 480 m s          | 480 ms           |                  |  |
|  | 3.Sweep<br>monitor<br>output   | 0 to 3.8V        | 0 to 3.8V        |                  |  |
|  | a.Calibration:                 |                  |                  |                  |  |
|  | 1. 2 gain cal.<br>output       | 1.8 V,<br>3.6 V. | 1.8 V,<br>3.6 V. | Accept-<br>able. |  |
|  | 2 10 gain cal.<br>output       | 0.9 V,<br>1.8 V. | 0.9 V,<br>1.8 V. |                  |  |
|  | b.Sweep zero-<br>outputs       |                  |                  |                  |  |
|  | 1.E M<br>Amplifier             | 35 mV            | 40 mV            | Accept-<br>able. |  |
|  | 2.2 gain<br>amplifier          | -20 mV           | -35 mV           |                  |  |
|  | 3.10 gain<br>amplifier         | -100 mV          | -135 mV          |                  |  |
| 4.Negative output<br>amplifier                         | 100 mV                         | 135 mV           |                  |                  |  |
| 5.Sweep<br>monitor                                     | 2 V                            | 2 V              |                  |                  |  |

| Type of test  | Parameter measured.          | Expected value.  | Obtained value   | Remarks     |
|---|------------------------------|------------------|------------------|-------------|
| IV.<br>Vacuum,<br>10 <sup>-5</sup> torr,<br>room<br>temp.,<br>10 mt | c. Sweep                     |                  |                  |             |
|   | 1. Sweep voltage             | +13V, -12V       | +13V, -12V       | Acceptable. |
|   | 2. Sweep period              | 480 m s          | 480 ms           |             |
|   | 3. Sweep monitor output      | 0 to 3.8V        | 0 to 3.8V        |             |
|   | a. Calibration:              |                  |                  |             |
|   | 1. 2 gain cal. output        | 1.8 V,<br>3.6 V. | 1.8 V,<br>3.6 V. | Acceptable. |
|   | 2 10 gain cal. output        | 0.9 V,<br>1.8 V. | 0.9 V,<br>1.8 V. |             |
|   | b. Sweep zero-outputs        |                  |                  |             |
|   | 1. E M Amplifier             | 25 mV            | 25 mV            | Acceptable. |
|   | 2. 2 gain amplifier          | 2 mV             | 2 mV             |             |
|   | 3. 10 gain amplifier         | 5 mV             | 5 mV             |             |
|   | 4. Negative output amplifier | 0                | 0                |             |
|   | 5. Sweep monitor             | 2 V              | 2 V              |             |
|   | c. Sweep                     |                  |                  |             |
|   | 1. Sweep voltage             | +13V, -12V       | +13V, -12V       | Acceptable. |
| 2. Sweep period   | 480 m s                      | 480 ms           |                  |             |
| 3. Sweep monitor output   | 0 to 3.8V                    | 0 to 3.8V        |                  |             |

| Type of test  | Parameter measured.                  | Expected value.  | Obtained value   | Remarks     |
|---|--------------------------------------|------------------|------------------|-------------|
| V.<br>Vibration,<br>3 axes,<br>X,Y&Z.<br>Sine<br>20 Hz to<br>2 kHz.<br>Random<br>20 Hz to<br>2 kHz. | a. Calibration:                      |                  |                  |             |
|   | 1. 2 gain cal output                 | 1.8 V,<br>3.6 V. | 1.8 V,<br>3.6 V. | Acceptable. |
|   | 2 10 gain cal output                 | 0.9 V,<br>1.8 V. | 0.9 V,<br>1.8 V. |             |
|   | b. Sweep zero-outputs                |                  |                  |             |
|   | 1. E M Amplifier                     | 25 mV            | 25 mV            | Acceptable. |
|   | 2. 2 gain amplifier                  | 2 mV             | 2 mV             |             |
|   | 3. 10 gain amplifier                 | 5 mV             | 5 mV             |             |
|   | 4. Negative output amplifier         | 0                | 0                |             |
|   | 5. Sweep monitor                     | 2 V              | 2 V              |             |
|   | c. Sweep                             |                  |                  |             |
|   | 1. Sweep voltage                     | +13V, -12V       | +13V, -12V       | Acceptable. |
|   | 2. Sweep period                      | 480 m s          | 480 ms           |             |
|   | 3. Sweep monitor output              | 0 to 3.8V        | 0 to 3.8V        |             |
|   | VI.<br>Acceleration.<br>35g,<br>1mt. | a. Calibration:  |                  |             |
| 1. 2 gain cal output  |                                      | 1.8 V,<br>3.6 V. | 1.8 V,<br>3.6 V. | Acceptable. |
| 2 10 gain cal output  |                                      | 0.9 V,<br>1.8 V. | 0.9 V,<br>1.8 V. |             |
| b. Sweep zero-outputs   |                                      |                  |                  |             |
| 1. E M Amplifier  |                                      | 25 mV            | 25 mV            | Acceptable. |
| 2. 2 gain amplifier   |                                      | 2 mV             | 2 mV             |             |
| 3. 10 gain amplifier  |                                      | 5 mV             | 5 mV             |             |

| Type of test | Parameter measured.          | Expected value. | Obtained value | Remarks     |
|--------------|------------------------------|-----------------|----------------|-------------|
|              | 4. Negative output amplifier | 0               | 0              | Acceptable. |
|              | 5. Sweep monitor             | 2 V             | 2 V            |             |
|              | c. Sweep                     |                 |                |             |
|              | 1. Sweep voltage             | +13V, -12V      | +13V, -12V     |             |
|              | 2. Sweep period              | 480 m s         | 480 ms         |             |
|              | 3. Sweep monitor output      | 0 to 3.8V       | 0 to 3.8V      |             |

Equipment used :

1. Tektronics oscilloscope.
2. Keithley Picoampere source.

Facility :

Vibration and acceleration test - V.S.S.C.  
All other tests - C E S S.

### 3.1.5 PAYLOAD LAYOUT:

The first two flights were conducted using M100-B rockets, and the remaining using Rohini-300s(RH-300). The M-100B has a steeple at the tip which can be split and ejected. The Gerdien condenser was mounted inside this steeple. In RH-300 rockets the sensor was mounted on the

top-most deck in the nose cone, and the nose cone was ejected. Sketches of sensor mounting in these two types of rockets is shown in Figure 3.5.

Figure 3.5. also shows the electronics box mounted just below the sensor in the case of RH-300 rocket. In the case of M-100B the electronics was mounted on the topmost deck namely DECK 1. In both the cases the electronics box had two connectors, one P.T.F.E insulated co-axial connector and another rack and panel connector. The co-axial connector was used for connecting the electrometer amplifier to the collector. Power inputs to and telemetry outputs from the electronics were taken through the rack and panel connector. An RG-178 P.T.F.E insulated cable was used to connect the collector to the electrometer amplifier. Amplifier end connection of the cable was accomplished through the co-axial connector and at the sensor end the inner conductor was soldered to a terminal at the lower end of the collector. The cable was anchored every few centimeters to reduce vibration. The shield of the cable was grounded only at the box end to avoid ground loop problems.

Experimental details of all rocket flights are given in table.3.3.

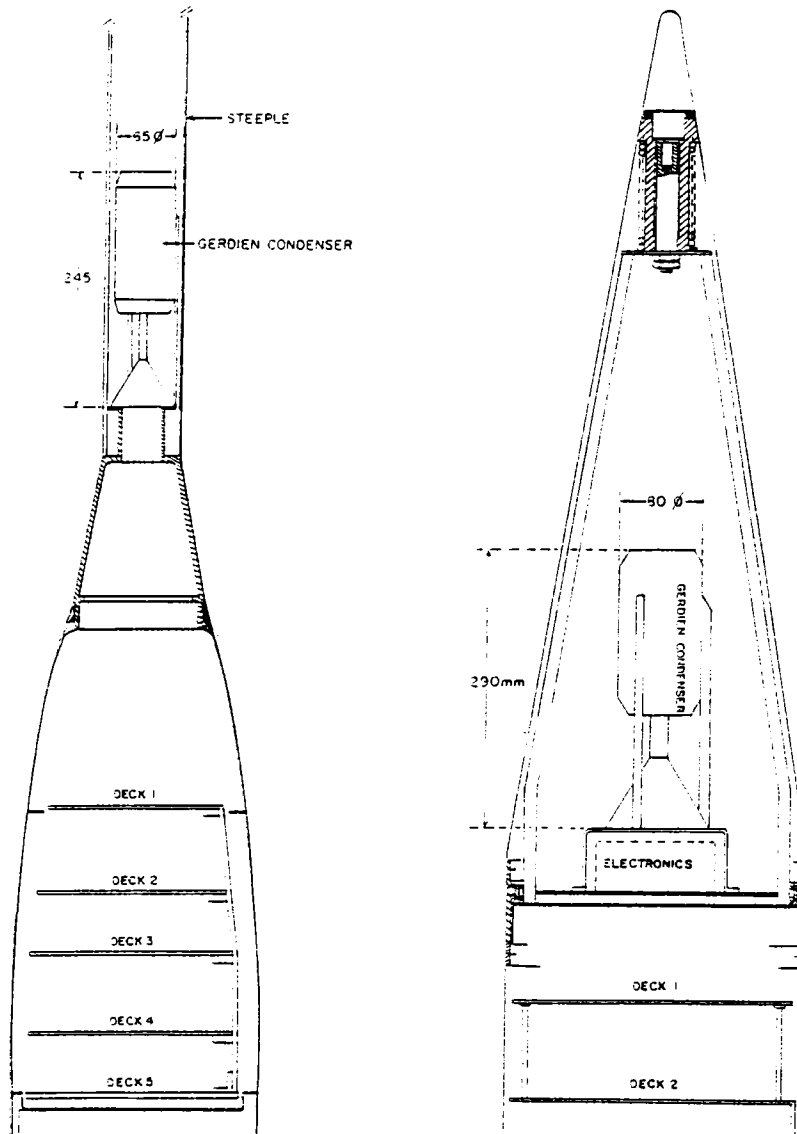


FIGURE 3.5. Gerdien condenser assembly in the steeple part of the rocket M-100B (left) and in the nose cone portion of the rocket RH-300.



Table 3.3

Details of rocket experiments

| Flight No | Type of rocket | Launch date | Launch time I S T | Solar zenith angle | 10.7 cm flux ( $F_{10.7}$ ) |
|-----------|----------------|-------------|-------------------|--------------------|-----------------------------|
| 1         | M-100B         | 29.11.1982  | 1051              | 34.6°              | 161                         |
| 2         | M-100B         | 9. 2.1984   | 1609              | 59.4°              | 140                         |
| 3         | RH-300         | 3.10.1986   | 0935              | 43.4°              | 72                          |
| 4         | RH-300         | 12. 4.1988  | 0910              | ----               | ---                         |
| 5         | RH-300         | 6.11.1988   | 0840              | 59°                | 161                         |

In all the flights the sensor was exposed at an altitude of about 50 to 55 km. Good data were obtained during the ascent. Air flow during descent is complicated and nonuniform and so descent data was not taken for analysis.

Data from the fourth flight was found to be not good and hence was not analysed.

### 3.2. DISCUSSION:

#### 3.2.1. POSITIVE ION DENSITIES:

The positive ion densities obtained from the four flights are shown in Figure 3.6. All these measurements show that the ion density decreases initially and reaches a minimum around 60-65 km. It then increases with altitude in the mesosphere. The production mechanisms of positive ions in the atmosphere indicate that while galactic cosmic rays constitute

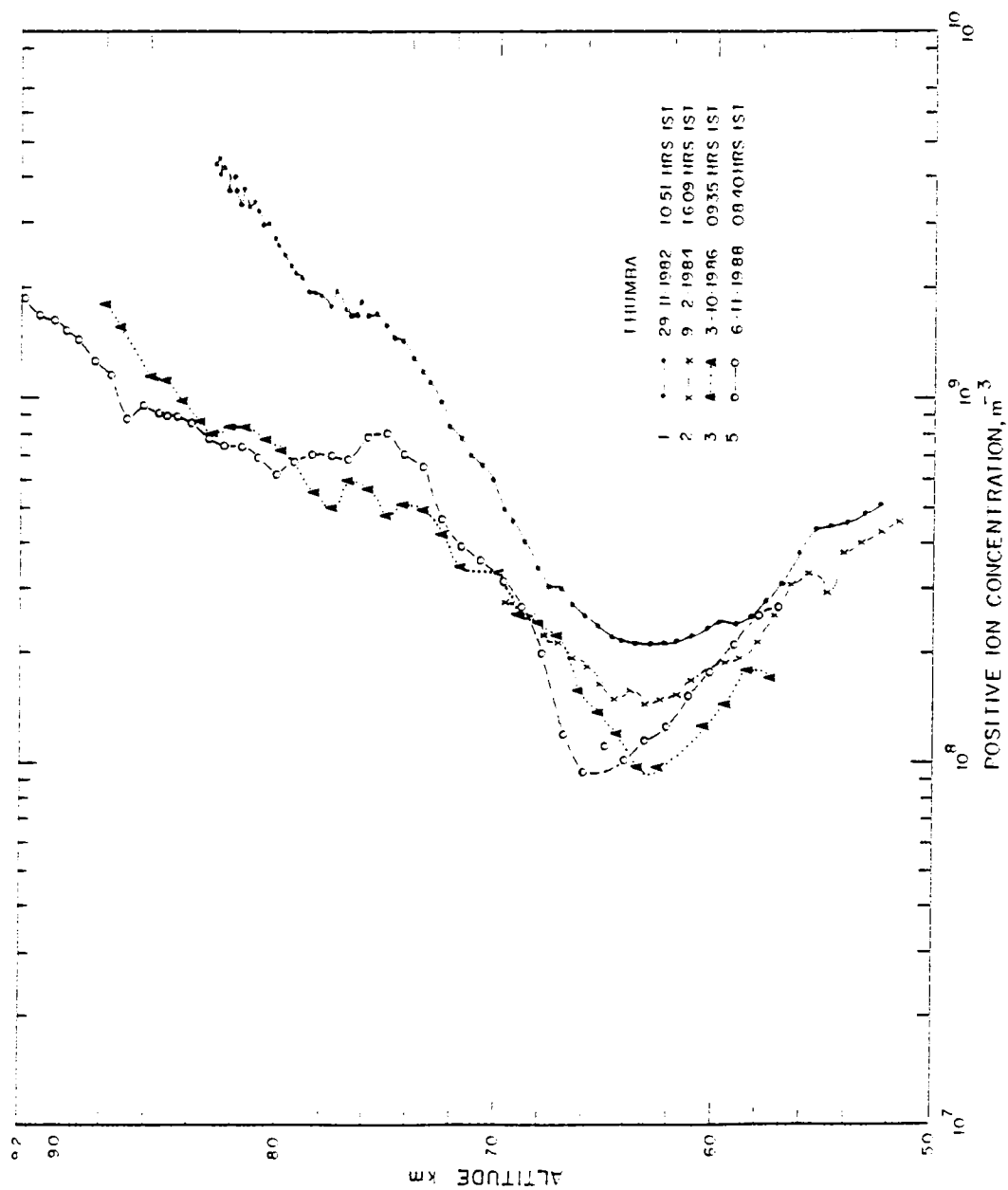


FIGURE 3.6. Positive ion density profiles obtained from the four rocket flights.

the main source of ionisation below about 60-65 km, solar Lyman- $\alpha$  (121.6 nm) is dominant above this altitude. The decreasing effect of cosmic rays and the increasing effect of Lyman- $\alpha$  beyond 60-65 km combine to produce a minimum in ion density at about 60-65 km. The measurements reported here are some of the first to show this minimum clearly; other two equatorial measurements that cover both sides of the minimum are those of Mitchell et al (1983 & 1985). In the measurements from a mid latitude station reported by Rose and Widdel (1972) also a minimum in ion density can be inferred at about 65 km.

In the region above the minimum, up to 85 km (D-region) ions are produced mainly by the Lyman- $\alpha$  radiation at 121.57 nm, the Lyman- $\beta$  radiation at 102.6 nm, the C-III radiation at 97.7 nm and radiation corresponding to a few other lines in the solar emission continuum in the far ultraviolet. Hard X-rays ( $< 1\text{nm}$ ) also contribute to D-region ionization and soft X-rays (1-10 nm) produce some ionization in the lower E-region (below 100 km).

The production of ionization by hard X-rays in the D-region is some what complex since it involves the absorption of an X-ray photon by a neutral particle, leading to the production of photo-electrons which are sufficiently energetic to ionize other particles. It thus becomes necessary to distinguish between primary and secondary ionisation. The mean number of secondary ion pairs produced depends on the

energy of the incident photon.

For low levels of solar activity, this source of ions is small compared to that produced by the Lyman- $\alpha$  line. On the other hand its contribution becomes more important during disturbed conditions. For example, solar irradiance of X-rays from 0.1nm to 0.8 nm intensifies by about 1000 times for active conditions, and may increase by an additional factor of 100 during solar flares.

The absorption of solar radiation in the spectral region from 102.7 nm to 111.8 nm represents an additional source of D-region ionization as suggested by Hunten and McElroy (1968), but the rate of ion formation is much smaller than that by Lyman- $\alpha$ .

Hence for typical conditions, most of the ionization in the D-region is due to the effect of the solar Lyman- $\alpha$  on Nitric oxide (Nicolet,1945). The ionization potential of NO molecule is 9.25 eV, which corresponds to a wave length of 134 nm. In the spectral region of the Lyman- $\alpha$  line an atmospheric window exists due to the low absorption cross section of O<sub>2</sub> in this interval, and thus the ionizing radiation can penetrate relatively far into the mesosphere.

Hence, above about 60-65 km the main source of ionisation is solar radiation, and ionisation in this region therefore will be dependent on solar zenith angle and solar activity. The ionisation is directly related to the level of solar activity but inversely to the solar zenith angle.

Therefore for the same level of solar activity, a lower zenith angle should give a higher ion concentration.

Here, results from four rocket experiments in which positive ion density were measured are presented. The measurements reported here were conducted as part of a programme on middle atmospheric investigations. From Table.3.3, it can be seen that two rocket flights have been done when the  $F_{10.7}$  values were the same, but the solar zenith angles were different. Two rocket experiments have been carried out on two days at the same zenith angles but the solar activity levels were different. Using the results from these experiments the effects of solar activity and solar zenith angle on positive ion density are discussed.

Figure 3.7.a shows positive ion density profiles obtained from first and fifth flights. The  $F_{10.7}$  value, which is indicative of level of solar activity, was same (161) for both flights, but the solar zenith angles were quite different. The zenith angles were  $34.6^\circ$  and  $59^\circ$  for the first and fifth flights respectively. From the figure it can be seen that the first flight which has a lower zenith angle has measured a higher ion density than the fifth, which is indicative of the influence of solar zenith angle on ion density.

The second and fifth flights had nearly equal zenith angles (about  $59^\circ$ ), but corresponding  $F_{10.7}$  values are different (140 and 161). The fifth flight conducted on a day

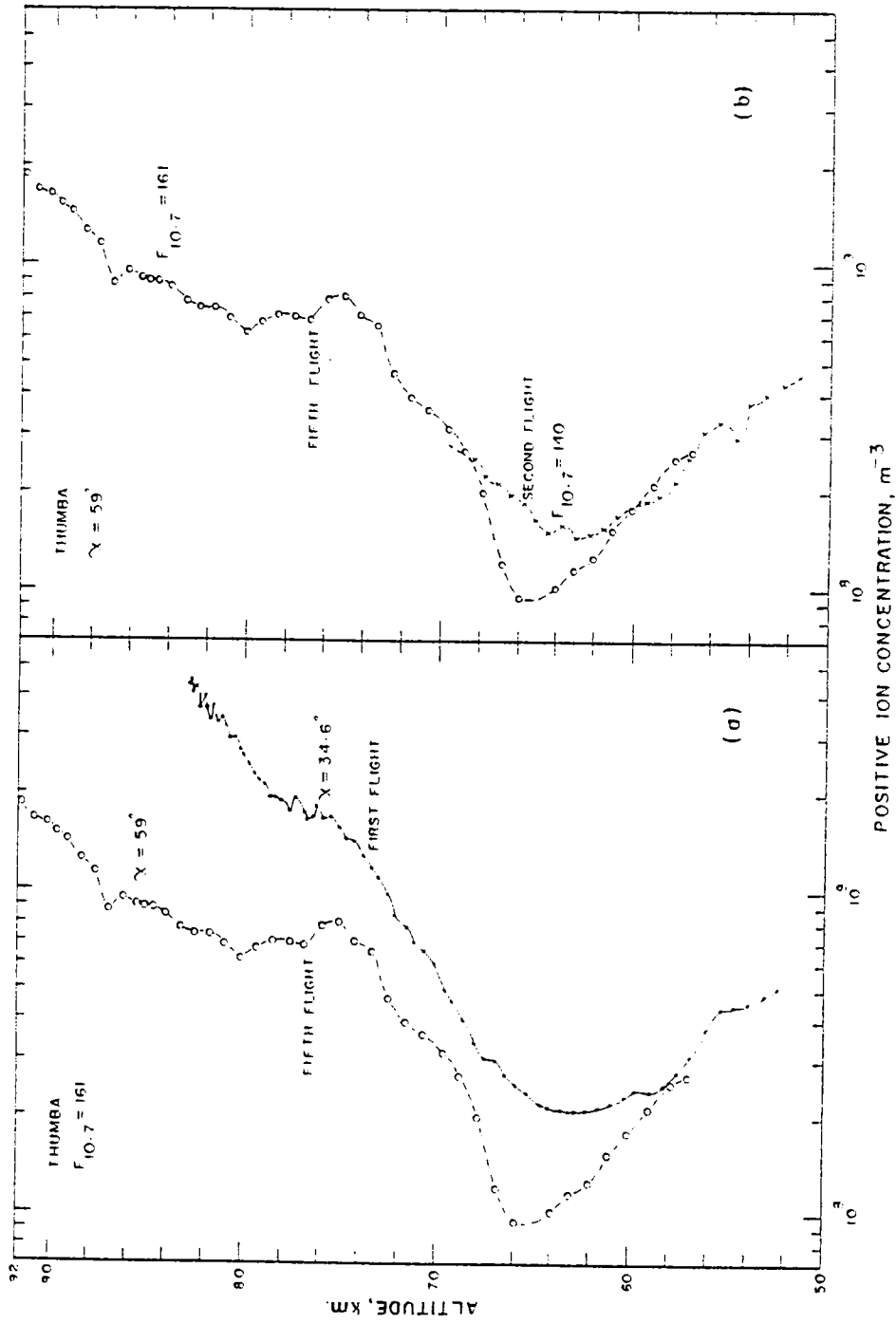


FIGURE 3.7. Positive ion density profiles showing the effect of (a) solar zenith angle (b) solar activity.

of higher solar activity has measured lower densities than the second, as seen from the profiles shown in Figure 3.7.b. One reason for this could be the difference in nitric oxide concentration. Seasonal variations of NO up to two or three orders of magnitude have been reported (Kopp and Herrmann, 1984). The two flights have been conducted in the months of November and February, though four years apart. Hence the seasonal effects may not be significantly felt in the measurements. But this effect cannot be completely ruled out. The second possibility is an asymmetry about noon in ionisation. A careful examination shows that the second flight was the only one conducted in the afternoon. A possible asymmetry in ionisation between forenoon and afternoon can be a reason for the ion densities in the second flight to be higher. Such an asymmetry in ion concentration with respect to noon has not been reported for comparison with these measurements.

However, asymmetries in electron concentration have been reported by Aikin et al (1972), Gregory and Manson (1969) and others. To be more specific Haug et al (1970) from partial reflection measurements at Crete ( $35^{\circ}\text{N}$ ) in May 1966 found electron density values to be maximised 2 hours after local noon at 80 km. But this was not apparent in the measurements made from the same station in the autumn of 1964 and 1965. Asymmetries were also observed in the partial reflection data at Urbana, Illinois, ( $40^{\circ}\text{N}$ ), with a tendency

for higher electron densities in the morning (Weiland et al., 1983). Chakrabarty et al (1983) try to explain this as due to a possible asymmetry in temperature. Temperature indirectly affects the electron loss coefficient in a way that it decreases with increase in temperature. A decrease in loss coefficient leads to a higher electron concentration. Thus, an increase in temperature can cause an increase in electron concentration and so an asymmetry in temperature about local noon would cause an asymmetry in electron density. The possibilities of such an asymmetry in temperature causing an asymmetry in ion density also needs to be studied. Simultaneous measurements of ion and electron densities at the same zenith angles at forenoon and after noon on the same day will help us to understand this. A perfect understanding may still elude us, as accurate measurements of temperature in the mesopause face certain problems.

Thus the ion density profiles obtained from these rocket flights show the effect of solar activity and zenith angle on positive ion density. Also the minimum in ion density at 60-65 km brought about by the combined effect of solar Lyman- $\alpha$  and galactic cosmic rays is seen clearly. A possible asymmetry in ion density with respect to noon is also suggested.



### 3.2.2. POSITIVE ION MOBILITIES:

The positive ion mobilities measured in the four rocket flights are shown in Figure 3.8. In these experiments mobilities were measured only up to a certain altitude. This is because, above this altitude continuum concepts are no longer valid for the condensers used and so the mobility measurements are invalid. Further, above this altitude the condensers were found to saturate at very small driving voltages making estimation of saturation voltage difficult. Therefore, in the experiments reported here, mobility data are available only up to an altitude of about 65 km.

Narcisi *et. al* (1970,1983) from their quadrupole mass spectrometric measurements have identified the type of ions present in this region. From their measurements it is seen that the  $\text{NO}^+$  ion which was predicted to be the predominant ion in the D-region is much less abundant and ions of  $\text{H}^+(\text{H}_2\text{O})_n$  type dominate the ion composition below about 82 km (for instance, Thomas 1983). Generally the ion  $37^+$ ,  $\text{H}_5\text{O}_2^+$  dominates the ion composition in the D-region with  $19^+$ ,  $\text{H}_3\text{O}^+$  and  $55^+$ ,  $\text{H}_7\text{O}_3^+$  also present but of lesser abundance. Heavier ions of mass greater than 40 amu are typically less than 10% of the total ionisation. This was found to be true during day and night through sun rise and sun set, during aurora, a meteor shower, a sporadic E event and total solar eclipse.

A positive identification of the value of  $n$  in

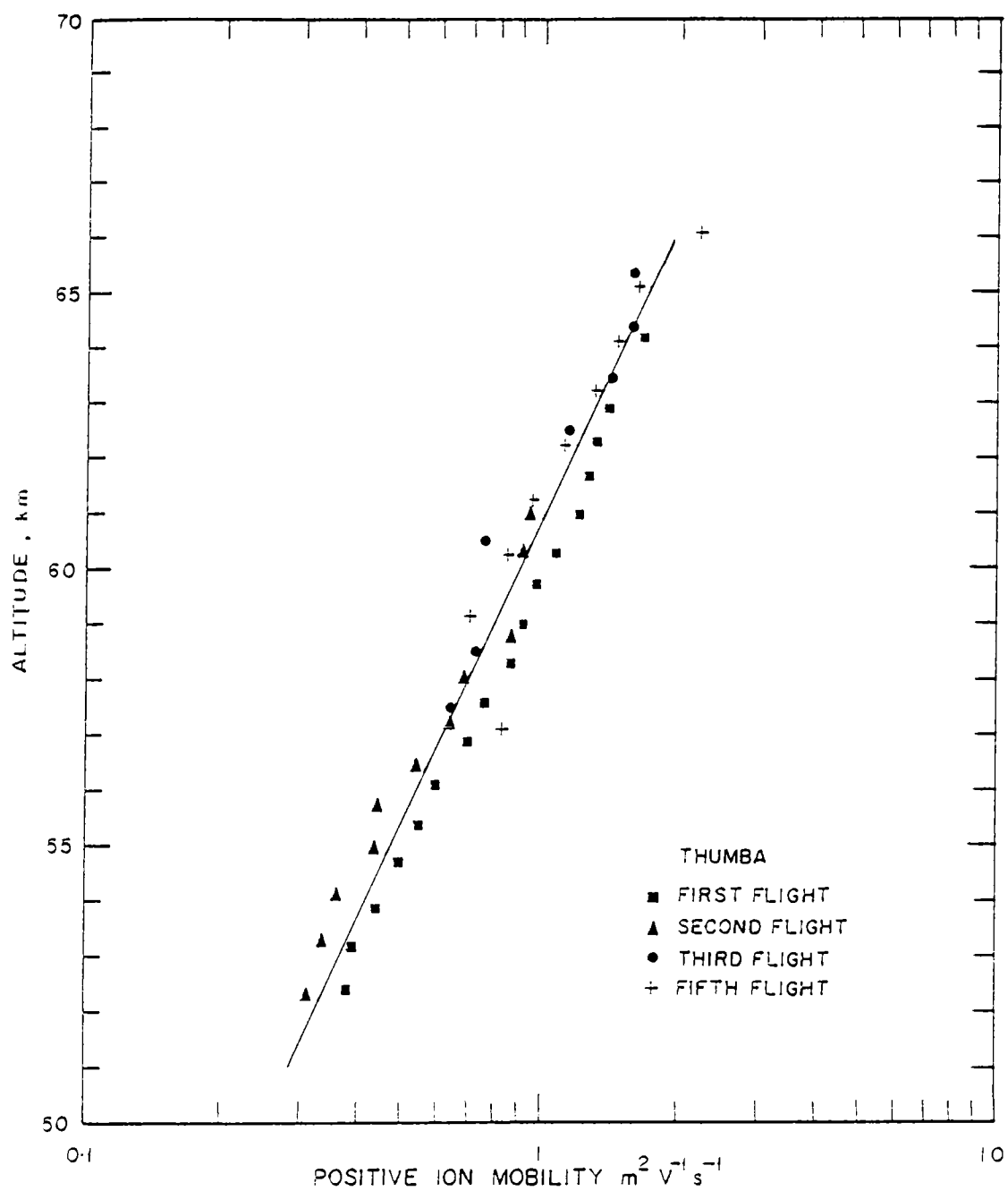


FIGURE 3.8. Positive ion mobility measured from four rocket flights. The straight line is a least square fit for all the values

$H^+(H_2O)_n$  cannot be made from Gerdien condenser measurements because mobility is not a sensitive function of ion mass. However, the values reported here are very close to those obtained using Gerdien condensers by Conley(1974), Rose and Widdel (1972) and others.

Measurements of mobilities of a large variety of molecular ions, both positive and negative, in dry nitrogen have been made by Kilpatrick (Meyerotte et. al.1980). Similarly Mitchell and Rider (Meyerotte et. al.1980) made reduced mobility measurements of a variety of positive atomic ions in dry nitrogen. Figure 3.9. shows the mass dispersion curves from these two measurements. The curve is reproduced from Meyerotte et al (1980). Measurements of mobilities of hydronium ions of masses 19,37 & 55 amu in nitrogen by Dotan (Meyerotte et. al.1980) and that of Huertas et al. (Meyerotte et. al.1980) of hydronium ions of masses 73,91 & 109 amu also follow these curves closely.

An attempt has been made to identify the mass of the observed ions from this mass dispersion curve. Figure 3.9 also shows the range of reduced mobility of positive and negative ions obtained from the measurements described here. By this method of evaluation it has been found that the measured mobilities correspond more or less to that of water cluster ions with  $n=2$  or  $3$ .

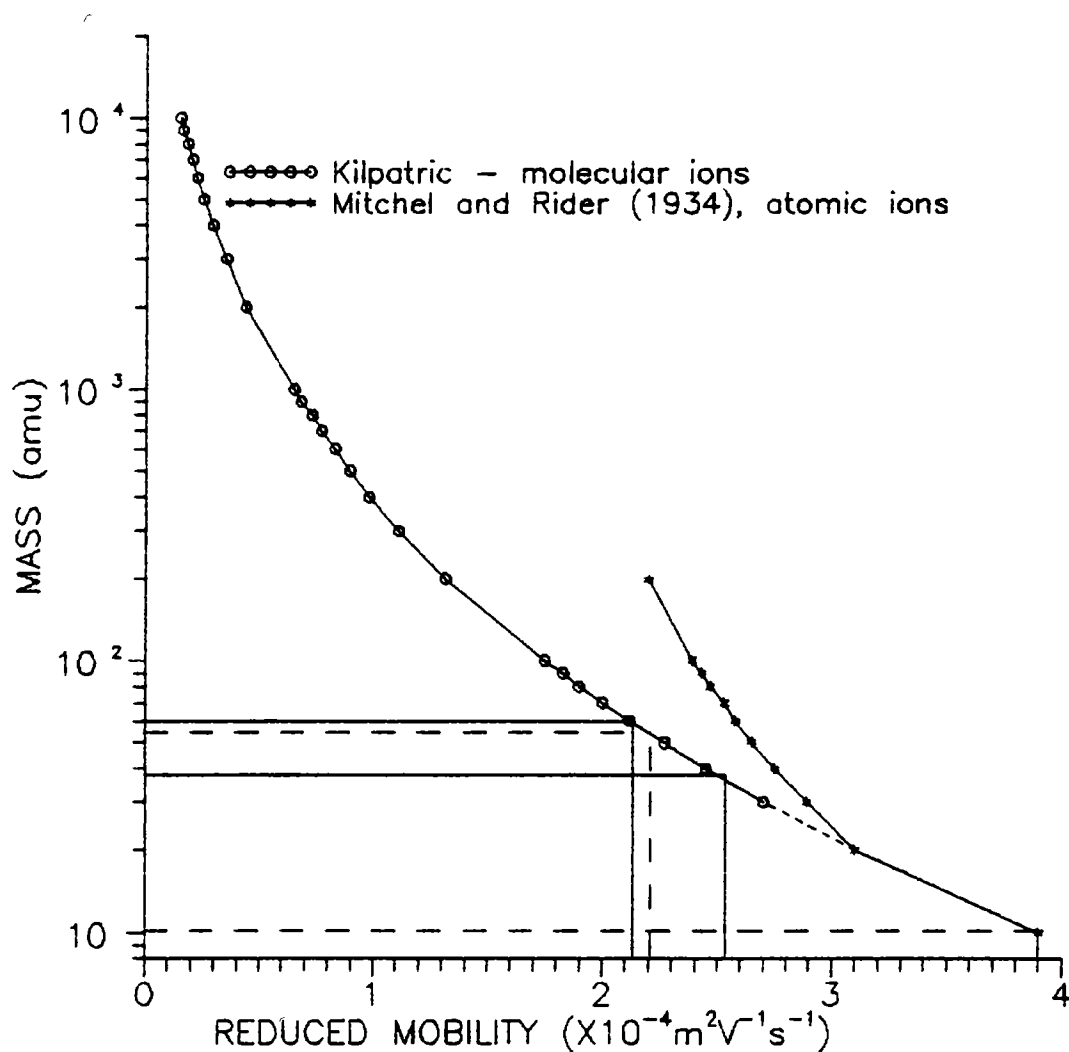


FIGURE 3. 9. Laboratory measurements of reduced mobility as a function of ion mass, in Nitrogen. The range of reduced mobility obtained from the rocket measurements and the corresponding mass range are shown. Solid lines indicate the range of positive ions and dashed lines indicate the range of negative ions.

### 3.2.3. NEGATIVE ION DENSITIES:

The profiles of negative ion densities obtained in the third and the fifth flights are shown in Figure.3.10. The density of negative ions is comparable to that of positive ions up to the altitude where positive ion density reaches the minimum. The negative ion density continues to decrease and reaches a minimum at a slightly higher altitude than the positive ions. It then increases gradually with altitude and reaches a broad maximum around 85 km. The ion density falls rapidly beyond and disappears around 90 km.

The first studies in ionosphere using radio wave techniques demonstrated that electrons are nearly absent below 65 or 70 km during day and 75 or 80 km during night. After the first measurement of Johnson et al (1958) there have been only a very few measurements of negative ions. Narcisi et al(1971) and Arnold et al (1971) observed the region at night. The presence of a transition zone above which the concentration of negative ion decrease was established by observation but the altitude of this layer seemed to vary considerably with time (Arnold and Krankowsky,1977).

The transition between electrons and negative ions appears to be located near 70 km during the day with the negative ion concentration reaching negligible levels at about 80 to 85 km. The theoretically derived ion density profile usually decreases above 70 to 75 km and disappears around 80 to 85 km (see for instance Nicolet and Aikin, 1960; Spjeldvik

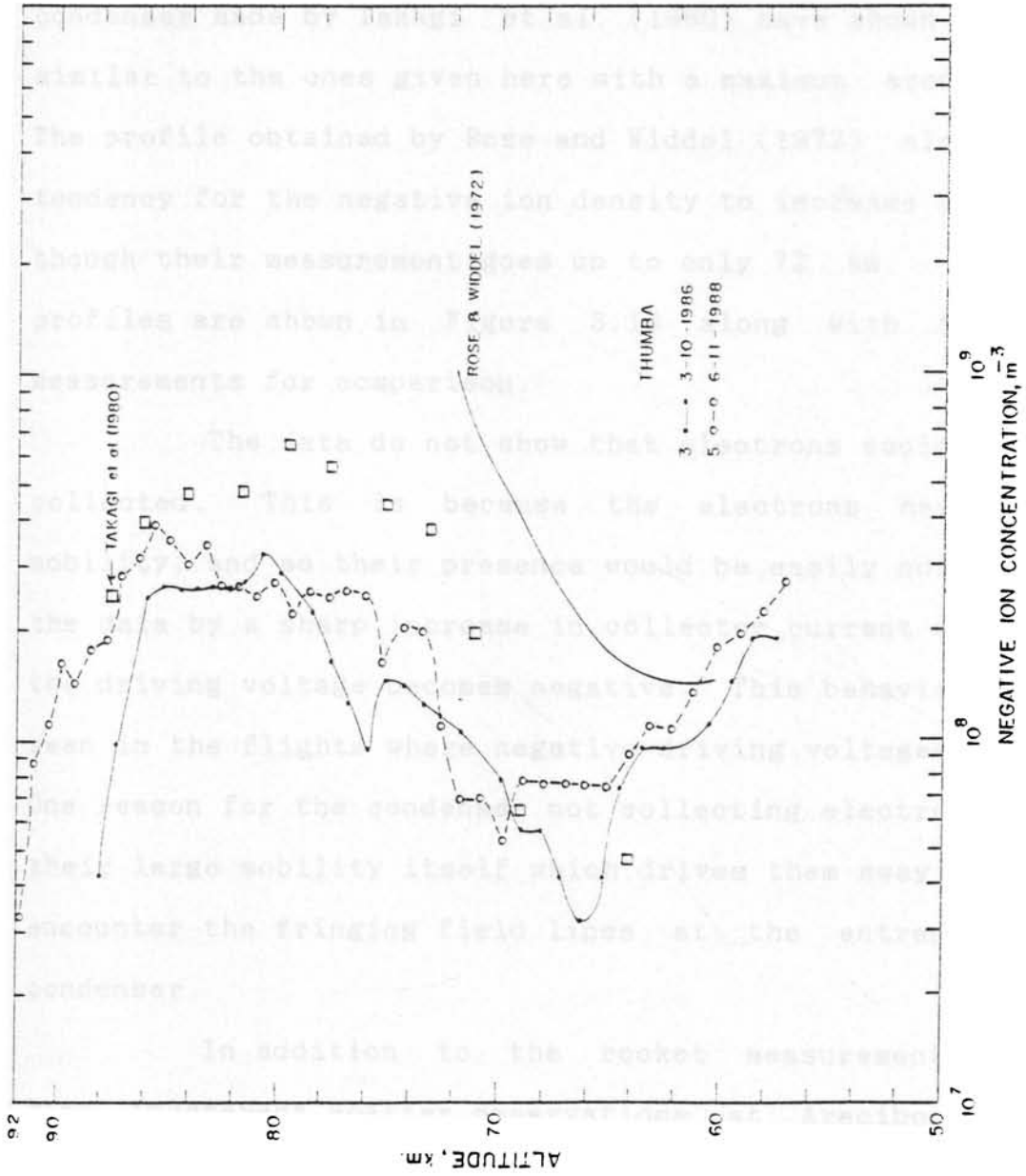


FIGURE 3.10. Negative ion density measurements from third and fifth flights along with those of Takagi et al. and Rose and Widdel.

and Thorne, 1975; Nath and Setty, 1976; etc.). The measurements reported here do not conform to these theoretical profiles. Negative ion density measurements using a Gerdien condenser made by Takagi et al. (1980) have shown a profile similar to the ones given here with a maximum around 80 km. The profile obtained by Rose and Widdel (1972) also shows a tendency for the negative ion density to increase above 70 km, though their measurement goes up to only 72 km. These two profiles are shown in Figure 3.10 along with the present measurements for comparison.

The data do not show that electrons could have been collected. This is because the electrons have a large mobility, and so their presence would be easily noticeable in the data by a sharp increase in collector current as soon as the driving voltage becomes negative. This behaviour was not seen in the flights where negative driving voltages were used. One reason for the condenser not collecting electrons may be their large mobility itself which drives them away, when they encounter the fringing field lines at the entrance to the condenser.

In addition to the rocket measurements reported here, incoherent scatter observations at Arecibo have also shown the presence, on several occasions, of a significant number of negative ions in the region from 85 to 95 km (Ganguly, 1984). Thus, the maximum in ion density around 85 km appears to be real. Some possible causes for large negative

ion densities to appear around the mesopause have been put forth by Chakrabarty and Ganguly (1989). Based on their ion chemical model, they show that either a large increase in the ozone number density (by a factor of about 1000) or a decrease in temperature by about 20 K from normal value around the mesopause could enhance the negative ion density to significant levels. Enhancement in ozone density near the mesopause have been reported, for example by Somayajulu et al.(1981) and a decrease in temperature by Tepley et al. (1981). The changes in the density of ozone could take place due to a variation in temperature. This is because several reactions controlling the chemistry of ozone are strongly dependent on temperature. Therefore enhancement in ozone density could be a cause for the high negative ion density reported.

Ionisation due to meteoric showers was suggested as a possible source for this layer (Prasad, 1989,1992). He in his model studies of the mesosphere, has used meteoric dust as a possible sink for electrons around mesopause and this results in negative ions. These ions are different from the negative ions found as a consequence of conventional gas phase chemistry. A meteor shower had been predicted a few days prior to the fifth flight. However unless by strange coincidence all these flights (the third and fifth reported here, that of Takagi et al., 1980, and of Rose and Widdel 1972) have been conducted either after or during meteor shower



periods, this layer in the negative ion density may not be caused by these showers.

Negative ion densities were measured by Conley et al (1983) from Canada during 26 February 1979 solar eclipse, but their data extend only up to about 70 km. However, they calculated the detachment coefficient based on their positive ion density measurements and the electron densities obtained in an accompanying experiment, and found that it was considerably less than theoretical expectations in the region from 60 to 80 km. Quadrupole mass spectrometric measurements carried out by Narcisi et al. (1983) as part of the same campaign showed the presence of two layers of negative ions, one of lighter ions below 75 km, and the other of heavier ions above 75 km. A heavy negative ion belt has been observed consistently by Narcisi et al. (1971,1972). Swider and Narcisi (1983) are unable to explain this phenomenon but suggest that they may be associated with meteoric debris. They as well as Conley et al. (1983), point out the inadequacy of current negative ion models.

#### 3.2.4.NEGATIVE ION MOBILITIES:

The negative ion mobilities measured in the two flights are shown in Figure. 3.11. Measurements of negative ion mobilities are very few and even mass spectrometric data appear to be conflicting. The first observation of negative ions suggested that the most abundant negative ion in the D

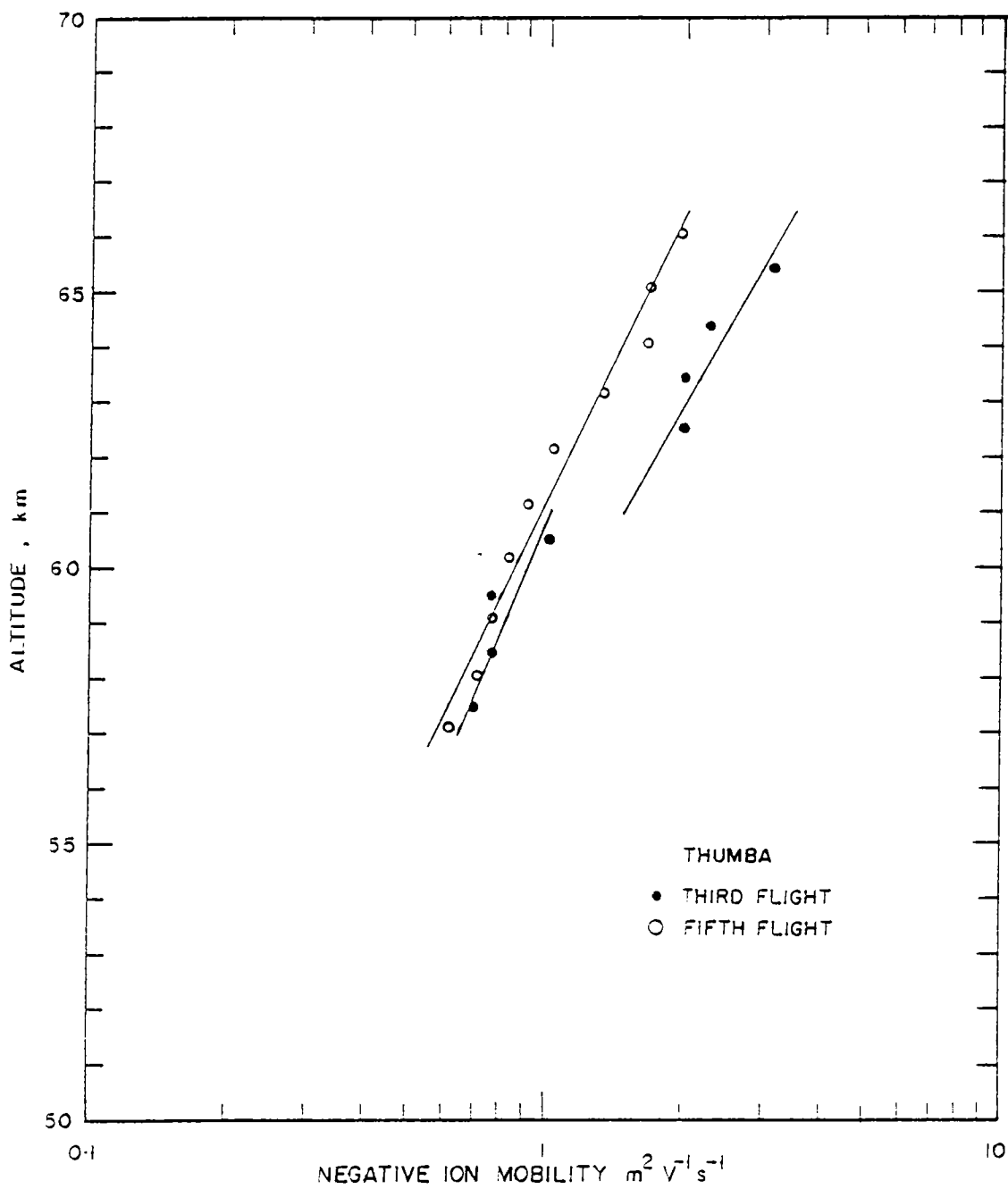


FIGURE 3.11. Negative ion mobility measurements from third and fifth flights. The straight lines are least square fits.

region is  $\text{NO}_2^-$  at mass 46 amu (Brasseur and Solomon, 1986). The measurement of Arnold et al. (1971) showed the significant ions to be  $\text{CO}_3^-$ ,  $\text{HCO}_3^-$  and  $\text{NO}_3^-$ . Narcisi et al. (1972) also found  $\text{NO}_3^-(\text{H}_2\text{O})_n$ , with possible admixtures of  $\text{CO}_3^-(\text{H}_2\text{O})_n$ , with  $n = 0$  to 5, as the major species. Viggiano et al. (1982) reported the most abundant ions below 80 km to be of mass  $61 \pm 2$  amu, which are considered to be the same as those seen by Arnold et al (1971). They also found ions with mass  $36 \pm 3$  amu and an ion of 76 amu, which was concluded to be  $\text{SiO}_3^-$ . The negative ion mobilities measured in the third flight were less (corresponding to a mass of about 35 to 50 amu) below about 62 km, while above this altitude larger mobilities (corresponding to 10 to 15 amu) were detected. The mobilities obtained in the fifth flight correspond to a mass of about 40 to 60 amu. Widdel et al. (1971) have measured such large mobilities as seen in the third flight, but Takagi et al. (1980) have measured only lower mobility ions. Thus more measurements are needed to obtain a better picture.

### 3.3. ERRORS IN MEASUREMENT:

The random error in computing ion densities and mobilities presented in this chapter have been estimated. This includes all estimable random errors in measurement from calibration to data reduction. It is found that in the regions of the profile where the ion densities and mobilities are the lowest a maximum error of  $\pm 20\%$  is present. Similarly

for those regions of the profile where the ion densities and mobilities are high it is found that a maximum error of  $\pm 6\%$  is present.

---

## CHAPTER - 4

### LOWER ATMOSPHERIC MEASUREMENTS

This chapter deals with the measurement of atmospheric electric parameters in the lower atmosphere using balloon-borne Gerdien condensers. This comprises of two sections. The first section deals with the technique of measurement. Here the details of design and fabrication of balloon payloads and the procedures followed in conducting the experiments are discussed. The balloon flights were conducted from T.I.F.R. Balloon Facility, Hyderabad, India (Geog. Lat:17.5°N, Long:78.6°E, AMSL 550m).

The results obtained from the measurements are discussed in the second section of the chapter.

#### 4.1. EXPERIMENTAL DETAILS:

Four balloon experiments were conducted using the Gerdien condenser technique. All the payloads were instrumented to measure polar conductivities, ion densities and their mobilities.

The range of altitude for balloon measurement is from ground to about 35 km and a balloon payload encounters a

different environment from that of a rocket payload. It does not encounter vibration, shock or spin, but has to function properly in a relatively sustained low temperature environment because of low ascent rate of balloons. Compared to a rocket, the space available for balloon payloads is relatively large. Typical dimensions of an integrated payload, called gondola, used in these experiments are about 3m × 1.5m × 1.5m in length, breadth and height respectively. Hence, the constraint on the dimensions of sensor or electronics of the payload is not severe in a balloon experiment. But the payload has to be designed and fabricated such that from the mechanical and electrical point of view the payload functions satisfactorily at very low temperatures.

In the first two experiments air flow through the sensor was accomplished by self aspiration; i.e. the sensor was mounted on the gondola in such a way that the ascent of the balloon created air flow through the sensor. In the later experiments a lobe pump was used to draw air through the sensor. The self aspirated and pumped measurements will be discussed separately.

#### 4.1.1.SELF ASPIRATED MEASUREMENTS:

The payload consists of a Gerdien condenser sensor and associated electronics. Figure.4.1 shows the block diagram of the payload. The parts of the diagram done in dashed lines indicate the changes incorporated from the second

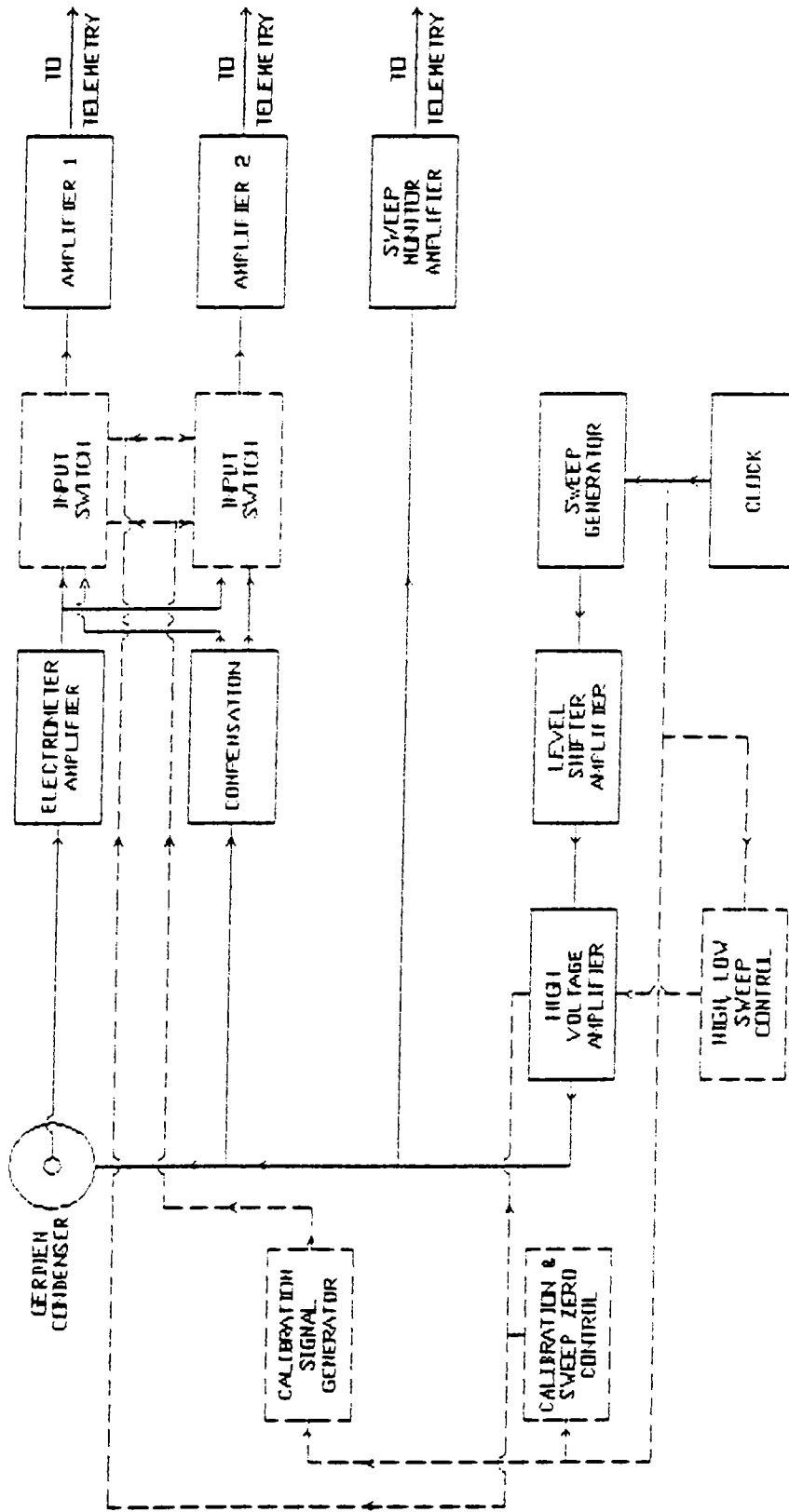


FIGURE 4.1. Functional block diagram of a Gerdien condenser balloon payload. Parts of the diagram done in dashed lines indicate the changes incorporated from the second flight onwards. A similar system with necessary changes in the gains of voltage amplifiers and high voltage amplifiers was used for pumped measurements also.

flight onwards. The blocks will be discussed in detail.

#### 4.1.1.1. The sensor:

A balloon payload does not encounter shock and vibration and so a sensor which is relatively simple in construction was designed and fabricated for balloon experiments. Details of construction of a typical balloon-borne Gerdien condenser is described here.

The balloon-borne sensor in its different stages of assembly, and a completed one, are shown in Figure 4.2. The sensor consists essentially of a shield, driving electrode, collector, a base to support the sensor and a set of insulators. The driving electrode is made of brass and nickel plated. The shield is made of mild steel and electroplated with nickel. The shield is slightly larger in diameter and much longer in length than the driving electrode. The difference between outer diameter of driving electrode and inner diameter of the shield is only 1mm. Over the driving electrode, about three layers of 0.15 mm thick high voltage insulator sheet is wound and then the assembly is inserted into the shield. The number of layers of the insulator sheet are adjusted such that the driving electrode sits tightly inside the shield and that the shield extends slightly at the inlet end. This extension of the shield does the function of guard ring. There are four P.T.F.E. stoppers, mounted diametrically opposite inside the shield, two at each end of



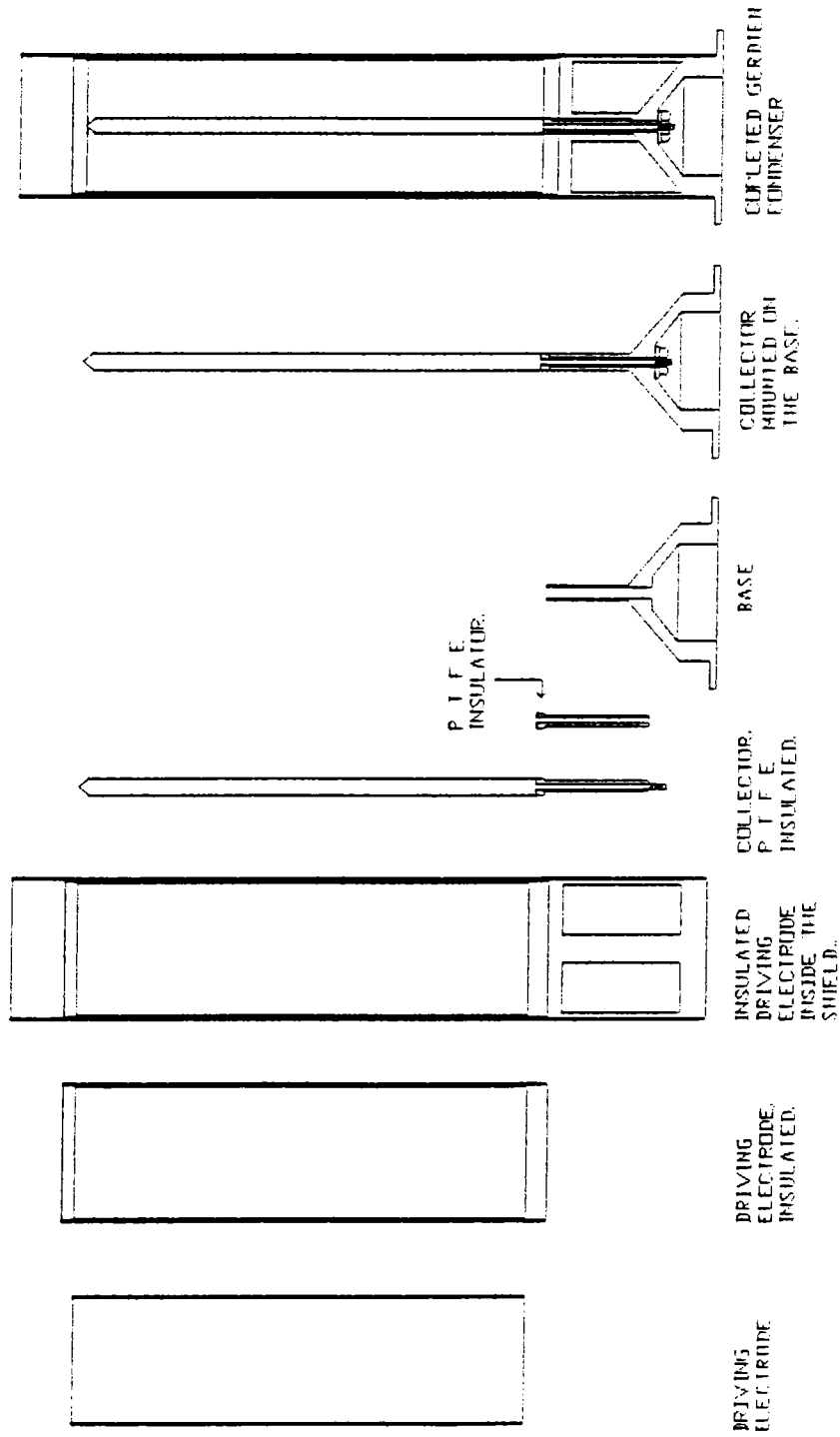


FIGURE 4.2. Stages of construction of a typical balloon-borne sensor for self aspirated measurements. Starting from the driving electrode different stages of assembly are depicted. a completely assembled sensor is also shown at the end.

the driving electrode. These stoppers are meant to arrest motion of driving electrode, if any. Electrical connection to the driving electrode is accomplished through a 10 mm port on the shield.

The shield is fabricated from a tube of same length as that of the sensor. The lower portion of the shield itself acts as the support legs. For this four similar and equally spaced slots of required dimensions are cut along the length at the lower end of the tube so that the remaining portion serve the function of support legs. The slots serve the function of outlets for air flow. The length of the legs are such that on completion of assembly of the sensor, the lower ends of both driving electrode and collector are exactly at the same level. The lower end of the legs slip over the base and are fastened to it using screws and nuts.

The collector is made exactly in the same way as in the rocket payload.

The base is made of mild steel and electroplated with nickel. The base has a flange at the bottom with four holes in it. The sensor is mounted with screws and nuts using these holes.

#### 4.1.1.2. Sensor design:

In designing a balloon-borne sensor, the objective is to make a sensor which can be operated in conductivity and ion-trap modes throughout the altitude range of measurement.

Here, the relationship between saturation voltage, sensor dimensions and mobility require careful consideration. Eqn. (21) in chapter.2, which shows the relationship between these parameters is reproduced here for the sake of convenience.

$$V_s = \frac{U (b^2 - a^2) \ln(b/a)}{2 L \mu} \quad (21)$$

For simultaneous measurement of conductivity, ion density and ion mobility a triangular sweep is used as the driving voltage. Then, the amplitude of the sweep should be such that the condenser operates in ion-trap mode at a voltage equal to or slightly less than the peak value of the sweep. From eqn.(21) it is seen that for a given velocity of ascent of the balloon, the saturation voltage  $V_s$  is directly proportional to the difference of squares of electrode diameters and inversely proportional to the length of the condenser and ion mobility. The variation of  $\ln(b/a)$ , relatively, is not of considerable significance.

Now, the ion mobility, which is inversely proportional to ambient air density, increases exponentially with altitude. Therefore very high driving voltages of the order of  $\pm 100$  V will be required to operate a condenser of a few centimeters in diameter and a few tens of centimeters in length in ion-trap mode, at ground and at low altitudes. This requirement can be met by an increase in length. However, the required length  $L$  would then make the condenser unwieldy.

There are some practical problems in fulfilling the requirement for a high driving voltage. First of all, a high driving voltage means that a high voltage, bipolar sweep of the order of  $\pm 100$  V will have to be generated to conduct simultaneous measurement of conductivity, ion density and ion mobility, which is not very easy. Also, the batteries required for such a high voltage sweep is large and their weight & cost becomes considerable. Further, for all balloon flights, at least two other sensors of different type were flown along with the Gerdien condenser and so, there was an apprehension among other experimenters of such a high field of the Gerdien condenser interfering with the performance of the other sensors.

In addition to the above mentioned constraints on driving voltage, self aspirated balloon measurements have another problem pertaining to the altitude range of measurement. For the first few kilometers after launch the data can be noisy due to swinging and rotation of the gondola. Therefore, in both the self aspirated measurements, ion trap mode of operation was attempted only above about 5 km. Hence, taking all the above mentioned aspects into consideration it was decided to operate the condenser with a driving voltage of about  $\pm 30$  V triangular sweep.

Once the sweep voltage has been decided, a and b values are chosen such that the collector current is measurable for the lowest expected ion density and lowest

expected ascent rate. The ascent rate of the balloon is expected to vary from about  $1 \text{ m s}^{-1}$  to about  $4 \text{ m s}^{-1}$ . For selecting the value of  $\mu$  for design, initially the lowest mobility value corresponding to an arbitrarily chosen altitude is taken. The length  $L$  is then calculated from eqn.(20) in chapter.2.

$$L = \frac{\ln(b/a) U (b^2 - a^2)}{2 \mu V_s} \quad (20)$$

On calculation if the sensor is found to be unwieldy in length, it is reduced to a practically feasible limit. Recalculation is then done to estimate the mobility value corresponding to the reduced length and the altitude corresponding to this mobility is found out. Above this altitude the sensor will operate in conductivity and ion-trap modes and below this altitude, it will operate only in the conductivity mode.

Table 4.1 shows the dimensions, sweep voltages and collector current range of the sensors used in the two balloon experiments.

TABLE - 4.1

Dimensions, sweep voltages and collector current range of sensors used in the first and second balloon experiments

| Flight No. | Driving electrode diameter. (m) | Collector diameter (m) | Length of condenser. (m) | Sweep voltage. (V) | Collector current range (pA) |
|------------|---------------------------------|------------------------|--------------------------|--------------------|------------------------------|
| IMAP-5     | 0.064                           | 0.016                  | 0.131                    | $\pm 35V$          | 0.5 to 20.                   |
| IMAP-8     | 0.064                           | 0.012                  | 0.30                     | $\pm 35, \pm 5$    | 0.5 to 20.                   |

#### 4.1.1.3. The sweep generator:

In balloon payloads also, as in the case of rocket payloads, an oscillator provides the basic sweep and a clock output. The sweep is amplified by a high voltage amplifier to obtain the required high voltage sweep. The clock output was used from the second flight onwards for synchronous control of in-flight calibration and sweep zero check. The functional block diagram and circuit diagram of the sweep generator are shown in Figure 4.3. a&b.

The basic sweep is a triangular wave of  $\pm 2.5V$  amplitude. This is amplified and level shifted in the level shifter amplifier to obtain a symmetric bipolar sweep. This is further amplified by the high voltage amplifier to obtain the desired driving voltage. The telemetry input range is from  $-5 V$  to  $+5 V$  and so this driving voltage is attenuated to  $\pm 4.5 V$  by the attenuator amplifier and fed to the telemetry

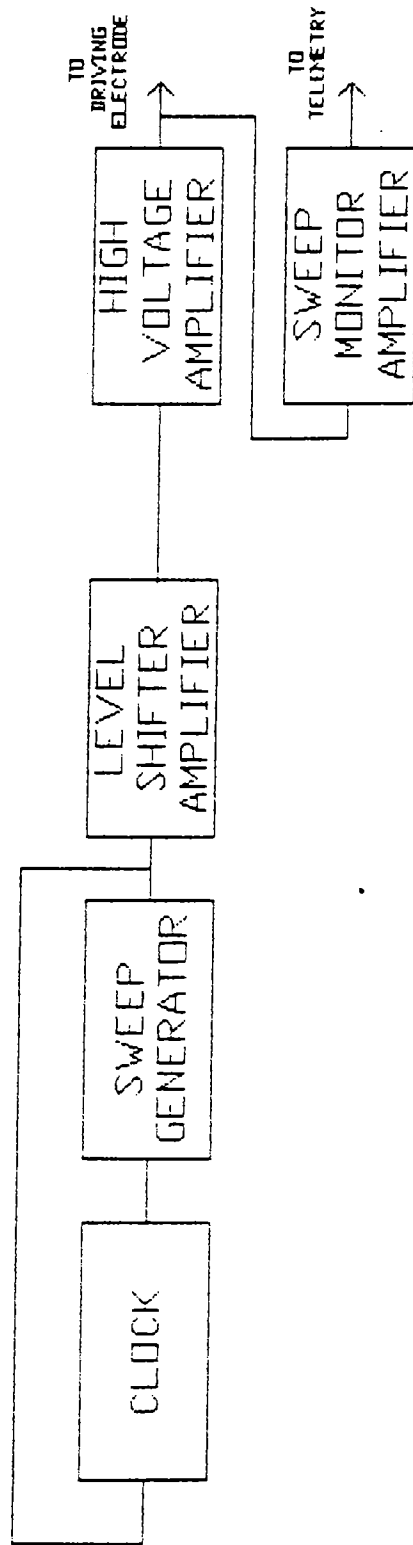
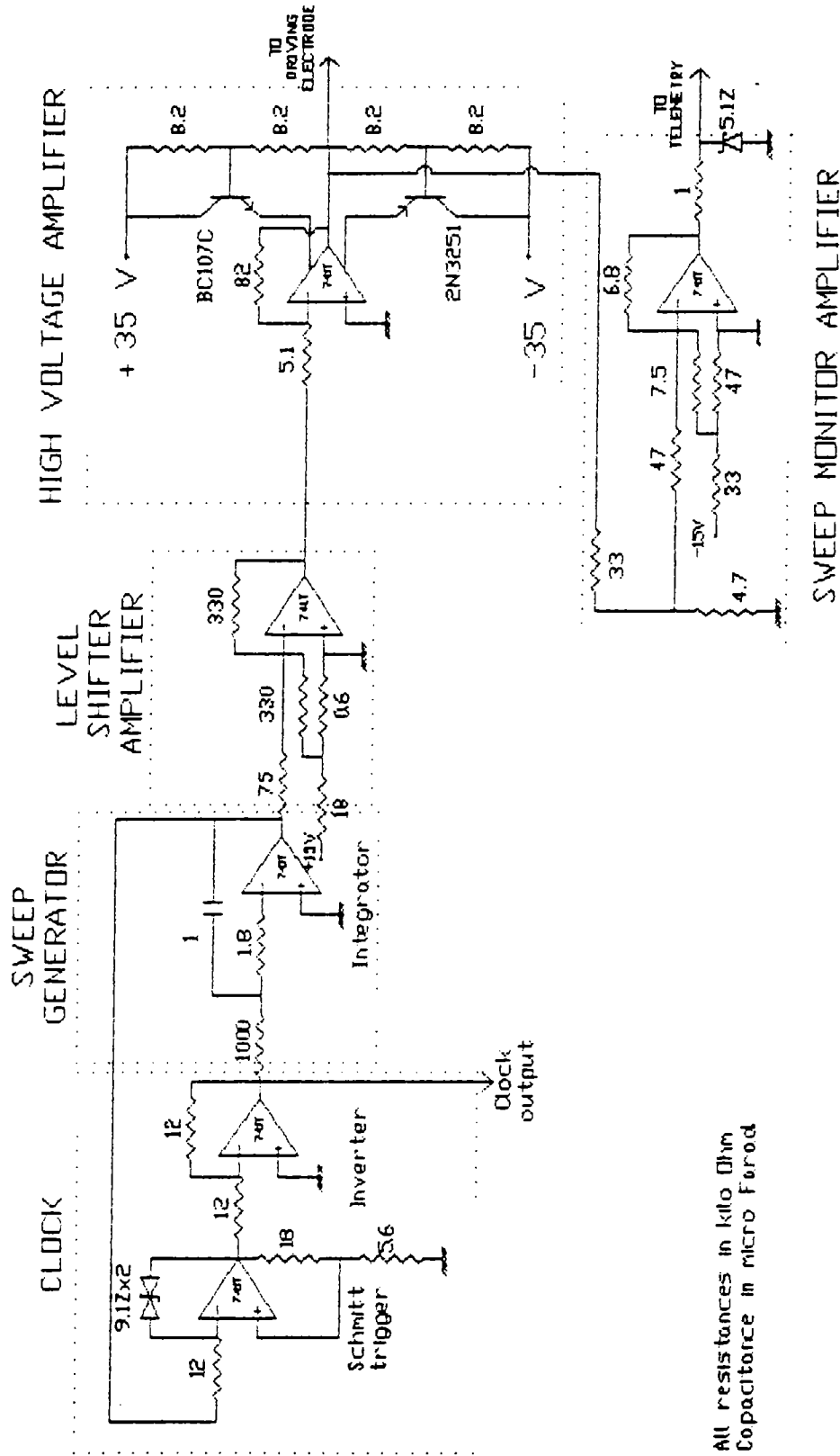


FIGURE 4.3.a. The sweep generator in balloon payload; a functional block diagram.



All resistances in kilo Ohm  
Capacitance in micro Farad

FIGURE 4.3.b.Circuit diagram of the sweep generator.



input. The frequency of sweep is determined by the time constant setting of the integrator in the sweep clock. Depending on the number of samples required for every kilometer of altitude the frequency of sweep is set. For example in the first flight a sweep of 0.05 Hz (20s period) was used. With a maximum balloon ascent velocity of 15 km/hr the sweep of 0.05 Hz yields twelve data samples for every kilometer of altitude.

From the second experiment onwards, sweeps of two amplitudes were alternated and fed to the driving electrode. That is, five cycles of  $\pm 30$  V sweep was alternated with five cycles of  $\pm 5$  V sweep. This was accomplished by incorporating a switching circuit which changed the gain of the high voltage amplifier after every five cycles to obtain the  $\pm 5$  V and  $\pm 30$  V sweeps. The introduction of low voltage sweep helped not only in obtaining good conductivity data at low altitudes but also in obtaining good ion density data at high altitudes.

In-flight calibration and sweep zero check were introduced from the second flight onwards. The sweep zero check was done by disconnecting and grounding the driving electrode. This was done at a repetition rate of 20 minutes. Each sweep zero check was followed by the in-flight calibration. The calibration signal was derived from the clock output.

#### 4.1.1.4. The current measurement system:

The block diagram and circuit diagram of the system used for measuring collector current is shown in Figure.4.4 a & b. An electrometer amplifier constructed with an AD515L operational amplifier converts the collector current to voltage. The required sensitivity of the electrometer amplifier is found out from the ascent rate of the balloon and sensor dimensions. For each balloon experiment, the expected collector current range was calculated and it was found that current of the order of a fraction of a pA could be expected. Therefore an electrometer amplifier of 0.1 V/pA sensitivity was designed and fabricated for all the balloon experiments.

The output of the electrometer amplifier is fed to two independent amplifiers of different gains wired around operational amplifiers. They provide two overlapping ranges of current measurement. The compensation for displacement current is done at these amplifiers. The sweep is fed to two compensation circuits, each consisting of a capacitor and a pre-set potentiometer. The outputs of these circuits are fed to the summing input of the amplifiers. The pre-set potentiometers control the amplitude of compensation signal fed to the amplifiers. During fabrication and testing these potentiometers are adjusted so that the signal due to displacement current gets nullified. The output of the amplifiers are fed to telemetry.

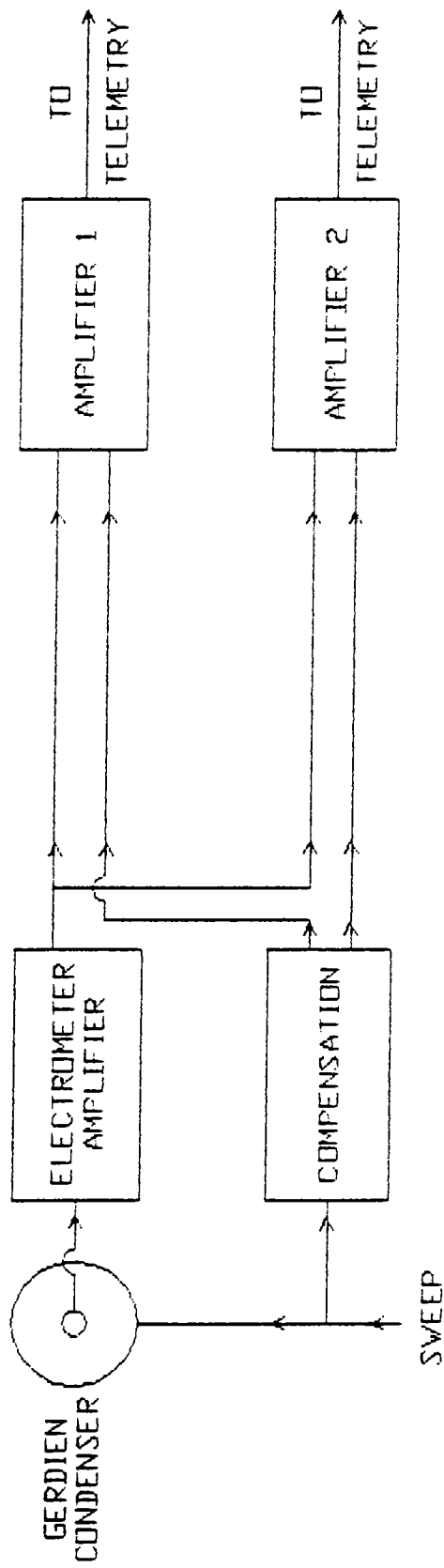


FIGURE 4.4.a. Current measurement system used in a balloon payload; a block diagram.

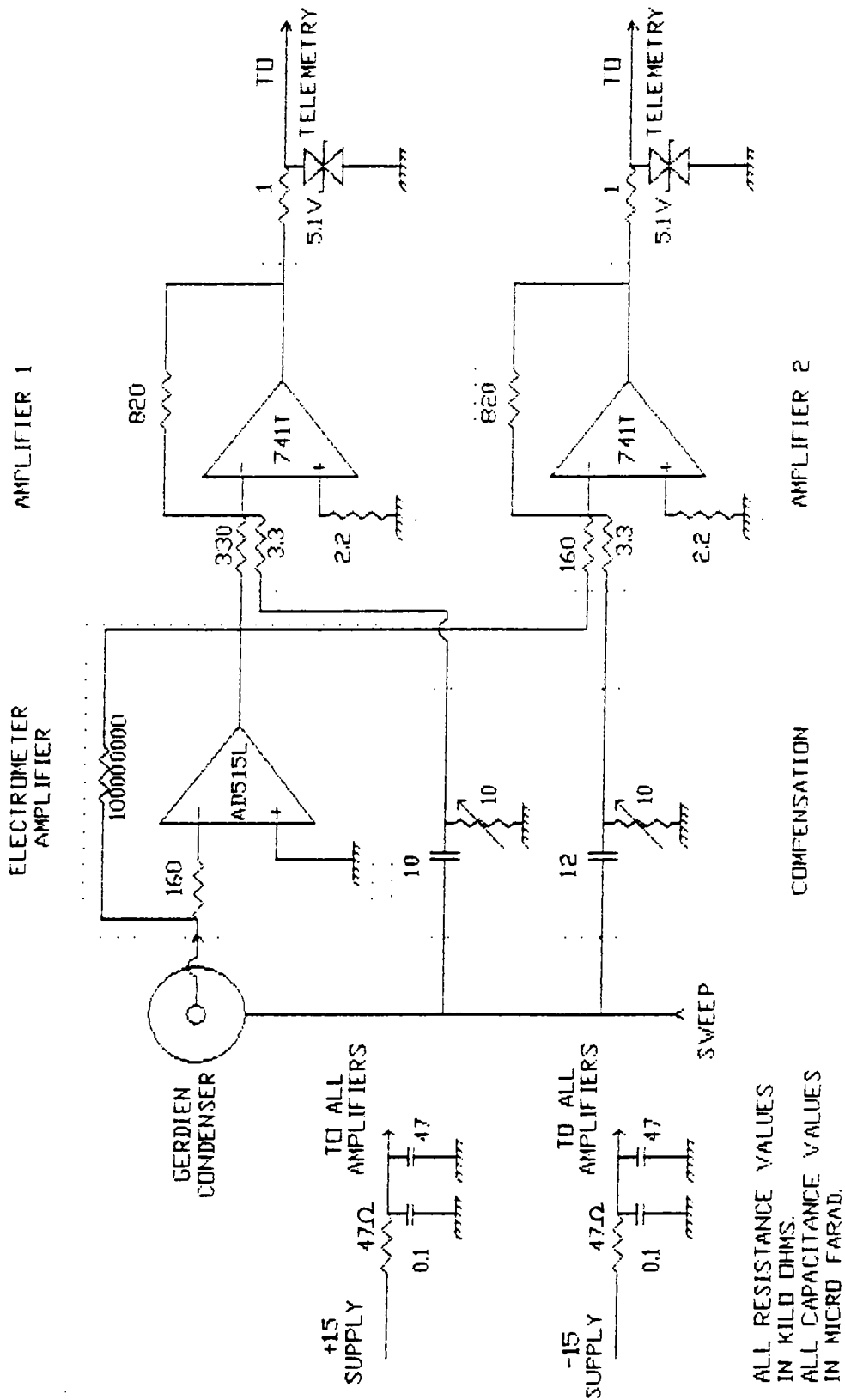


FIGURE 4.4.b. Circuit diagram of the system used for measurement of collector current in a balloon payload.

With a telemetry input range of  $-4.5$  to  $+4.5$  V, the overall sensitivity and range of measurement for each experiment is determined by the dimensions of the sensor, speed of air flow, the electrometer amplifier sensitivity and gain of amplifiers. Therefore, taking all these factors into consideration the gain of amplifiers for each experiment is decided.

The current measurement system was calibrated at various temperatures encountered during flight, with the Keithley picoampere current source. Also, the attenuation factor between the sweep applied to the sensor, and the output of the sweep monitoring channel were noted. The calibration and compensation for displacement current were done along with the cable connecting the sensor to the electrometer amplifier.

#### 4.1.2. PUMPED CONDENSER MEASUREMENTS:

##### 4.1.2.1. Need for pumped condenser measurements:

In Gerdien condenser measurements, for computing the values of ion density and mobility from the raw data, it is essential that the speed of air flow through the condenser is known. The self-aspirated condensers make use of the ascent of the balloon to generate air flow through them and so the speed of air flow through the sensor is assumed to be equal to the ascent rate of the balloon. This can lead to, two types of errors. One concerning the reduction of air flow inside the condenser has already been discussed in section 2.3.2 on

flow considerations. The other is, not exactly an error but a difficulty in estimating the speed of air flow for computation of ion density and mobility. This arises because ascent rate is estimated from the position of the balloon which is taken at a much larger interval, about 5 minutes, compared to the sampling time of 5 seconds. The problem is aggravated when the ascent of the balloon is not smooth.

One way to eliminate this problem is to draw air through the condenser at a known constant rate. This method of operation has certain advantages. The air flow through the sensor becomes independent of the motion of the balloon and so measurement is not affected even when the motion of the balloon is highly erratic. Also measurement is possible at ground and at float.

#### 4.1.2.2. The Pump:

The balloon payload encounters pressures from about 1000 mb at surface to about 5 mb at float altitude and temperature from about 25°C to -20°C. The pump used for aspiration should function satisfactorily within this temperature and pressure range and should also have a constant pumping rate. A pump that can satisfy these requirements and is convenient to use is the lobe pump. Fabrication of a lobe pump is also difficult because it involves machining to a very high degree of tolerance.

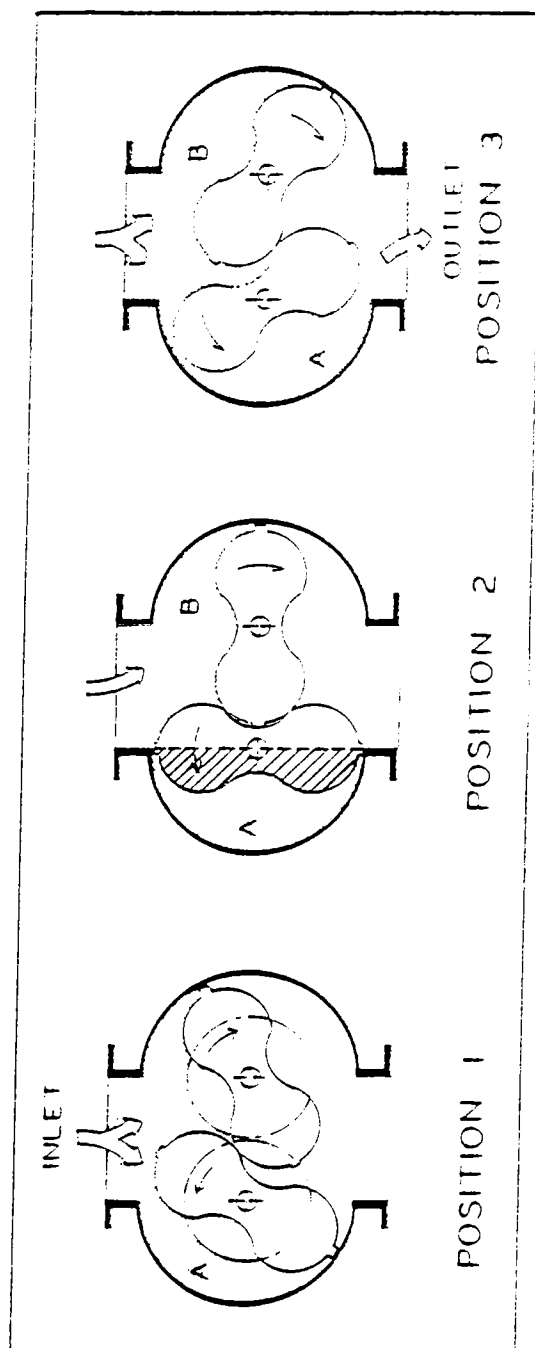
Therefore commercially available lobe-type gas flow

meters were converted and used as pumps in the pumped condenser measurements. This was found to be easy and cost-effective compared to fabricating a lobe pump.

The lobe-type flow meter essentially consists of two figure of eight lobes, coupled to each other by two similar gear wheels for synchronous rotation. The meter also has a counter type display unit. The operation of the meter is shown schematically in Figure 4.5. In order to convert the meter into a pump, its display section was disconnected and the lobes were driven using an AC synchronous motor. The required AC voltage for running the motor was generated with an inverter. The mechanical coupling between motor and meter was established through a third gear wheel attached to the motor. The performance of the pump at various pressures encountered during flight was determined with the help of a vacuum chamber. A similar meter was used to measure the flow rate delivered. The calibration curve is shown in Figure 4.6. The pumping rate was found to remain essentially constant with pressure. The fourth flight carried a higher capacity pump compared to the third so that a larger current could be obtained, thus improving the sensitivity of the instrument.

#### 4.1.2.3. The sensor and pump assembly:

Figure 4.7 shows the schematic diagram of the sensor, pump and their assembly. The sensor is similar in construction to self aspirated sensors. A two inch tube is



POSITION 1.- As the left impeller rotates in a counter clockwise direction toward vertical position, air enters the space between impeller and cylinder. POSITION 2.- At vertical position, a definite volume of air is contained in the compartment marked A. POSITION 3.- As the impeller continues to turn, the volume of gas is discharged. The whole process is repeated twice for each complete revolution of impeller shafts.

FIGURE 4.5. Principle of operation of a lobe type meter.



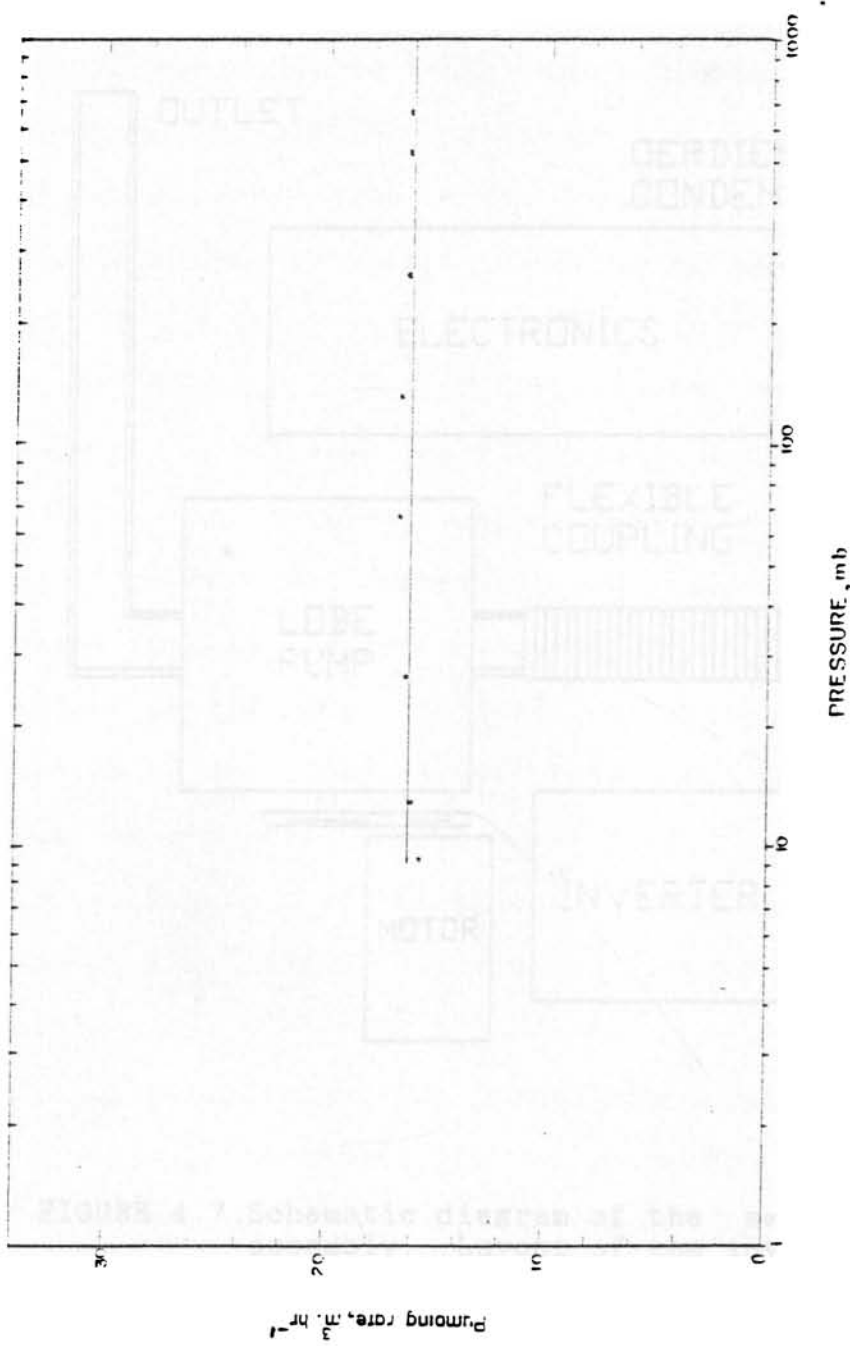


FIGURE 4.6. Variation of the pumping rate with pressure of the lobe pump used in the flight IMAP - CO1. The straight line corresponds to the mean value of the pumping rate of 16.24 m hr<sup>-1</sup>, with a standard deviation of 0.37m hr<sup>-1</sup>.

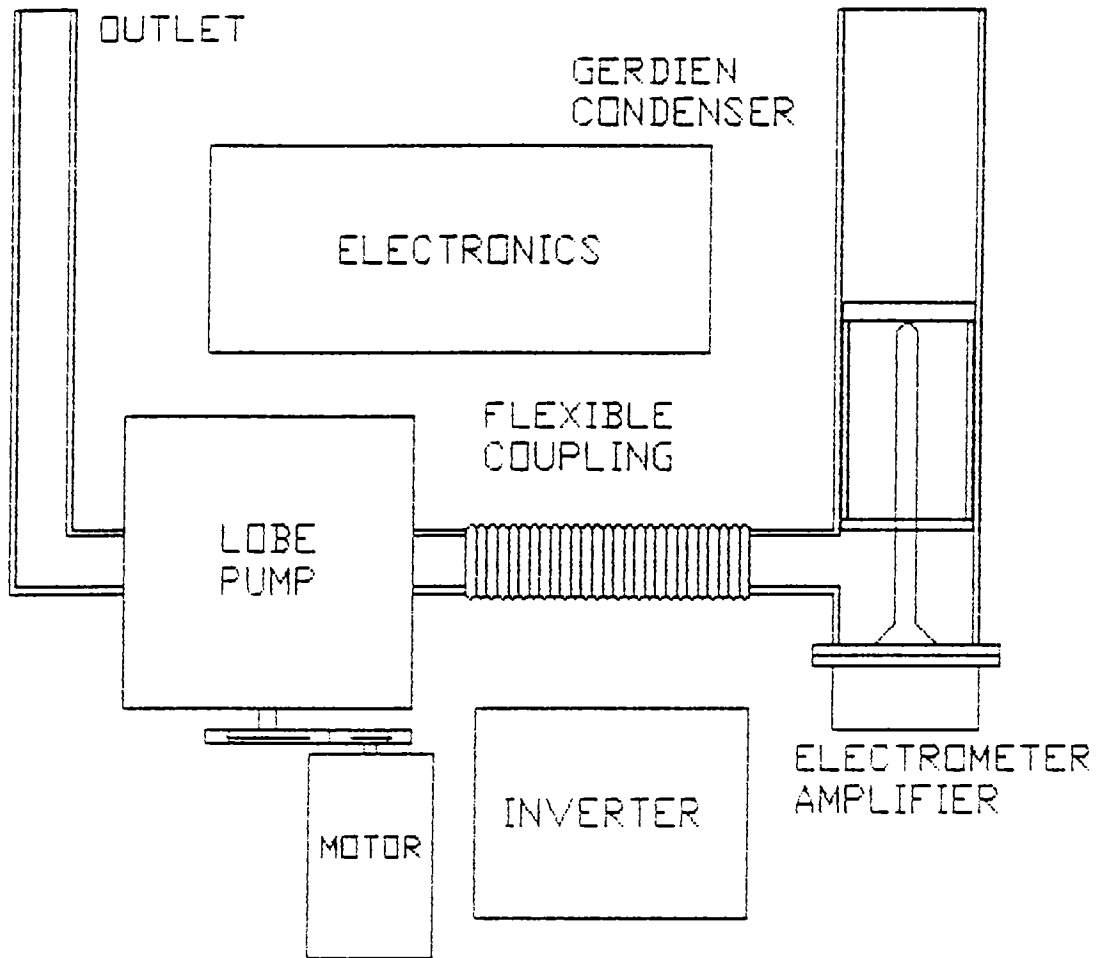


FIGURE 4.7. Schematic diagram of the sensor, pump and their assembly. Layout of the inverter and electronics are also shown.

welded to the shield near the base of the condenser for outlet of air to the pump. The connection between the pump and Gerdien condenser is established through a flexible coupling. The flexible coupling is meant to reduce transmission of vibration of the pump to the Gerdien condenser. During the balloon flight the pump and sensor assembly is kept inside the gondola and inlet and outlet tubes only protrude outside the thermal dressing. For this reason the shield is extended by about 30 cm to serve the function of inlet tube also.

In the first pumped measurement, the electrometer amplifier was kept separately and it was connected to the sensor through a graphite coated P.T.F.E. insulated coaxial cable. In the second payload the electrometer amplifier was mounted on the sensor itself. As shown in the diagram the mounting was done in such a way that the electrometer became virtually a part of the sensor. This helped in eliminating the P.T.F.E. coaxial cable which is a source of triboelectric noise.

#### 4.1.2.4. Electronics for pumped measurements:

Electronics of the pumped condenser measurement payload consisted of two systems, namely the measurement system and the drive system for the pump.

The drive system consisted of electronics necessary for driving the pump. As mentioned earlier the pump was driven by an AC synchronous motor. The power supply requirement of 220 V AC at 50 Hz of the motor was provided by

a square wave AC inverter running on 20 V DC power supply. The DC supply was provided by a battery of lithium cells. To take care of the on load reduction in voltage with time of the lithium cells the 20 V DC supply was derived through a series regulator from a 32 V supply.

The measurement system was similar to the one used in self aspirated measurements. The dimensions, sweep voltages and collector current range of the pumped condensers are given in Table 4.2.

TABLE - 4.2  
Dimensions, sweep voltage and collector current range of sensors used in pumped condenser measurements.

| Flight No. | Driving electrode diameter. (m) | Collector diameter (m) | Length of condenser. (m) | Sweep voltage. (V) | Collector current range (pA) |
|------------|---------------------------------|------------------------|--------------------------|--------------------|------------------------------|
| IMAP-C1    | 0.08                            | 0.0116                 | 0.15                     | ±20, ±2.           | ±0.05 to ±2.5                |
| IMAP-C05   | 0.08                            | 0.0116                 | 0.15                     | ±20, ±2.           | ±0.05 to ±2.5                |

The measurement system, in addition, had a circuit to monitor the speed of the motor. This was done in an indirect way by monitoring the inverter frequency. The inverter being a relatively high power sub-system of the payload, it was electrically isolated from the measurement system

to avoid interference. Therefore the inverter signal was fed to the measurement system through an opto-isolator. This signal, after necessary scaling in amplitude and frequency was fed to a 0 to 6 V telemetry channel.

#### 4.1.3. TEST, INTEGRATION AND FLIGHT DETAILS:

##### 4.1.3.1. Test and integration:

After fabrication the payload is subjected to a set of tests stipulated by the Balloon Facility. As in the case of rocket payloads, these tests are meant to weed out weaklings and are based on the environment encountered by a balloon payload. The ambient temperatures during balloon flight can reach as low as  $-82^{\circ}$  C. However, the payloads are mounted inside a gondola and are insulated by a thermal dressing, as described later. The temperatures inside the gondola usually remain within a few degrees around zero, which is also due to its large thermal capacity. But the payloads are tested for temperatures down to  $-20^{\circ}$  C. First, the payload is tested for satisfactory performance at various temperatures from  $-20^{\circ}$  C to  $10^{\circ}$  C. Further the performance of the payload at various pressures encountered during flight is checked. The payload is then integrated with other systems in the gondola and checked for proper functioning. A final flight worthiness test is conducted on the integrated payload by keeping it on for 24 hr. The payload is also checked for satisfactory performance before and after each test.

#### 4.1.3.2. Thermal dressing:

On completion of all the tests a three layer thermal dressing is done on the gondola to protect it from low temperature environment. First the gondola is covered with an aluminised mylar film in such a way that the reflecting surface faces inside. This reflecting surface helps in trapping infra-red radiation inside. Also, the mylar film absorbs the infrared radiation and reradiates back to the gondola. Further the gondola is covered with a layer of 2 inch thick polystyrene foam. Over the foam, for further insulation is given, a covering of two layers of mylar film.

#### 4.1.3.3. Payload layout:

In both the self-aspirated measurements the sensor was mounted on a platform, extending from one side of the gondola by about 0.5 m. Layouts of self-aspirated and pumped condenser balloon payloads are shown in Figure 4.8.

As shown in Figure 4.8 the sensor was mounted on the extended platform and the box containing the electronics was mounted inside the gondola on the nearest flight deck. The box had two connectors, one P.T.F.E insulated co-axial connector for connecting the electrometer amplifier to the collector and another rack and panel connector for all the other connections. An RG-178 P.T.F.E insulated co-axial cable of about 60 cm length was used to connect the collector to the

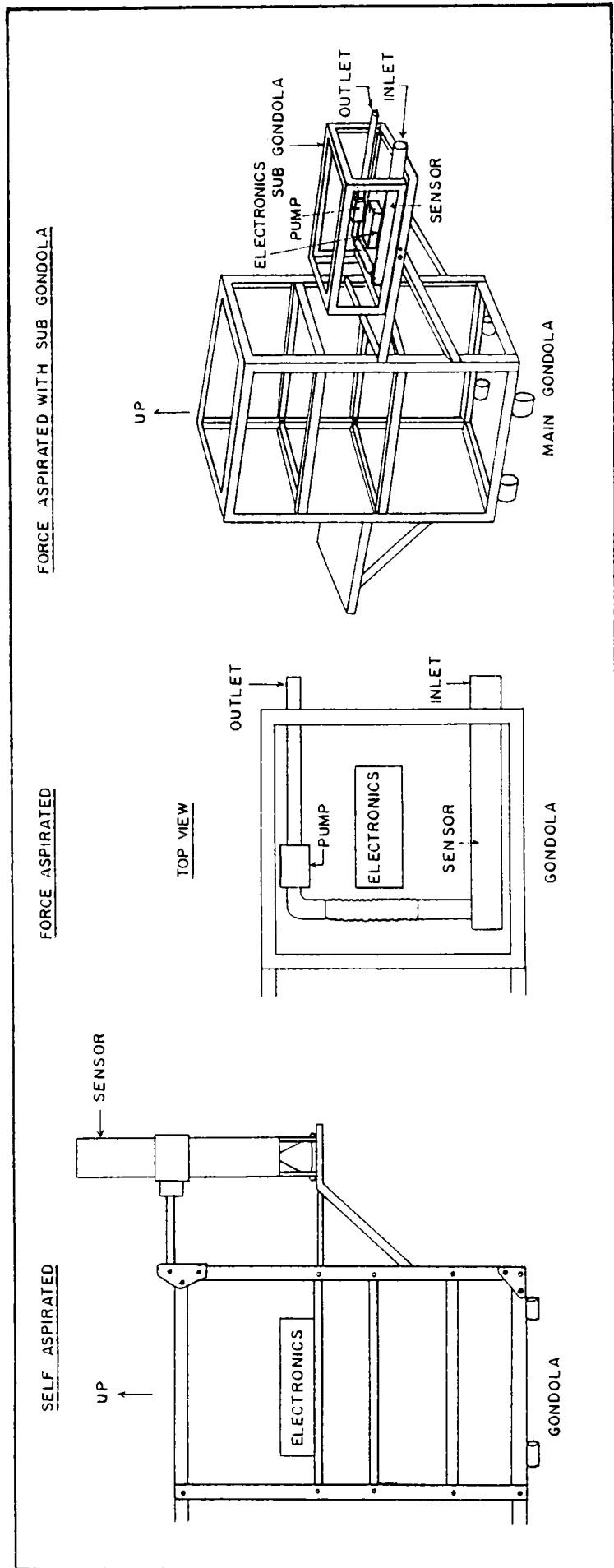


FIGURE 4.8. Payload layout in balloon gondola. Layout in the case of self aspirated and pumped measurements are shown. The sensor can be seen to be mounted on an extended platform in the self aspirated case. A sub-gondola used in IMAF C-05 is also shown.

electrometer amplifier. Amplifier end connection of the cable was accomplished through the co-axial connector and at the sensor end the inner conductor was soldered to a terminal at the lower end of the collector. The cable was anchored at every few centimeters. The shield of the cable was grounded only at the box end to avoid ground loop problems.

The flights were conducted from TIFR Balloon facility, Hyderabad. Table 4.3 summarises the details of the four flights. For both the self aspirated measurements data were obtained from about 4 km.

For the first pumped condenser flight data were obtained from about 4 km. For the last flight namely IMAP-C05, continuous conductivity data were obtained from ground to float altitude of 35.8 km. Ion density and mobility data could be obtained only at float from about 0441 hr to 0800hr.

TABLE 4.3

| Flight no. | Launch date | Launch time (Hr,IST) | Float altitude (km) |
|------------|-------------|----------------------|---------------------|
| IMAP - 5   | 16-2-1985   | 0121                 | 27.3                |
| IMAP - 8   | 6-12-1985   | 2351                 | 33                  |
| IMAP - C1  | 22-12-1986  | 0142                 | 33                  |
| IMAP - C05 | 22-4-1989   | 0158                 | 35.8                |



#### 4.1.3.4. Flight details:

A typical balloon load line is shown in Figure.4.9. The part marked main instrument (also called gondola) contains all scientific payloads, control instrumentation and telemetry.

The Gerdien condenser instrument worked satisfactorily in all the flights. Only ascent data were taken for analysis. The descent data was found to be noisy. Conductivities, ion densities and mobilities of both positive and negative ions were obtained in IMAP-5. In IMAP-8, both positive and negative ions were collected up to an altitude of about 15 km. Above this altitude, the collection of positive ions began to reduce and from about 18 km onwards, no positive ions were collected. In the case of IMAP-C1, no positive ion data were obtained at all. Negative ion data were obtained normally in both flights. This was found to be the case with other types of sensors, flown along with the Gerdien condenser, also. The gondola seems to have been collecting charges of one polarity, and not discharging as expected. As the relaxation times of a conductor are very small in the upper troposphere and above, the gondola, in normal circumstances, should reach equilibrium with the surroundings very quickly. However the flight results do not indicate this.

To eliminate this problem, it was felt necessary to

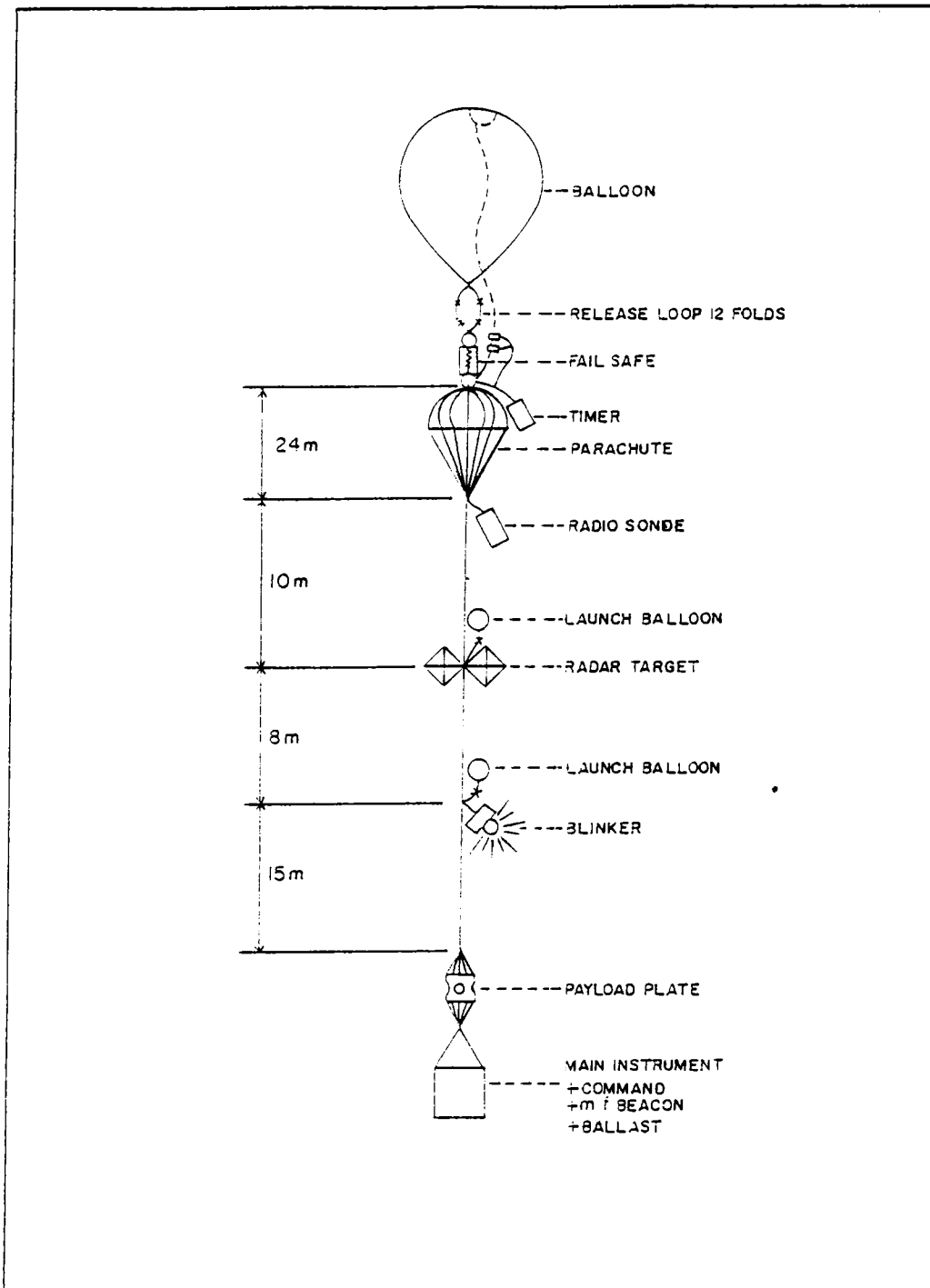


FIGURE 4.9.A typical balloon load line. The part marked main instrument (gondola) contains all scientific payload loads, control instrumentation and telemetry

separate the experiments into smaller sub-gondolas attached to the main one. In IMAP-C05 flight, therefore, the payload was made into a self-contained package (sub-gondola), except for telemetry and power, and attached to the side of the main gondola. Possibly due to this and other steps taken to prevent gondola charging, both positive and negative ions were measured in this flight. In Figure.4.8, along with the layout of the self-aspirated payload, layouts of the two pumped condenser payloads are also shown.

## 4.2. RESULTS AND DISCUSSION:

### 4.2.1. CONDUCTIVITY

As mentioned earlier, polar conductivities were measured in all the flights from about 4 km onwards. In the last flight continuous conductivity data are available from the ground level to float altitude. Float data were obtained in both pumped condenser measurements. In IMAP-C1 flight the balloon remained afloat for about an hour from 0440 hr. In IMAP C-05 float data was obtained from about 0441 hr to 0800 hr.

The conductivity profiles from the self-aspirated condensers are shown in Figure 4.10.a. The positive and negative conductivities obtained in the first flight were very close to each other and well within the experimental errors. Therefore a profile of average polar conductivity was derived,

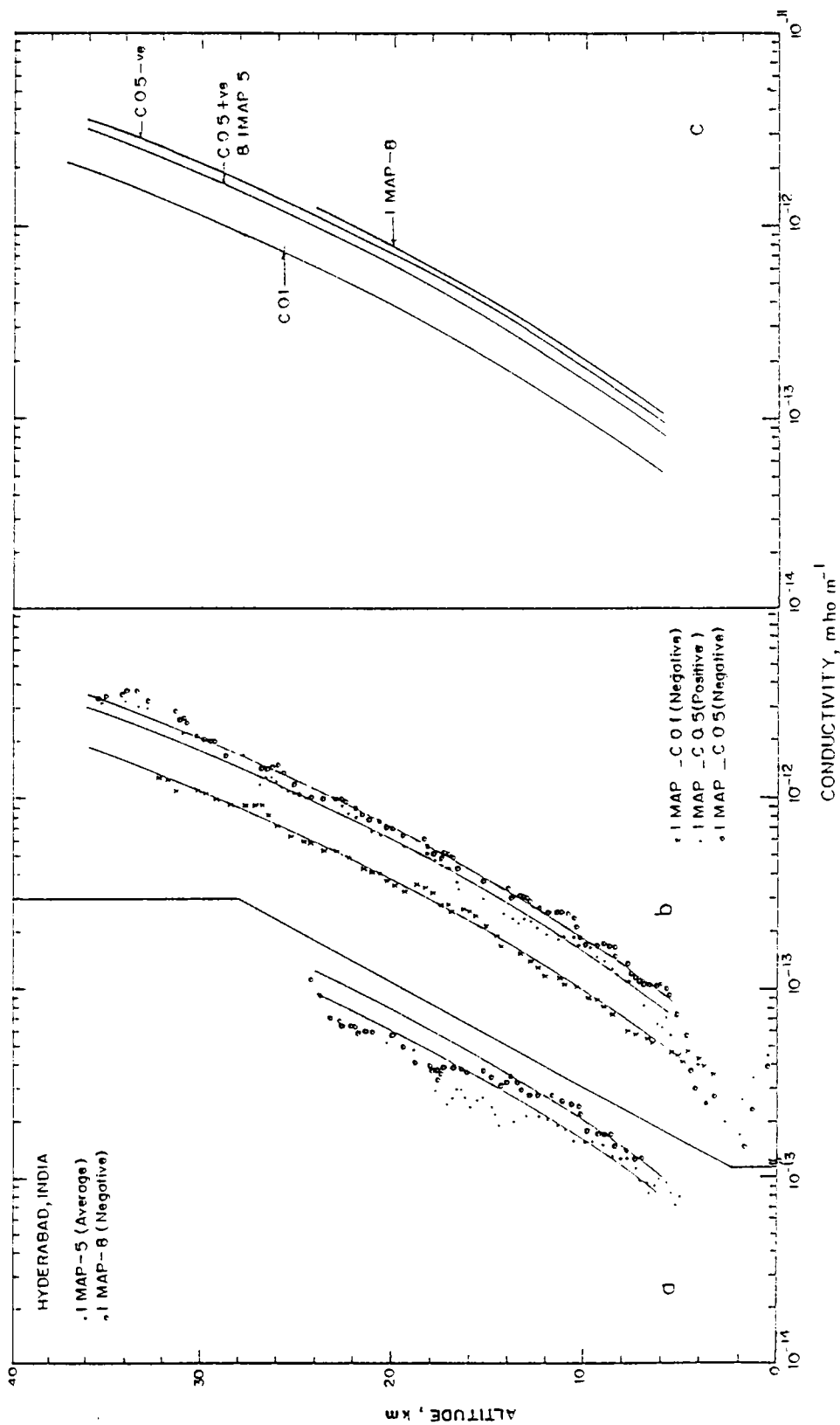


FIGURE 4.10. Variation of conductivity with altitude; a) measured with self aspirating condensers; b) measured with pumped condensers and c) fitted curves using the equation (24) for all the measurements.

which is shown here. As mentioned earlier, only negative conductivities could be obtained in the second flight.

Rosen and Hofmann (1981b) have conducted a few conductivity measurements from a mid latitude region. They found that their conductivity data follow an expression of the form

$$\sigma = A p^{-B} \exp(-Cp) \quad (24)$$

where,  $\sigma$  is the conductivity at the altitude at which

$p$  is the pressure and

$A, B, C$  are empirical constants.

The constants  $B$  and  $C$  express the variation with pressure (altitude) while  $A$  is a constant of proportionality. Similar expressions were fitted to the data of the two measurements reported here. The smooth curves shown in the Figure.4.10.a represent the expression. In the case of Rosen and Hofmann (1981b) the values of  $A$  (3789),  $B$  (0.6975) and  $C$  (0.002899) were the same for all the flights. In the present case, however, although  $B$  (0.6327) and  $C$  (0.001539) remain the same for both the flights,  $A$  (IMAP-5, 882 average; IMAP-8, 1119 negative) varies slightly from flight to flight. A change in  $A$  from flight to flight apparently means a change in the conductivity with time.

The conductivity profiles from the force-aspirated condensers are shown in Fig.4.10.b. Curve fitting as per the eqn.(24) was done for the data from these

flights also. It may be pointed out here that the expression to fit the profile will be valid only down to about 3 to 4 km, below which the effect of surface radioactivity and radioactive gases tend to increase the conductivity towards the surface. In the case of IMAP-C05 flight curve fitting was done only for the region above about 4 km. The B and C values for the pumped measurements were found to be the same as those of the self-aspirated ones. A was found to be different namely 538(IMAP-C1;negative), 870(IMAP-C05;positive) and 1000 (IMAP-C05;negative).

Thus, the nature of variation of conductivity is found to be same for all the four experiments. But A varies slightly from flight to flight. This difference could be attributed to seasonal changes in conductivity. The flights reported here were conducted within a span of four years. Of the four two were conducted in winter and the other two close to summer. The three flights of Rosen & Hofmann, for which A, B and C were same, were all conducted in the same season.

The profiles from the self-aspirated measurements show large fluctuations around the tropopause region. At the time these flights were conducted, these fluctuations were attributed to the effect of aerosols. Similar fluctuations were also observed by Kondo *et al.* (1982 a,b). However no other observation of this phenomenon appears to have been reported. The profiles from the two pumped measurements also

do not show any similar fluctuation. Further, Rosen *et al.* (1985) indicate that the effect of aerosols on conductivity could be limited. It may be mentioned here that the balloon during its flight always slows down in the tropopause region, where the fluctuations in conductivity are observed. Near tropopause the ascent rate of the balloon becomes very low and unstable. The balloon is then accelerated by telecommand and attains the proper ascent rate on crossing the tropopause region. Under such circumstances air flow along the length of the condenser could have become non-uniform and this could have caused large errors in the conductivity measurements, as suggested by Paltridge (1965). This problem is not present in pumped condenser measurements because the flow through the sensor is not dependent on the ascent rate of the balloon.

The smooth fitted curves for the conductivities measured in all these flights are shown in Figure.4.10.c. The conductivity measured in the third flight is much smaller than, in fact almost half that of, the other flights. The entire profile seems to have shifted to a lower value by a constant factor. The reason for this is not very clear. The calibration and other house-keeping circuitry shows that the electronics has behaved properly during the flight. On the other hand, it is difficult to understand how the conductivity could have gone down so much. The profiles from the other three flights are close together, with only the value of  $A$  varying slightly from flight to flight. Therefore a

by taking the average  $A$  from these three flights - namely 882 (IMAP-5; average), 1119 (IMAP-8; negative), 870 (IMAP-C05; positive) and 1000 (IMAP -C05; negative). As positive and negative polar conductivities normally do not differ very much, a general expression for polar conductivity for this region can be given by :

$$\sigma_{\pm} = 968 p^{-0.6327} \exp(-0.001539 p) \quad (2)$$

where  $p$  is in millibars and  $\sigma$  is in units of  $10^{-14}$  mho  $m^{-1}$ .

This representative profile for Hyderabad (low latitude) may be compared with a mid latitude measurement to see how these measurements fit into the general understanding of the galactic cosmic ray ionisation processes in the lower atmosphere. In Figure.4.11, this representative profile is compared with a mid latitude measurement of Rosen & Hofmann (1981b). It can be seen that, in general, the mid latitude values are higher than those of low latitude ones. Also, the two profiles tend to diverge with altitude. To understand this, the ion production rates over these two places are also given in Figure.4.11. The values corresponding to Hyderabad, India are taken from Datta *et al.* (1984) for a geomagnetic latitude of  $11^{\circ}$  and the values for mid latitude are taken from Rosen *et al.* (1979). Here also, the mid latitude values are higher and the two profiles tend to diverge with altitude.

The ion production rate ( $q$ ) is related to ion



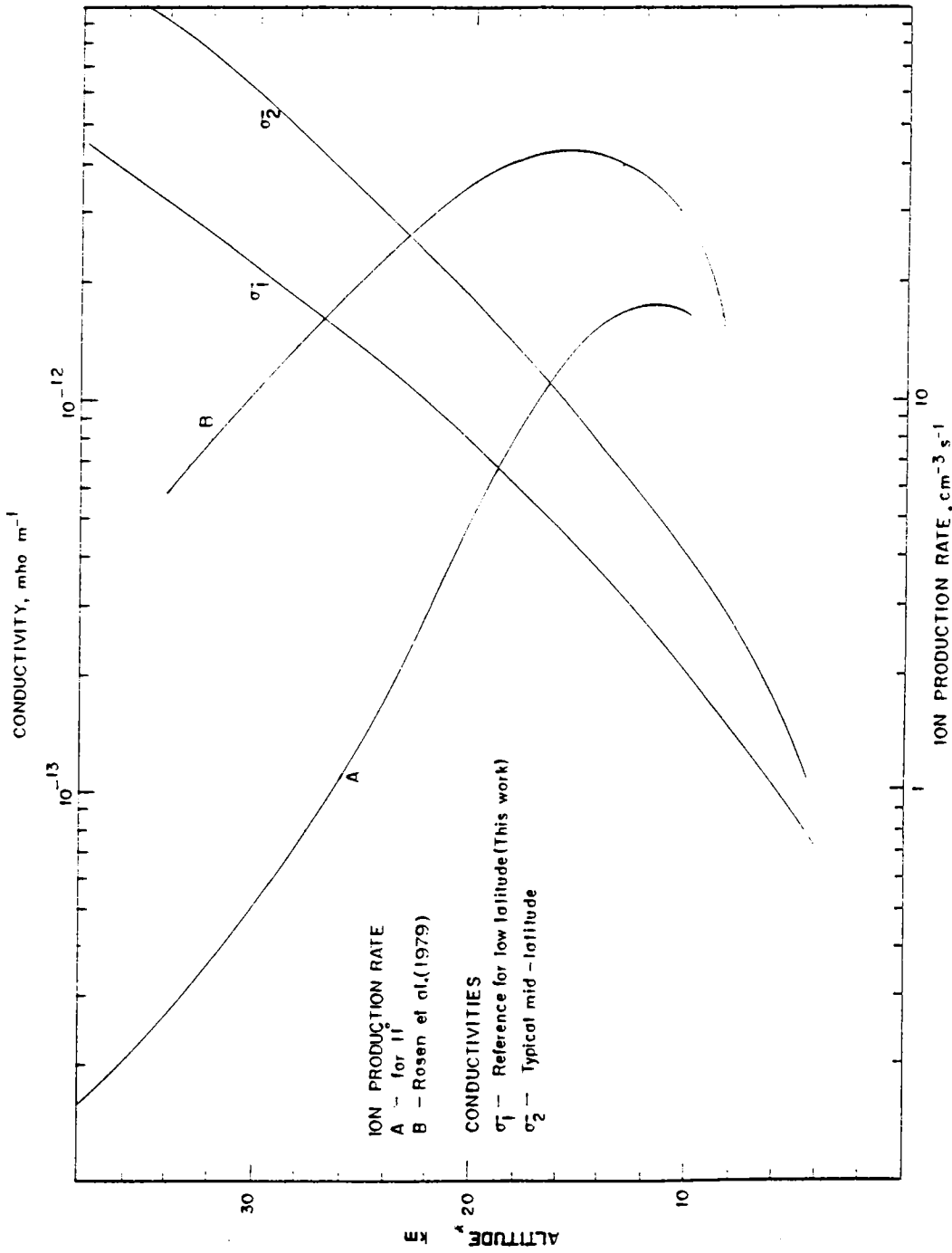


FIGURE 4.11. The derived representative profile for polar conductivity for low latitudes. This is compared with a typical mid latitude profile. To understand the divergence with altitude of the two profiles, the ion production rates for these latitudes are also shown.

density ( $n$ ) and the recombination coefficient ( $\alpha$ ) by the expression :

$$q = \alpha n^2 \quad (3)$$

and the conductivity ( $\sigma$ ) is related to the ion density and mobility ( $\mu$ ) by :

$$\sigma = n e \mu \quad (4)$$

where  $e$  is the electronic charge. Therefore, the ion density and hence the conductivity are proportional to the square root of the ion production rate. If it is assumed that  $\alpha$  and  $\mu$  do not differ very much at these latitudes, then the conductivity and the ion production rate profiles at these latitudes can be quantitatively compared. The ratio of  $q$  at mid latitude to that at low latitude around 15 km is about 3. The corresponding ratio for  $\sigma$  at 15 km is about 1.5 to 2, which is close to the square root of 3. Similarly, the ratio of  $q$  at 30 km is about 12 and the corresponding value for  $\sigma$  is about 3 to 4, which is also close to the square root of 12. Thus, the low latitude measurements fit well with mid latitude measurements both qualitatively and quantitatively within the limits of experimental errors. Therefore, the profile derived here can be taken as a representative one for the low latitudes.

The fourth flight has measured the conductivity from the surface itself. This has therefore succeeded in observing the effect of surface radioactivity and radioactive gases on the conductivity profile (Murali Das *et al.* 1991). The average conductivity for a land station is known to be

about  $1.8 \times 10^{-14} \text{Ohm}^{-1} \text{m}^{-1}$  (Chalmers 1967). The polar conductivities measured near ground at Hyderabad in the last flight is about  $4 \times 10^{-14} \text{Ohm}^{-1} \text{m}^{-1}$ . This is attributed to a high level of terrestrial (nuclear) radiation at Hyderabad (Sankaran et al, 1986).

Below 15 km, ionisation due to galactic cosmic rays decreases continuously down to the surface. At low altitudes, ionisation due to surface radioactivity and radioactive gases begins to dominate. They contribute almost eighty percent of the ionisation near the surface (Bricard, 1965).

The effect of surface radioactivity decreases with altitude and above a certain altitude where the ionisation due to galactic cosmic radiation begins to dominate, the conductivity starts increasing. At a given latitude, this point of inflexion depends on the strength of the radio activity at the surface. A mid latitude measurement of Rosen & Hofmann (1981) also shows a tendency for the ion density to increase below 3 km.

In the last flight (IMAP C05) the point of inflexion in conductivity was seen to occur at a height of 2 km. The height at which the point of inflexion occurs is not a constant, as it depends on many factors, and is expected to change with the time of the day.

The altitude up to which the surface radioactivity can be effective is dependent on the distribution of radon and its derivatives with altitude. Gamma rays from the soil

contribute significantly to the ionisation at and near the surface. Their influence falls rapidly with height and within a few tens of meters the contribution to ionisation by gamma rays becomes relatively insignificant (Bricard,1965). Ionisation in the upper layers is essentially due to radioactive gases transported by turbulence. Among the radioactive gases, only Rn and Tn are important. Again, Tn which has a half life of 54.5 s is not of importance in the upper layers. The Rn content of surface air depends on exhalation rate and the turbulent transport into upper layers. But the latter seems to be the dominant factor. During days of fair weather the Rn content of surface air is known to show a maximum around sunrise when turbulent mixing is at a minimum and a minimum during afternoon when mixing is at a maximum (Junge,1965). The reverse must be true for the upper layers. This diurnal variation in Rn concentration consequently could affect the height at which the minimum or point of inflexion in the altitudinal profile of conductivity occurs. Therefore, the point of inflexion in conductivity seen at 2 km at about 0215 hr in the last flight can possibly shift to a higher level during day time. A reduction in the surface value of conductivity must accompany this increase in height.

#### 4.2.2. MOBILITY:

As mentioned in the introduction, the speed of airflow through the condenser was assumed to be equal to the

ascent rate of the balloon in the case of the self-aspirated condensers. Since the ascent rate is not known accurately, and also since the assumption is not strictly valid, the ion density and mobility data from the two self-aspirated condensers have relatively large uncertainties. Of the two force-aspirated condensers, only the first measured mobilities.

The variation of mobility with altitude does not give a picture of the ion mass distribution if any, since mobility is a function of temperature and pressure also. To eliminate the effects of temperature and pressure, the measured mobilities have been reduced to STP values using the expression

$$\mu_o = \mu (T_o/T) (p/p_o)$$

where the subscript o refers to STP values. The reduced mobilities obtained from the three flights are shown in Figure.4.12. In the case of the force-aspirated sensor the measured values are seen to be almost constant with altitude, implying that the ion species in this altitude region have more or less the same mass. The average reduced mobilities obtained in the three flights fall in the range from  $1.7 \times 10^{-4}$  to  $2.4 \times 10^{-4} \text{ m}^2 \text{ V}^{-1} \text{ s}^{-1}$ . Various experimenters have obtained mobility values which fall between  $0.5 \times 10^{-4}$  and  $5 \times 10^{-4} \text{ m}^2 \text{ V}^{-1} \text{ s}^{-1}$  (Meyerotte et al. 1980). However, most of the measurements give values around  $2 \times 10^{-4} \text{ m}^2 \text{ V}^{-1} \text{ s}^{-1}$ . The present measurements also give values close to this. Till now

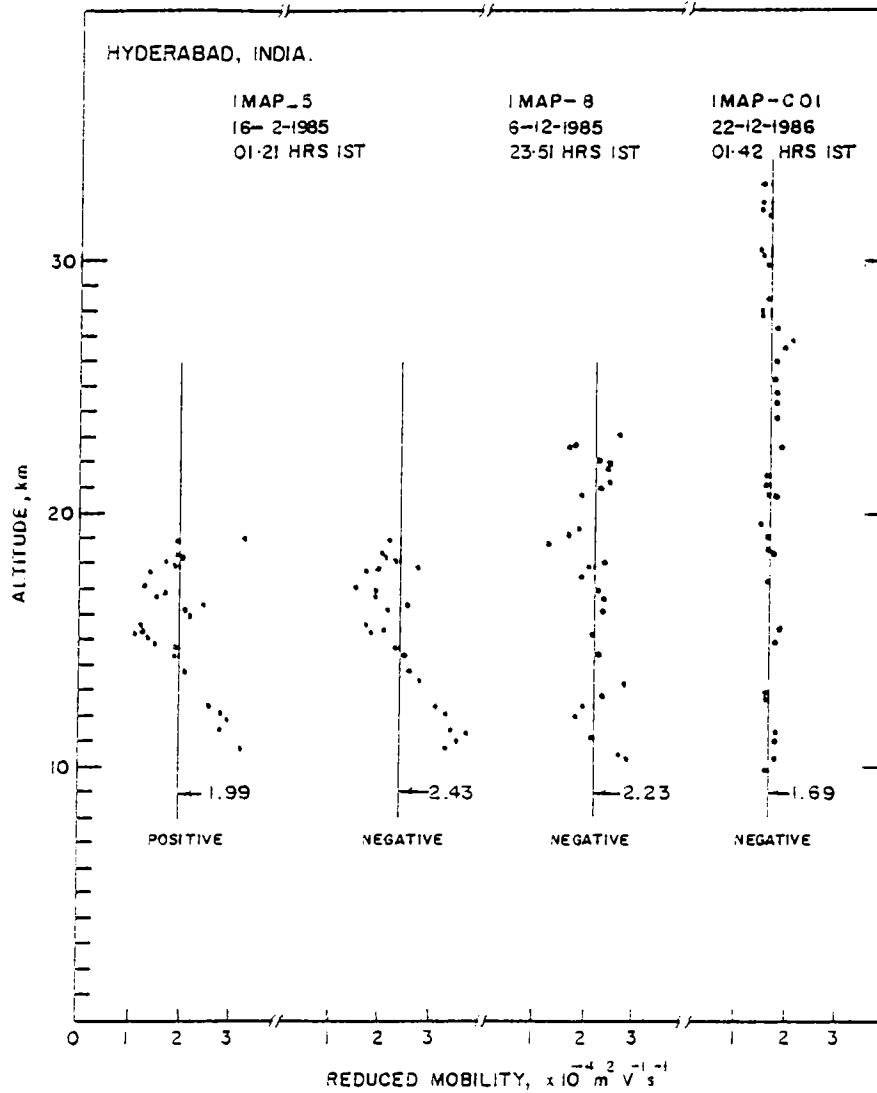


FIGURE 4.12. The variation of reduced mobility with altitude, derived from measurements reported here. The straight lines are least square fits of the data points.

only two sets of mobility measurements using force-aspirated Gerdien condensers have been reported. They are the ones presented here and those of Rosen & Hofmann (1981b). While the former have yielded negative ion data the latter have data only of positive ions. Also, the two measurements are from two different latitudes. Therefore they cannot be directly compared. Yet, it may be stated that the average reduced mobility obtained from the force-aspirated condenser measurements of IMAP-CO1,  $1.69 \times 10^{-4} \text{ m}^2 \text{ V}^{-1} \text{ s}^{-1}$  for negative ions, compares well with the value  $1.5 \pm 10\%$  obtained using a pumped condenser by Rosen & Hofmann for positive ions.

The mobility values obtained from the self-aspirated measurements show large scatter so that they cannot be of use in attempting to identify the ion masses. The scatter in the reduced mobilities obtained from the pumped condenser, however, is low. These values, along with Kilpatrick's mass dispersion curve (shown in Figure 3.9) gives ion mass values between 85 and 150 amu for the negative ions observed in the third flight.

#### 4.2.3. ION DENSITIES:

The ion densities measured using the self-aspirated sensors are shown in Figure.4.13.(a). The wild fluctuations are due to uncertainties in the airflow velocity, as explained earlier.

The ion densities obtained with the force-aspirated

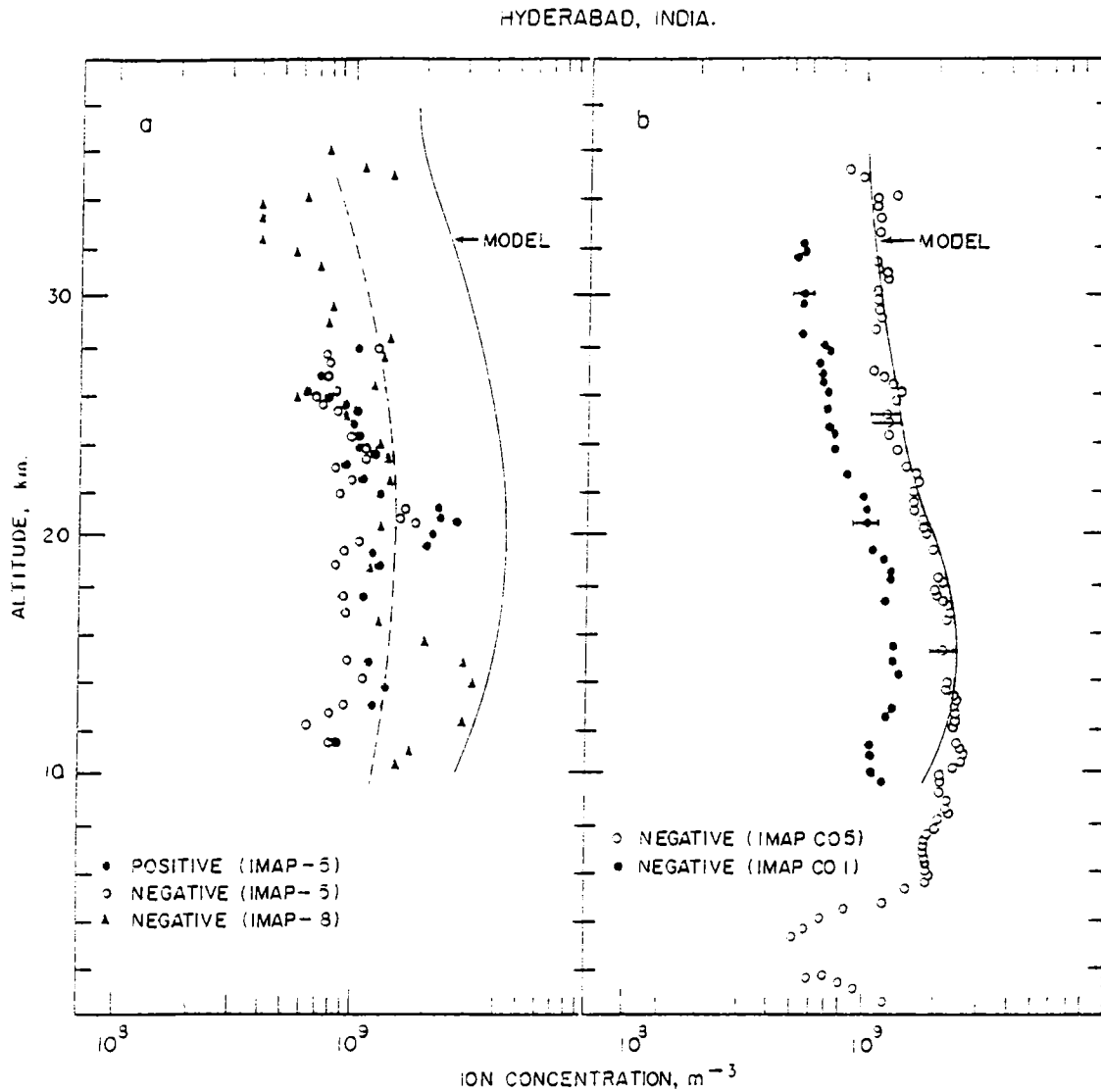


FIGURE 4.13. Ion density profiles measured a) using self aspirated sensors and b) using pumped condensers. An improvement in the quality of data in the pumped condenser measurements is seen.



condensers are shown in Figure 4.13.(b). The scatter in the data can be seen to be much less than that in the self-aspirated measurements. As in the case of the conductivities, the values from the flight IMAP-CO1 are much less than the others.

Since only conductivities could be measured directly in the last flight during the ascent, the profile shown was derived from the conductivity by using the reduced mobility obtained in the earlier flight. The average reduced mobility obtained in IMAP-CO1 (force-aspirated) was used for negative ions. The ion density profile also clearly shows the effect of surface radioactivity and radioactive gases. The ion density values are comparable to the theoretical values calculated from ion pair production rates and recombination coefficients as given in *Datta et al.* (1984).

#### 4.2.4.FLOAT DATA:

The fourth flight has measured conductivity, ion density and mobility at float. The balloon reached the float altitude of 35.8 km at 0441 hr, IST and continued to float at this altitude till 0800 hr. Figure 4.14 shows all the parameters measured during float. No significant change is observed in any of these parameters with time or sunrise.

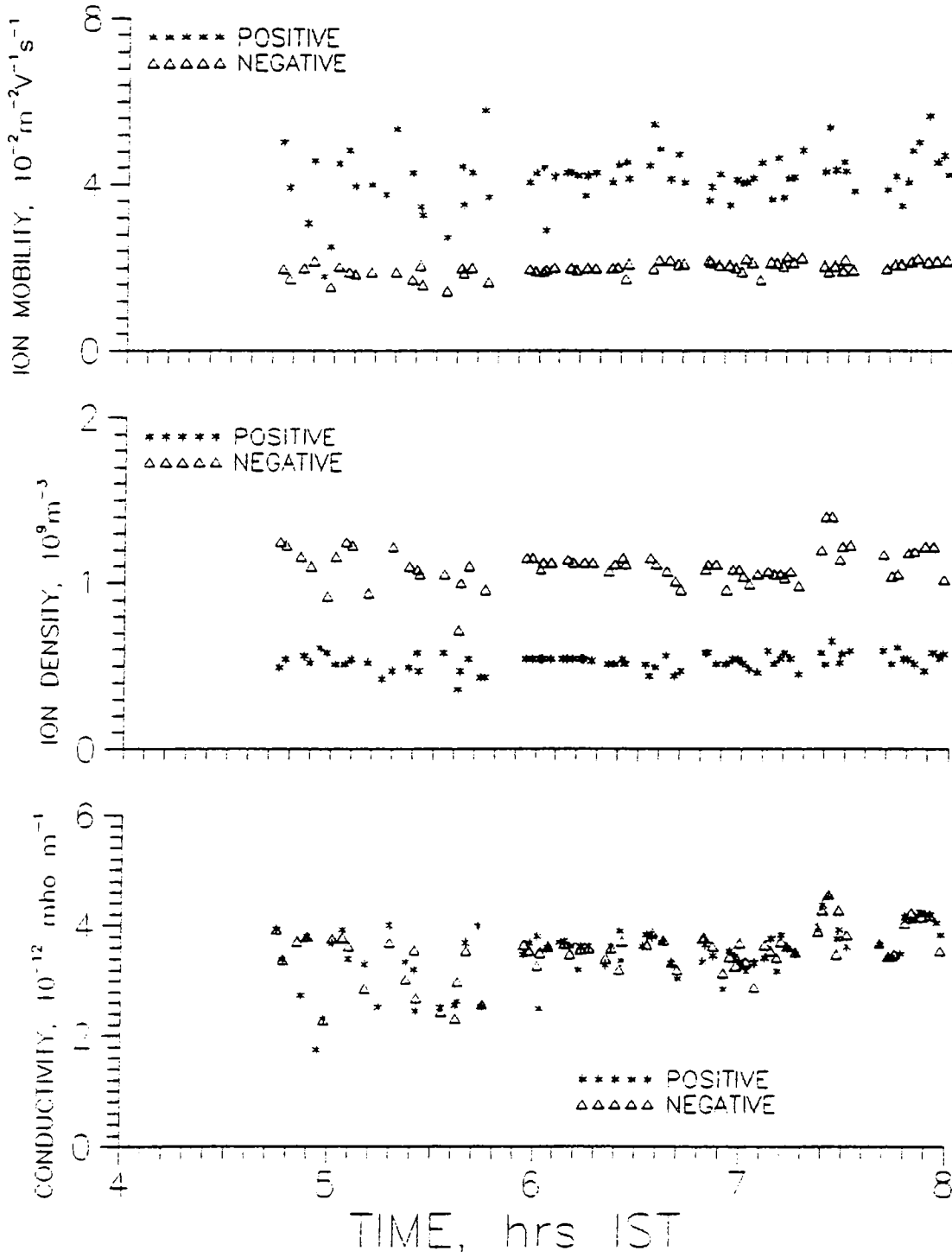


FIGURE 4.14. Float data from the flight IMAP-C05.

#### 4.3. ERRORS IN MEASUREMENT:

In the case of balloon experiments also random error in computing polar conductivities, ion densities and mobilities have been estimated. This includes all estimable random errors in measurement from calibration to data reduction. It is found that in the regions of the profile where the ion densities and mobilities are the lowest a maximum error of  $\pm 9\%$  is present. Similarly for those regions of the profile where the ion densities and mobilities are high it is found that a maximum error of  $\pm 5\%$  is present. The error in conductivity measurement is lower, and has a maximum value  $\pm 6\%$  and a minimum of  $\pm 3\%$ .

## CHAPTER 5

### SUMMARY AND CONCLUSION

A summary of the work described in this thesis, its main achievements, and a discussion of the investigations that can be carried out as an extension, are given in this chapter.

#### 5.1 SUMMARY:

The thesis describes the development of Gerdien condenser payloads for balloon-borne and rocket-borne measurements of atmospheric electrical polar conductivities, ion densities and mobilities. For balloon-borne measurements, a force-aspirated Gerdien condenser has also been designed, fabricated and successfully used in two flights, for the first time in India. Four balloon flights and five rocket flights have been carried out with these payloads. All of them, except one rocket flight, have given good data, some of them for the first time in India.

The rocket measurements have shown the minimum in ion density around 62 km. These are some of the few flights to have observed this minimum. The positive and negative ion densities match up to an altitude of about 70 km, beyond which the negative ion densities are seen to decrease. However, as

opposed to the accepted model profiles, the measured negative ion density profile shows a broad maximum around 80 to 85 km. Only one or two previous in-situ measurements conducted from elsewhere have observed such a behaviour. The measured positive and negative ion mobilities agree with those from other measurements.

The balloon-borne measurements have given some of the first results from the Indian zone. One flight has succeeded in obtaining a continuous profile of conductivity from the ground to the float altitude of around 35 km. The observed ion densities agree with model values, except in the case of one flight. The observed reduced mobilities show that the ion species remain more or less the same in the region of measurement. The mobility values are in good agreement with other observations. Measurements during float, covering a period from night to day, do not show any change in any of the parameters with sun rise.

## 5.2 ACHIEVEMENTS OF THE WORK:

One of the important achievements of the work has been the development and establishment in India of the Gerdien condenser technique for the measurement of polar conductivities, ion densities and mobilities in the region from the surface to about 90 km. The instrument has been almost standardised for balloon-borne and rocket-borne measurements. For balloon-borne measurements, the feasibility

of converting a commercially available lobe type flow meter into a pump, and using it for the forced aspiration of the Gerdien condenser has been successfully demonstrated.

One of the balloon-borne measurements has given a continuous profile of polar conductivities from the surface to about 35 km, where the effect of surface radioactivity and radioactive gases on the profile is clearly seen. This is probably the first balloon measurement, at least from the equatorial region, that has given a continuous profile from the surface, and observed the effect of radioactivity. The balloon measurements reported here are also the first simultaneous measurements from India of the polar conductivities, ion densities and mobilities of both positive and negative species in the troposphere and the stratosphere.

The rocket-borne measurements reported here are the first simultaneous measurements from India of positive and negative ion densities and mobilities in the mesosphere. The observations of the minimum in ion densities, reported here, are some of the few such observations. The large negative ion densities around 80 to 85 km seen in the last two flights reported here have been observed only very rarely. Only one or two in-situ measurements and a few ground based soundings have observed this earlier.

### 5.3 AN OVERVIEW OF THE RESULTS

Atmospheric electric polar conductivities have been obtained in the region from ground to 35 km, and from 55 to 70 km. Although the measurements in the two altitude regions have been made from two different stations, namely Thumba at the dip equator, and Hyderabad, India, a low latitude station, they can be combined to give the altitude profile over a typical low latitude station. The two data sets can be combined because in this region dominated by galactic cosmic ray ionisation, the difference between these two stations will not be large. Similarly, the ion density and mobility data from the two stations also can be combined to give typical profiles for this region.

The profile for positive polar conductivity is shown in Figure 5.1, where the values from the fourth balloon flight (IMAP C05) alone has been shown for the lower region. The smooth curve is from the empirical equation discussed in Chapter 4. The data for the two regions are seen to merge well, showing the mutual consistency of the measurements. Figure 5.2 shows the positive ion density profile for the whole region. Here, the profile for the lower region has been derived from the conductivity values obtained in the fourth balloon flight. This has been preferred over direct measurements made in the earlier flights because the fourth flight has shown a greatly improved performance compared to

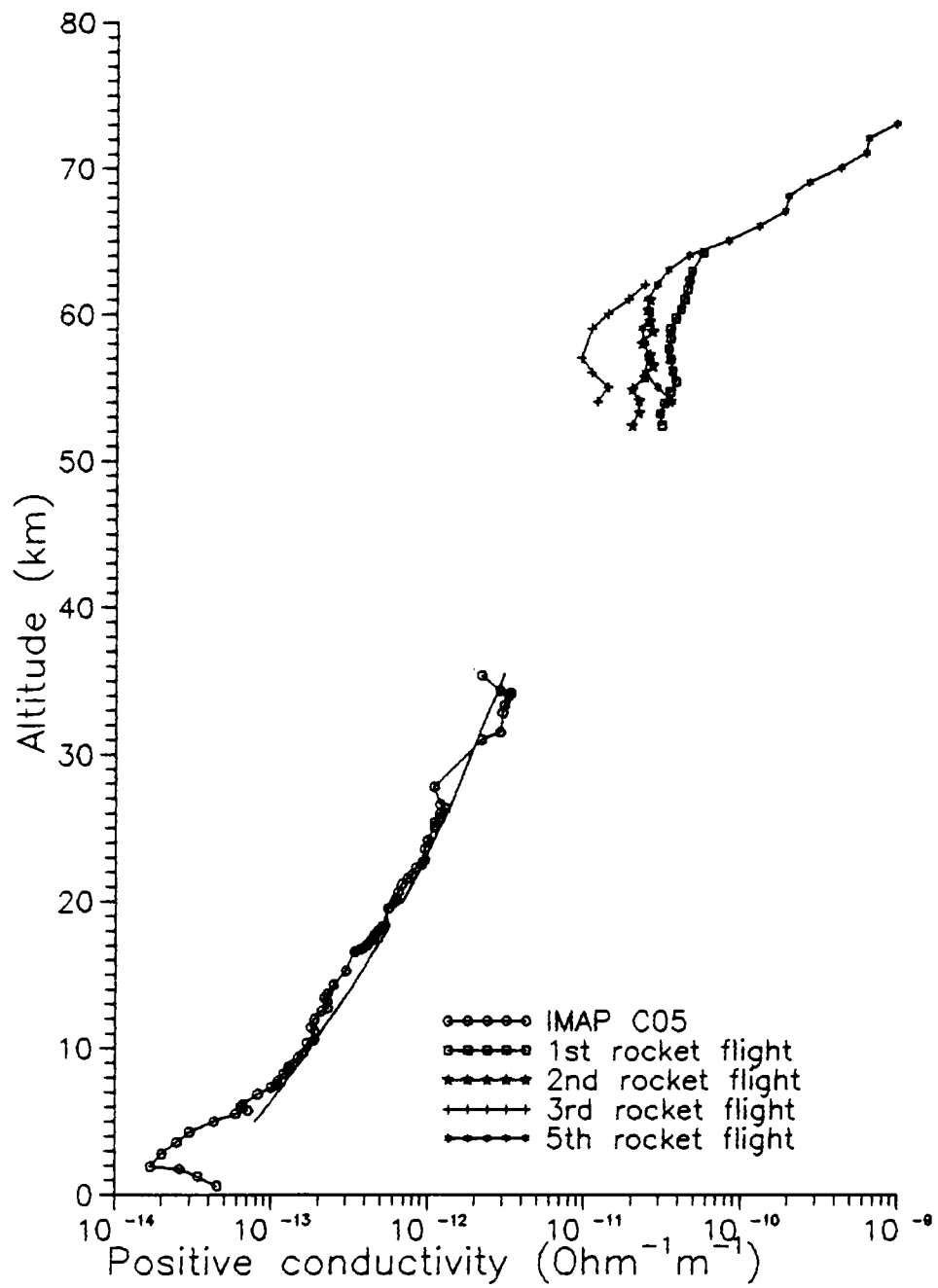


FIGURE 5.1 Positive conductivity from rocket and balloon experiments.



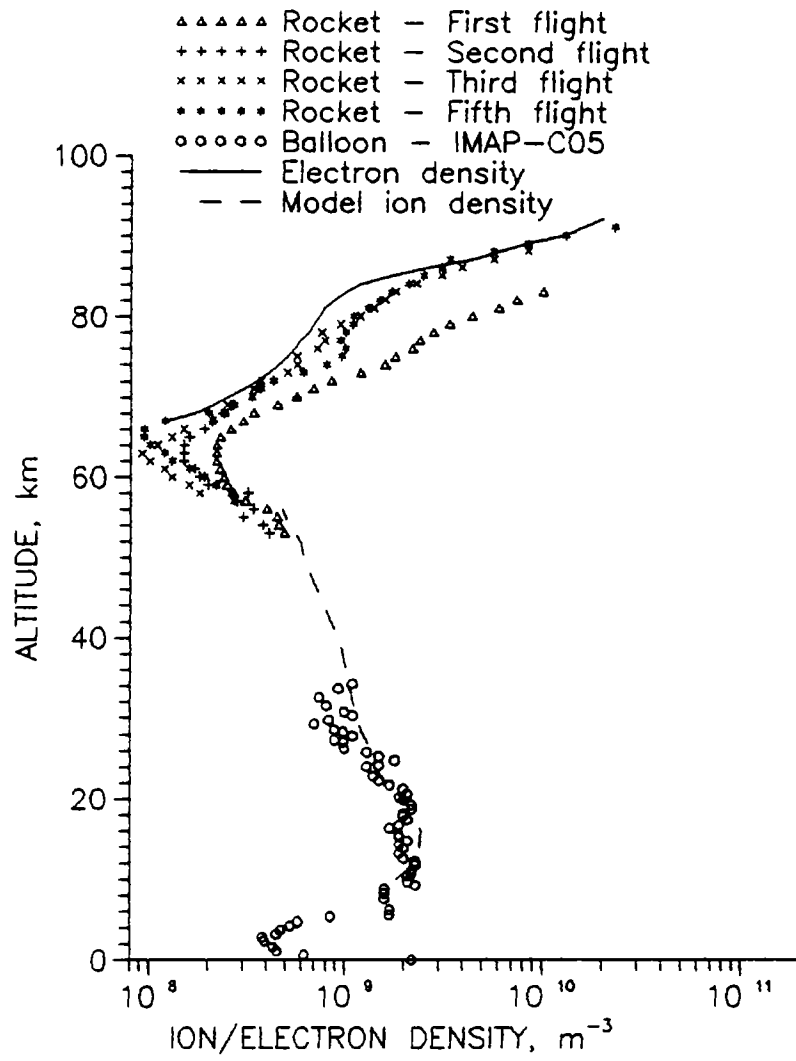


FIGURE 5.2. Positive ion density from rocket and balloon experiments

the others, and the data are seen to be of better quality and consistency. The figure also shows a model profile derived from cosmic ray ionisation rates taken from Deshpande et al. (1985) and a parametrised recombination coefficient taken from Datta et al. (1985). The measured profile agrees well with this model profile.

In the upper region of the atmosphere, especially above about 60 to 65 km, ionisation is mainly due to solar ultraviolet radiation, and the ion chemical processes are more complex than in the lower regions. A number of models have been developed for explaining the observations during different normal and disturbed conditions (for instance, Nicolet and Aikin, 1960; Ferguson, 1971; Mitra and Rowe, 1972; Reid, 1977; Chakraborty and Chakraborty, 1978; Deshpande et al., 1985; etc.). In the region above about 70 km, negative ions are displaced by electrons. A large number of electron density measurements have been made from Thumba, which can therefore be compared with the present measurements. Figure 5.2 shows a typical normal days profile for noon time taken from Subbaraya et al. (1983). This is seen to agree well with the ion densities reported in this thesis. The ion density profiles in this region, shown in the figure, have been corrected for the variation in mass flow efficiency as reported by Conley (1974). The correction is not exact, since it was made using the curve given by Conley (1974) for his sensor for a rocket velocity of Mach 3. However, the

agreement between these values and the electron density profile shows that the correction has not been far off the mark.

The measured ion mobilities are plotted in Figure 5.3. The straight line shown is a least square fit for the entire data. The fact that the straight line fits well with the entire data indicates that the ion masses are more or less uniform over this region.

#### 5.4 FUTURE PERSPECTIVES

Several problems remain to be tackled with regard to the area of the present investigation. One of the gaps in data is between the regions covered by the balloon measurements and the rocket measurements, namely the altitude region between about 35 km to about 55 km. While it is difficult to make reliable in-situ measurements in this region, since the only access is by using a parachute, the lack of data close to the region where the transition in the main ionising source takes place also creates difficulties in obtaining a complete picture.

One of the problems to be sorted out is regarding the effect of aerosols on polar conductivities. While the first two balloon flights using self-aspirated Gerdien condensers reported here showed some fluctuations close to the tropopause, which were assumed to be due to aerosols, later flights using force-aspirated condensers failed to do so.

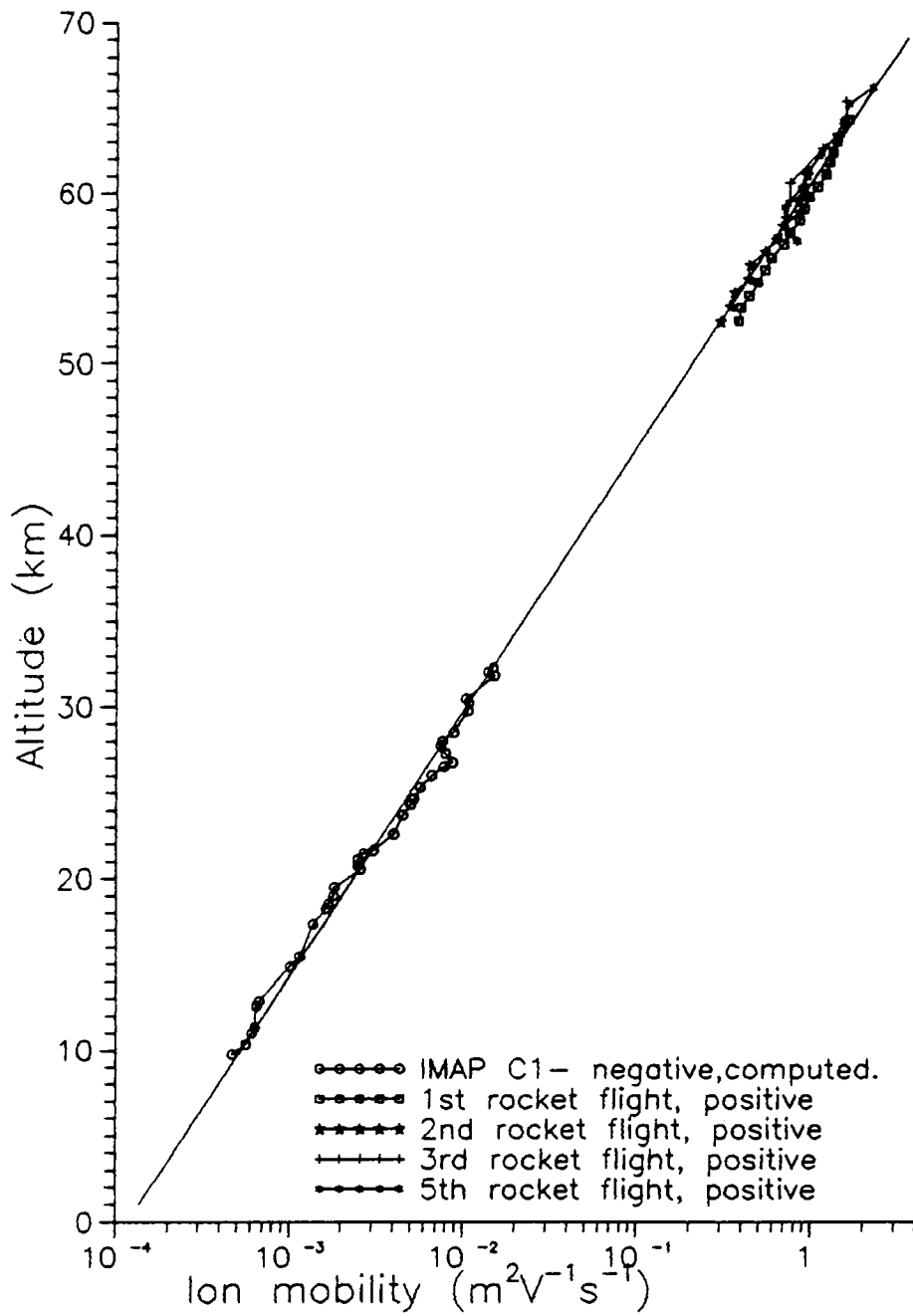


FIGURE 5.3. Ion mobility from rocket and balloon experiments

Similar fluctuations have been observed by some other experimenters also (for instance, Kondo et al., 1982 a,b). On the other hand, Rosen and Hofmann (1985) report that aerosols have hardly any effect on the conductivity.

A third problem that needs to be looked into is the negative ion maximum seen around 80 to 85 km. This contradicts the accepted model predictions, and some efforts have been made to interpret them in terms of chemistry. But more observations, and perhaps more model computations are also needed.

=====

## REFERENCES:

- Aikin, A.C. , R.A. Goldberg , Y.V.Somayajulu, and M.B.Avadhanulu, Electron and positive ion density altitude distributions in the equatorial D-region, Journal of Atmospheric and Terrestrial Physics, 34, 1483-1494, 1972.
- Anna Mani and B.B.Huddar, Atmospheric electricity measurements in the upper air over Poona, Proceedings of the Indian Academy of sciences, LXI, 5, Sec.A, 1965.
- Anna Mani, C.R Sreedharan, B.B.Huddar and Y.Ramanathan, Atmospheric electricity measurements over Indian ocean, Pure and Applied Geophysics, 100, VIII, 101-108, 1972.
- Arijs, E, D.Nevejans, J.Ingels and P. Frederick, Positive ion composition measurements between 33 and 20 km altitude, Annales Geophysicae, 1, 2, 161- 166,1983.
- Arnold, F., J.Kissel, H.Wieder and J.Zhringer, Negative ions in the lower ionosphere, a mass spectrometric measurement, Journal of Atmospheric and Terrestrial Physics, 33, 1669, 1971.
- Arnold, F.,D.Krankowsky and K.H.Marien, First mass spectrometric measurements of positive ions in the Stratosphere, Nature,267, 30-32, 1977.
- Beig, G, J.S.Siddhu, S.R.Das, and D.K.Chakrabarty, Balloon-borne measurements of stratospheric ion density and conductivity at low latitude, Geophysical Research Letters, 15, 12, 1357- 1360, 1988.
- Beig, G, J.S.Siddhu, S.R.Das, and D.K.Chakrabarty, Balloon-borne measurement of the stratospheric ion conductivity profile at low latitude, Journal of Geophysical Research, 94, D8, 11070-11073, 1989,
- Bordeau,R.E., F.C.Whipple,Jr, J.F.Clarke, Analytic and experimental electrical conductivity between the stratosphere and the ionosphere, Journal of Geophysical Research, 64, 40, 1363-1370, 1959.
- Brasseur, Guy., and Susan Solomon, Aeronomy of the middle atmosphere,Reidel publishing company,1986.
- Bricard, J, Action of radioactivity and of pollution upon parameters of Atmospheric electricity, Problems of atmospheric and space electricity, Ed. S.C.Coroniti, 1965.
- Byrne, G.J, J.R.Benbrook, E.A.Bering, D.M. Oro, C.O.Seubert and W.R.Sheldon, Observation of the stratospheric conductivity and its variation at three latitudes, Journal of Geophysical Research, 93, D4, 3879- 3891, 1988.

- Byrne, G.J, J.R.Benbrook, E.A.Bering and D.M. Oro, Solar radiation in the stratosphere : Implications for photoelectric emissions from instrumentation at balloon altitudes, *Journal of Geophysical Research*, **95**, 5557, 1990.
- Chakrabarty,D.K., and P.Chakraborti, An attempt to identify the obscured paths of water cluster ions build-up in the D-region, *Journal of Atmospheric and Terrestrial Physics*, **40**, 437- 442, 1978.
- Chakrabarty, D.K., C.E.Meek and A.H.Manson, Assymetry in the diurnal variation of temperature and electron loss coefficient in the mesosphere, *Journal of Atmospheric and Terrestrial Physics*, **45**, 5, 309-314, 1983.
- Chakrabarty, D.K., and S.Ganguly, On significant quantities of ions observed around mesopause, *Journal of Atmospheric and Terrestrial Physics*, **51**, 11/12, 983-989, 1989.
- Chalmers, J.A., *Atmospheric electricity*, Second edition, Pergamon press, Oxford, 1967.
- Cobb, W.E., Ion losses in the Gerdien condenser intake system, *Journal of Applied Meteorology*, **7**, 456-458, 1968.
- Conley, T.D, Mesospheric positive ion concentrations, mobilities and loss rates obtained from rocket-borne Gerdien condenser measurements, *Radio Science*, **9**, 6, 575-592, 1974.
- Conley, T.D, E.R.Hegblom and R.S.Narcisi, D - region positive and negative ion concentration and mobilities during the February 1979 eclipse, *Journal of Atmospheric and Terrestrial Physics*, **45**, 7, 499- 513, 1983.
- Deshpande, S.D.,V.C.Jain and A.P.Mitra, Models of ion production in the middle atmosphere, Scientific report, Indian Space Research Organisation, 1985.
- Deshpande, S.D.,V.C.Jain and A.P.Mitra, Models of rate of ion production in the middle atmosphere, Scientific report, Indian Space Research Organisation, 1986.
- Dotan, I.,D.L.Albritton, W.Lindinger and M. Pahl, Mobilities of  $\text{CO}_2^+$ ,  $\text{N}_2\text{H}^+$ ,  $\text{H}_3\text{O}^+$ ,  $\text{H}_3\text{O}^+\cdot\text{H}_2\text{O}$ ,  $\text{H}_3\text{O}^+(\text{H}_2\text{O})_2$  ions in  $\text{N}_2$ , *J.Chem Phys.* **65**, 5028- 5030, 1976.
- Farrokh, Hashem. Design of a simple Gerdien condenser for ionospheric D-region charged particle density and mobility measurements, Scientific report, The pennsylvania state university, 1975.
- Ferguson,E.,D-region ion chemistry, *Rev.Geophys Space Phys* **9**, 997, 1971.

- Garg, S.C, Thomas John, K.S.Zalpuri, P.Subramaniam, and Y.V.Somayajulu, measurement of stratospheric electrical conductivity using balloon-borne Langmuir probe, *Indian Journal of Radio and Space Physics*, **18**, 285- 289, 1989.
- Gerdien, H., The absolute measurement of specific conductivity and density of the air-earth conduction current in the atmosphere, *Terr. Magn. Atmos. Elect.*, **10**, 69-75, 1905.
- Goldberg, Richard.A, Middle atmospheric electrodynamic status and future, *Journal of Atmospheric and Terrestrial Physics*, **46**, 11, 1083- 1101, 1984.
- Goldberg, Richard.A., Middle atmospheric electrodynamic status and future, *Journal of Atmospheric and Terrestrial Physics*, **46**, 11, 1083- 1101, 1984.
- Goldberg, R.A, J.R.Barcus, L.C.Hale and S.A.Curtis, Direct observation of magnetospheric electron precipitation by lightning, *Journal of Atmospheric and Terrestrial Physics*, **48**, 3, 1986.
- Goldberg, R.A, S.A.Curtis and J.R.Barcus, Detailed spectral structure of magnetospheric electron bursts precipitated by lightning, *Journal of Geophysical Research*, **92**, A3, 2505-2513, 1987.
- Gras, J.L, Lower stratospheric small-ion conductivity measurements, *Journal of Atmospheric and Terrestrial Physics*, **37**, 1285-1286, 1975.
- Gregory, J.B., and A.H.Manson *Journal of Atmospheric and Terrestrial Physics*, **31**, 703,1969 (cited in Chakrabarty et al 1983).
- Gupta S.P. and A. Narayan : Balloon-borne measurements of ion conductivity over low latitude stratosphere *Planet. Space Sci.* **35**, 439-443, 1987.
- Harris and Crede, (Ed.), *Shock and Vibration Hand book - Basic theory and measurements*, McGraw Hill, p 19-10, 1976.
- Hashem Farrokh, Design of a simple Gerdien condenser for ionospheric D-region charged particle density and mobility measurements, *Scientific report- Ionospheric Research Laboratory, University Park, Pennsylvania*, 1975.
- Haug, A., E.V.Thrane, E.Tsagakakis and Anastassiades, *Journal of Atmospheric and Terrestrial Physics*, **32**, 1865, 1970 (cited in Chakrabarty et al 1983).
- Holzworth,R.H., K.W.Norville, P.M.Kintner and S.P.Powell, Stratospheric conductivity variations over thunderstorms, *Journal of Geophysical Research*, **91**, D12, 13257- 13263, 1986.



- Holzworth, Robert.H, Conductivity and electric field variation with altitude in the stratosphere, Journal of Geophysical Research, 96, D7, 12857- 12864, 1991 (a).
- Holzworth, R.H., Atmospheric electrodynamics in the US: 1987 - 1990, Reviews of geophysics, supplement, 115- 120, April 1991 (b).
- Hoult, D.P., D region Probe theory, Journal of Geophysical Research, 70, 3183- 3187, 1965.
- Hua Hu, Robert H.Holzworth and Ya Qi Li, Thunderstorm related variations in stratospheric conductivity measurements, Journal of Geophysical Research, 94, D13, 16429- 16435, 1989.
- Hunten, D.M., and McElroy, Metastable  $O_2(^1\Delta_g)$  as a major source of ions in the D-region, Journal of Geophysical Research, 73, 2421, 1968.
- Iverson, I.B, M.M.Madsen and N.D'Angelo, Measurement of the vertical atmospheric field and of the electrical conductivity with stratospheric balloons, Annales Geophysicae, 3, 1, 51-56, 1985.
- Iribarne, J.V., and H.R.Cho, Atmospheric physics, Reidel publishing company, 8- 10, 1980.
- Israel, H., Atmospheric Electricity, Vol.1&2, Israel program for scientific translations, (1970).
- Jayati Datta, S.C.Chakravarty and A.P.Mitra, Cosmic rays ion production rates in the middle atmosphere, Scientific report, Indian Space Research Organisation, 1984.
- Jespersen, M., A.J.Kane and B.Landmark, Electron and positive ion measurements during auroral absorption, Journal of Atmospheric and Terrestrial Physics, 30, 1955- 1963, 1968.
- Junge, Christian.E., Air chemistry and radio activity, Academic press, 217, 1963.
- Kamra, A.K, Fair weather space charge distribution in the lowest 2 m of the atmosphere, Journal of Geophysical Research, 87, C6, 4257- 4263, 1982.
- Kamra, A.K, J.K.S.Teotia and A.b.Sathe, Measurements of electric field and vertical distribution of space charge close to the ground during the solar eclipse of February 16 1980, Journal of Geophysical Research, 87, C3, 2057- 2060, 1982.

- Kelly, M.C., C.L.Siefring, R.F.Pfaff, P.M.Kintner, M.Larson, R.Green, R.H.Holzworth, L.C.Hale, J.D.Mitchell and D.Le Vine, Electrical measurements in the atmosphere and ionosphere over an active thunderstorm, 1. Campaign overview and initial ionospheric results, *Journal of Geophysical Research*, **90**, 9815- 9823, 1985.
- Kondo Y., R.Reiter, H.Jaeger and M.Takagi: Stratospheric aerosol inferred from electrical conductivity during a volcanically quiescent period *Pure Appl. Geophys.* **120**, 1-10, 1982(a).
- Kondo Y., R.Reiter, H.Jaeger and M.Takagi: The effect of the Mt. St. Helens eruption on tropospheric and stratospheric ions. *Pure Appl. Geophys.* **120**, 11-17, 1982(b).
- Mani, A. and B. B Huddar, Variations in atmospheric electricity in the lower troposphere over Poona, *The Indian Journal of Meteorology and Geophysics*, **13**, Spl. No., 179-187, 1962.
- Mani, A, B.B.Huddar and G.P.Srivastava, Electrical conductivity and potential gradient measurements in the free atmosphere over India, *Indian Journal of Pure and Applied Geophysics*, **9**, 992-996, 1971.
- Markson, Ralph., Atmospheric electricity and sun-weather relationships, *Nature*, **273**, 5658, 103- 109, 1978.
- Markson, Ralph., Atmospheric electricity and the sun-weather problem, *Solar-Terrestrial Influences on Weather and Climate*, Reidel publishing company, 215- 232, 1979.
- Maynard,N.C, L.C.Hale, J.D.Mitchell, F.J.Schmidlin, R.A.Goldberg, J.R.Barcus, F.Soraas and C.L.Croskey, Electrical structure in the high-latitude middle atmosphere, *Journal of Atmospheric and Terrestrial Physics*, **46**, 9, 807-817, 1984.
- Meyerott,R.E, J.B.Reagan and R.G.Joiner, The mobility and concentration of ions and the ionic conductivity in the lower stratosphere, *Journal of Geophysical Research*, **85**, A3, 1273- 1278, 1980.
- Mitchell, J.D, R.S.Sagar and R.O.Olson, Positive ions in the middle atmosphere during sunrise conditions, *Cospar space research*, **XIII**, 199- 204, 1977.
- Mitchell, J.D, L.C.Hale, and C.L.Croskey, Eclipse-related measurements of middle-atmosphere electrical parameters, *Journal of Atmospheric and Terrestrial Physics*, **45**, 7, 515-525, 1983.

- Mitchell, John.D, Middle atmospheric\* positive ion measurements during solar eclipses, *Annales Geophysicae*, 3, 1, 95- 102, 1985.
- Mitra,A.P.and Rowe, Ionospheric effects of solar flares - VI changes in D-region ion chemistry during solar flares, *Journal of Atmospheric and Terrestrial Physics*, 34, 795-806, 1972.
- Morita, Y, Recent measurements of electric conductivity and ion production rate in the lower stratosphere, *Research letters on atmospheric electricity*, 1, 49- 52,1981.
- Muir,M.S., The Ionosphere as the source of atmospheric electric sunrise effect, *Journal of Atmospheric and Terrestrial Physics*, 37, 553-559, 1975.
- Muir,M.S., A possible mechanism linking solar events and terrestrial weather, *South African Journal of Physics*, 2, 33- 35, 1979 (a).
- Muir,M.S., The role of atmospheric electricity in sun-weather relationships, *Solar-Terrestrial Influences on Weather and Climate*, Reidel publishing company, 259- 262, 1979 (b).
- Muralidas,S., S.Sampath and V. Saikumar, Effect of surface radio activity on vertical distribution of atmospheric electrical conductivities, *Indian journal of radio and space physics*, 20, 444- 445, 1991.
- Narcisi, Rocco.S and Walter Roth, The formation of cluster ions in laboratory sources and in the ionosphere, *Advances in electronics and electron physics*, , Academic press Inc.,New York, 29 pp 79- 113, 1970.
- Narcisi,R.S.,A.D.Bailey, L.Della Lucca, C.Sherman and D.M.Thomas, Mass spectrometric measurements of Negative ions in the D-and lower E-regions, *Journal of Atmospheric and Terrestrial Physics*, 33, 1147, 1971.
- Narcisi, R.S., A.D.Bailey, L.E.Wlodyka and C.R.Philbrik, *Journal of Atmospheric and Terrestrial Physics*, 34, 647,1972.
- Narcisi,R., A. Bailey, G.Frederico and L.Wlodyka, Poitive and negative ion composition measurements in the D and E regions during the 26 February 1979 Solar eclipse, *Journal of Atmospheric and Terrestrial Physics*, 45, 7, 461- 478, 1983.
- Nath,N., and C.S.G.K.Setty, the D-region ion composition, *Pure and applied Geophysics*, 114, 891- 908, 1976.

- Neils Jonassen and Marvin H. Wilkening, Conductivity and concentration of small ions in the lower atmosphere, Journal of Geophysical Research, 70, 9, 779-784, 1965.
- Nicolet, M., Contribution a l'etude de la structure de l'ionosphere, Mem. Inst. Meteorol. Belg., 19, 83, 1945.
- Nicolet, M., and A.C. Aikin, The formation of the D-region of the ionosphere, Journal of Geophysical Research, 65, 5, 1960.
- Ogawa, Toshio, Analysis of measurement techniques of electric fields and currents in the atmosphere, Contributions, Geophysical Institute, Kyoto university, 13, 111- 137, 1973.
- Paltridge, G.W, Experimental measurement of small ion density and electrical conductivity of the stratosphere, Journal of Geophysical Research, 70, 12 1965, pp 2751- 2761.
- Paltridge, G.W, Time variation in small ion density at 32 kilometers altitude, Journal of Geophysical Research, 71, 8, 2169- 2170, 1966.
- Prakash, S, B.H. Subbaraya, and S.P. Gupta, Some features of the equatorial D region as revealed by the Langmuir probe experiments conducted at thumba, Proceedings of the Cospar symposium on Methods of measurements and results of lower ionosphere structure, 259- 265, Akademie-Verlag. Berlin, 1974.
- Prasad, B.S.N., V.S. Jain and A.P. Mitra, IRI models of electron density distribution over Indian sub continent, Scientific report, Indian Space Research Organisation, 1982.
- Prasad, B.S.N., N. Srinivas and S. Chandramma, A simplified ion-aerosol model for balloon measurements of ion conductivity and aerosol concentration, Indian Journal of Pure and Applied Geophysics, 20, 304- 306, 1991.
- Prasad, B.S.N, Personal communication (1989 & 1992).
- Ratcliffe, J.A., An introduction to the ionosphere and magnetosphere, Cambridge university press, 1972.
- Reid, G.C., The production of water cluster ions in the Quiet time D-region, Journal of Geophysical Research, 25, 275, 1977.
- Reiter, Reinhold, Influence of solar activity on electrical potential between the ionosphere and the earth, Solar-Terrestrial Influences on Weather and Climate, Reidel publishing company, 243- 251, 1979.

- Rosen J.M., D.J.Hofmann and W.Gringel, Atmospheric electrical measurements workshop, Data report, Atmospheric physics report No.AP-49, University of Wyoming, 82071, 1979.
- Rosen, J.M, D.J.Hofmann, W.Gringel, S.Michnowski, Y.Morita, T.Ogawa and D.Olson, Balloon-borne atmospheric electrical measurements to 33 km, Part--1: Smallion density, air-earth current density, conductivity, ion density, ionisation and electric field, Atmospheric physics report No.AP-60, University of Wyoming, 82071, 1980.
- Rosen, J.M, and D.J Hofmann, Balloon borne measurement of electrical conductivity, mobility and recombination coefficient, Journal of Geophysical Research, **86**, C8, 7406-7410, 1981.
- Rosen, J.M, D.J.Hofmann, W.Gringel, J.Birlinski, S.Michnowski, Y.Morita, T.Ogawa, and D.Olson, Results of an international workshop on atmospheric electrical measurements, Journal of Geophysical Research, **87**, C2, 1219-1227, 1982.
- Rosen, J.M, D.J.Hofmann, W.Gringel, Measurements of ion mobility to 30 km, Journal of Geophysical Research, **90**, D4, 5876- 5884, 1985.
- Rose, G, H.U. Widdel and R. Borchers, A mesosphere payload to measure the concentration and mobility of positive and negative ions in the height range between 72 and 40 km, Journal of British Inter planetary Society, **24**, 215-231,1971.
- Rose, G and H.U Widdel, Results of concentration and mobility measurements for positively and negatively charged particles taken between 85 and 22 km in sounding rocket experiments, Radio Science, **7**, 1, 81- 87, 1972.
- Schmeer, H and A.Hack, Z.Angew Phys.,**14**, 398,1962 (cited in. Farrokh 1975.).
- Spjeldvik, W.N., and R.M.Thorne, A simplified D-region model and its application to magnetic storm after effects, Journal of Atmospheric and Terrestrial Physics, **37**, 1313- 1325.
- Srivastava ,G.P, B.B.Huddar and Anna Mani, Electrical conductivity and potential gradient measurements in the atmosphere over India, Pure and Applied Geophysics, **100**, VIII, 81-93, 1972.
- Somayajulu Y.V., K.S.Zalpuri and S.Sampath, Indian Journal of Pure and Applied Geophysics, **10**, 197, 1981.
- Sonin, A.A., Theory of ion collection by a super sonic atmospheric sounding rocket, Journal of Geophysical Research, **72**, 4547- 4557, 1967.

- Stergis, C.G., S.C. Coroniti, A. Nazerk, D.E. Kotas, D.W. Seymour and J.V. Werme, Conductivity measurements in the stratosphere, *Journal of Atmospheric and Terrestrial Physics*, **6**, 233- 242, 1955.
- Subbaraya, B.H, Satya Prakash and S.P Gupta, Electron densities in the equatorial lower ionosphere from the Langmuir probe experiments Conducted at Thumba during the years 1966 - 1978, Scientific report, Indian Space Research Organisation, 1983.
- Swider, W., and R.S. Narcisi, *Journal of Atmospheric and Terrestrial Physics*, **45**, 493, 1983.
- Takagi, Masumi, Yutako Condo and Akira Iwata, Measurement of ion concentration and ion mobility in the mesosphere at dusk by rocket-borne Gerdien probes, *Journal of Geomagnetism and Geoelectricity*, **32**, 715- 719, 1980.
- Thomas, L., Modelling of the ion composition of the middle atmosphere, *Annales Geophysicae* **1**, 1, 61-73, 1983.
- Tepley, C.A., J.D. Mathews and S. Ganguly, *Journal of Geophysical Research*, **86**, 11330 (cited in Chakrabarty and Ganguly 1989).
- Udare, R.S., R. Rajaram, T. Ogawa and M. Yashuhara, Height profile of vertical electric field and conductivity over HYderabad, *Indian Journal of Pure and Applied Geophysics*, **20**, 307- 309, 1991.
- Viggiano, A.A, F. Arnold, D.W. Fahey, F.C. Fehsenfeld and E.E. Ferguson, *Planet. Space Sci.* **30**, 499, 1982.
- Weiland, R.M., T.S.N. Somayaji, and Bowhill S.A, *Journal of Atmospheric and Terrestrial Physics*, **45**, (cited in Chakrabaty et al 1983).
- Widdel, H.U, and R. Borchers, Results of concentration and mobility measurements of positively and negatively charged particles taken by a rocket-borne parachuted aspiration (Gerdien) probe in the height region from 72 to 39 km, *Pure and applied Geophysics*, **84**, pp 154- 160, 1971.
- Widdel, H.U, G. Rose and R. Borchers, Experimental results on the variation of electric conductivity and ion mobility in the mesosphere, *Journal of Geophysical Research*, **81**, 34, 6217- 6220, 1976.
- Widdel, H.U, G. Rose and R. Borchers, Payload B-III - An instrument for the measurement of conductivity concentration and mobility of positive and negative ions in the mesosphere, *Journal of Geophysics*, **44**, 179- 188, 1977.

Widdel, H.U, G.Rose and R.Borchers, Results of conductivity ion mobility and ion concentration measurements obtained with a parachuted Gerdien aspiration analyser probe in the heights below 70 km, Journal of Atmospheric and Terrestrial Physics, 41, 1141-1147, 1979.

Willet, J.C., Solar modulation of the supply current for Atmospheric electricity? Journal of Geophysical Research, 84, c8, 4999- 5002, 1979.

Wilson, C.T.R., Investigation on lightning discharges and on the electric field of thunderstorms, Phil. Trans. R. Soc. London, (A), 221, 73- 115, 1920.

Woessner, R.H, W.E. Coebb and Ross Gun, Simultaneous measurements of the positive and negative light ion conductivities to 26 Kilometers, Journal of Geophysical Research, 63, 1, 171-180, 1957.

---

Sankaran, A.V., B.Jayaswal, K.S.V.Nambi, and C.M.Sunta, U, Th and K distributions inferred from regional geology and the terrestrial radiation profiles in India, Scientific report - Babha Atomic Research Centre, Bombay, India, 29, 1986.

PUBLICATION IN JOURNALS / PRESENTED IN SYMPOSIA :

1. S. Murali Das, V. Sasi Kumar and S. Sampath : Measurement of electrical conductivities, ion densities & mobilities in the middle atmosphere over India. *IND. J. RAD. SPACE PHYS.* 16 215-220 1987.
2. S. Sampath, S. Murali Das and V. Sasikumar Electrical conductivities, ion densities and mobilities in the middle atmosphere over India.- balloon measurements. *J. ATMOS. TERR. PHYS.* 51 6 533-540 1989.
3. S. Murali Das , S. Sampath and V. Sasi Kumar: Effect of surface radioactivity on the vertical distribution of atmospheric electrical conductivity : *IND. J. RAD. SPACE PHYS.* 20, 444-445, Dec. 1991.
4. S. Sampath, V. Sasikumar and S. Murali Das : Positive and negative ion densities and their mobilities in the middle atmosphere over India - Rocket measurements *J. ATMOS. TERR. PHYS.* 54, 347-354, 1991.
5. V. Sasi Kumar, S. Sampath, S. Murali Das & K. Vijayakumar Effect of radioactive deposits at the surface on atmospheric electricity - *COMMUNICATED FOR PUBLICATION TO THE SPECIAL ISSUE OF J. GEOPHYS. RES. ON 9th Int. CONFERENCE ON ATMOSPHERIC ELECTRICITY.*
6. S. Murali Das, S. Sampath and V. Sasi Kumar : Balloon-borne pumped Gerdien condenser measurement of ion densities, mobilities and conductivities. *COMMUNICATED FOR PUBLICATION TO THE SPECIAL ISSUE OF J. GEOPHYS. RES. ON 9th Int. CONFERENCE ON ATMOSPHERIC ELECTRICITY.*
7. S. Sampath , S. Murali Das and V. Sasi Kumar : Balloon-borne measurement of ion densities, mobilities and conductivities in India - Presented at the Solar Terrestrial Symposium - COSPAR - held at Toulouse, France during June 30 - July 12, 1986.



8. S.Sampath , S. Murali Das and V.Sasi Kumar : Middle atmospheric ion densities, mobilities and conductivities over India - Presented at the IAGA symposium in the IUGG conference held at Vancouver, Canada during August 9 - 22, 1987.

9. S.Sampath, S. Murali Das and V.Sasikumar : Measurement of middle atmospheric electrical conductivities, ion densities and mobilities in the middle atmosphere over India. *IMAP SCIENTIFIC RESULTS. ISRO SCIENTIFIC REPORT ISRO-IMAP-SR-32-88 87-94 1988.*

10. S . Murali Das, V. Sasi Kumar and S SAMPATH : A Gerdien conductivity meter for surface measurements : Technical report submitted as a part of the project sanctioned by the D.S.T., Govt. of India.

-----